



RAPPORTSERIE

Nr. 56 – Oslo 1990

V. LØVØ, A. ELVERHØI, P. ANTONSEN,
A. SOLHEIM, G. BUTENKO, O. GREGERSEN &
O. LIESTØL:

**Submarine permafrost and gas hydrates in
the northern Barents Sea**

**NORSK
POLARINSTITUTT**

Nr. 56 – Oslo 1990

**V. LØVØ, A. ELVERHØI, P. ANTONSEN,
A. SOLHEIM, G. BUTENKO, O. GREGERSEN &
O. LIESTØL:**

**Submarine permafrost and gas hydrates in
the northern Barents Sea**

**Vigdis Løvø, Anders Elverhøi, Petter Antonsen, Anders Solheim and Olav Liestøl
Norsk Polarinstitutt
Rolfstangveien 12
1330 Oslo Lufthavn**

**George Butenko
Veritec A/S
Veritasveien 1
1322 Høvik**

**Odd Gregersen
Norges Geotekniske Institutt
Sognsveien 72
0855 Oslo 8**

PREFACE

The present report is the result of a project that was initiated by the Norwegian Polar Research Institute (NP) and the Norwegian Petroleum Directorate (NPD) and carried out jointly between NP, NPD, the Norwegian Geotechnical Institute (NGI) and Veritec A/S. NPD also provided financial support, the and the project was led by a steering committee with participants from each of the institutions.

CONTENT

CHAPTER 1

1. GAS HYDRATES AND SUBMARINE PERMAFROST	1
1.1 General aspects of gas hydrates	1
1.1.1 Introduction	1
1.1.2 Crystal structure and stability	2
1.1.3 Hydrate-prone physical environment	6
1.1.4 Gas hydrate sampling	8
1.1.5 Origin of gas hydrates and hydrate-forming gas	10
1.2 Acoustic and thermal properties of gas hydrates	12
1.3 Geophysical and geochemical evidence for gas hydrates	12
1.3.1 Seismic evidence	12
a) Reflection seismic	12
b) Refraction seismic	13
1.3.2 Log evaluation	14
a) Mud log	15
b) Dual Induction Log	15
c) Spontaneous Potential (SP)	15
d) Caliper Log	15
e) Velocity tools	16
f) Neutron Porosity	16
g) Density Log	16
h) Drilling Rates	16
i) Cross Correlations	16
1.3.3 Sediment sampling and geochemical analysis	18
1.3.4 In situ testing of gas hydrates	18
1.3.5 Sediment mass movements	19
1.4 General aspects of submarine permafrost	20
1.4.1 Introduction	20
1.5 Physical properties of frozen sediments	23
1.5.1 Acoustic properties	24
1.5.2 Electrical properties	26
1.5.3 Thermal properties	26
1.5.4 Mechanical properties	27
a) Temperature	27
b) Soil type	28
c) Water content	28
d) Salinity	30
e) Rate of stress application	31
1.6 Geophysical methods for detection of submarine permafrost	32
1.6.1 Seismic methods	33
a) Refraction	33
b) Reflection	35
1.6.2 Electrical methods	38
1.6.3 Well log evaluation	39
a) Resistivity log	39
b) Sonic log	39
c) Caliper Log	39
d) Spontaneous Potential	39
e) Drilling Rates	40
f) Density Log	40
g) Neutron Porosity log	40
h) Gamma log	40
i) Crystal cable log	40

CHAPTER 2

2. PHYSICAL AND GEOLOGICAL SETTING OF THE WESTERN/NORTHERN BARENTS SEA	42
2.1 General overview	42
2.1.1 Physical setting	42
a) Physiography	42
b) Hydrography	44
c) Sea ice conditions	47
2.1.2 Geological setting	50
a) Pre-Quaternary history	50
b) Bedrock geology	51
c) Sediments above bedrock	54
d) Arctic silts	56
2.2 Selected study areas: physical and geological setting	57
2.2.1 Physical setting	57
a) Air temperature	57
b) Water temperature and salinity	58
c) Water depth	59
2.2.2 Sediments above Upper Regional Unconformity	59
a) Thickness	59
b) Composition	59
c) Total organic carbon (TOC) and total carbon (TC) content	60
d) Geothermal gradient	61
e) Seismic velocity	62
f) Pockmarks	63
2.2.3 Bedrock characteristics	64
a) Total organic carbon	64
b) Porosity	65
c) Seismic velocity	65
2.3 Late Cenozoic History	65
2.3.1 Summary - Late Cenozoic paleoenvironment Svalbard - Barents Sea	68
a) Late Miocene/Early Pliocene (5 - 2.6 Ma)	68
b) Mid/Late Pliocene/Early Pleistocene (2.6 - 1.2 Ma)	69
c) Pleistocene: pre-Weichselian (1.2 - 0.12 Ma)	69
d) Weichselian/Holocene (0.12 Ma - present)	69
2.3.2 Weichselian sea level changes and paleogeography of the Barents Sea	75
2.3.3 Ice profiles and sub-glacial conditions (Late Weichselian)	77
a) Extensive ice cover	80
b) Limited ice cover	81
2.4 Glacial erosion and its influence on the Late Cenozoic evolution of the Barents Sea	83
2.4.1 Glacial erosion	83
a) Indirect measurements of glacial erosion	86
b) Further comments on the recent glacial erosion from Svalbard	87
c) Estimates of glacial erosion in the Barents Sea	88
2.4.2 Late Cenozoic development of the Barents Sea, glacial versus fluvial erosion	90

CHAPTER 3

3. EVALUATION OF THE POSSIBILITIES OF SUBMARINE PERMAFROST AND GAS HYDRATES IN THE BARENTS SEA AND SVALBARD	94
3.1 Permafrost conditions in Svalbard	94
3.1.1 Spitsbergen	94
a) Permafrost depth	94
b) Glaciers and lakes, influence on permafrost depth	96
3.1.2 Bjørnøya	98
3.1.3 Hopen	98
3.2 Thermal regimes and geological history	99
3.2.1 Mid Weichselian/Early stage of the Late Weichselian (~50 - 20ka)	99
3.2.2 Late Weichselian (18 - 14ka)	99
3.2.3 End of the Late Weichselian (14 - 10ka)	101
3.2.4 Holocene	103
3.2.5 Conclusions	104
3.3 Distribution of permafrost and ice-bearing sediments and rocks in the Barents Sea	108
3.3.1 In situ temperature measurements	110
3.3.2 Temperature profiles, Hopen - the Barents Sea	111
3.3.3 Conclusions	114
3.4 Possible occurrence of gas hydrates in the Barents Sea and in Svalbard	114
3.4.1 Thermal prediction of gas hydrate occurrence in the Barents Sea.	115
3.4.2 Gas composition and hydrate stability	117
3.4.3 Thermal prediction of gas hydrate occurrence in Svalbard.	118

CHAPTER 4

4. DATA ANALYSIS	120
4.1 Seismic interpretation	120
4.1.1 Bjørnøya South	121
a) Gas hydrates/free gas	125
b) Shallow gas	128
c) Diagenesis	132
4.1.2 The Sentralbanken and the Olga Basin areas	132

CHAPTER 5

5. WELLS AND BOREHOLES IN OFFSHORE ARCTIC REGIONS WHERE PERMAFROST AND GAS HYDRATES MIGHT BE ENCOUNTERED.	136
5.1 Introduction	136
5.2 Permafrost	136
5.2.1 Thaw subsidence	136
a) Excess ice	136
b) Thaw-consolidation with fluid expulsion	137
c) Pore pressure reduction	137
d) Stiffness reduction	137
5.2.2 External Freezeback	137
5.2.3 Hydrate Decomposition	138
5.3 Examples of measured parameters in thaw/freeze processes	139
5.3.1 Radius of thawing around a well	139
5.3.2 Thaw-subsidence induced loads	140
5.4 Drilling problems in permafrost areas	141
5.4.1 Hole sloughing and washouts	141
5.4.2 Drilling through hydrates	141
5.5 Drilling mud in permafrost areas	142
5.5.1 Mud types, properties	142
5.5.2 Air and foam	142
5.6 Casing and completion equipment in permafrost areas	143
5.6.1 Casing design	143
5.6.2 Completion equipment	143
5.6.3 Thermal production systems	144

CHAPTER 6

6. RELEVANT GEOPHYSICAL METHODS FOR DETECTION OF SUBSEA PERMAFROST AND GAS HYDRATES IN THE BARENTS SEA.	145
6.1 Detection of subsea permafrost	145
6.2 Detection of gas hydrates	147

CHAPTER 7

7. CONCLUSIONS	149
7.1 Geological history and physical setting	149
7.2 Permafrost	150
7.3 Gas hydrates	151

REFERENCES	153
------------	-----

1. GAS HYDRATES AND SUBMARINE PERMAFROST

1.1 General aspects of gas hydrates

1.1.1 Introduction

Gas hydrates are crystalline substances composed of water and natural gas formed under certain conditions of low temperature and high pressure. Natural gas contains mainly methane, often accompanied by hydrocarbons of higher molecular weight; ethane, propane, and butanes, as well as inorganic gases such as nitrogen, carbon dioxide and hydrogen sulphide (Kvenvolden 1982).

Gas hydrates were first discovered by Sir Humphry Davy in 1810 when he noticed ice-like crystals forming upon cooling of an aqueous solution (Davy 1811). However, detailed studies of hydrates and their physical properties were not undertaken until Hammerschmidt (1934) published data pertaining to the plugging of natural-gas pipelines due to gas hydrate formation. The geological occurrence of gas hydrates was first detected in deep ocean bottom sediments on the Blake Outer Ridge offshore the United States (Markl et al. 1970). An anomalous reflection paralleling the sea bed was identified in seismic profiles from the area. It is now commonly accepted that this "Bottom Simulating Reflector" (BSR) originates from the base of a gas hydrate layer. During the last few years, several reports of gas hydrate occurrence have been published, based on both seismic interpretation and sediment sampling.

The occurrence of gas hydrates is important for several reasons. As well as being a possible energy source, gas hydrates may pose severe problems with regard to drilling and operation of wells.

Large volumes of gas can be contained in hydrated form and may constitute an important, relatively shallow reserve of natural gas. However, current technology can probably not produce the hydrated gas in commercial quantities. The main economic advantage of the gas hydrates may reside in their ability to act as an impermeable seal under which free gas can accumulate (Kvenvolden & Barnard 1983).

Drilling and operation of wells in a gas hydrate zone may result in pressure increase, mud gasification, and consequently a possible loss of control, due to decomposition of the hydrates (Davidson et al. 1978). The decomposition of hydrates occurring in sediments close to the sea floor, may cause problems of thaw settlements or heave to sea bottom installations. Furthermore, interpretation of seismic reflection data may be complicated by the presence of a substantial

thickness of gas hydrates. The hydrates have higher seismic velocities than unconsolidated sediments and lateral variations in thickness of the hydrate layer may cause problems in the interpretation (Judge 1982).

1.1.2 Crystal structure and stability

The crystalline structure in gas hydrates results from hydrogen bonding between water molecules, but the geometry is quite different from the hexagonal ice-structure. The water is crystallized in the isometric (cubic) system, and the lattice contains voids large enough to accommodate molecules of gas. The interaction between the gas molecules and the surrounding network of water is not chemical in nature, but is due to the van der Waals forces similar to that found between adjacent molecules in liquids (Hand et al. 1974).

Two structures of the cubic lattice are possible. In Structure I, the cages are arranged in body-centered packing and include small hydrocarbon molecules such as methane, ethane, and nonhydrocarbons such as CO_2 and H_2S . In Structure II, diamond packing is present; not only can methane and ethane be included in the voids, but, in order to stabilize the structure, propane and isobutane are needed to occupy some of the larger voids. Hydrocarbons larger than isobutane do not appear to form hydrates, primarily because they are too large to fit in the biggest solute cages in the lattice (Hand et al. 1974). In general, appreciable quantities of hydrate are only expected as structure I unless the gas is relatively rich in higher hydrocarbons (Davidson et al. 1978).

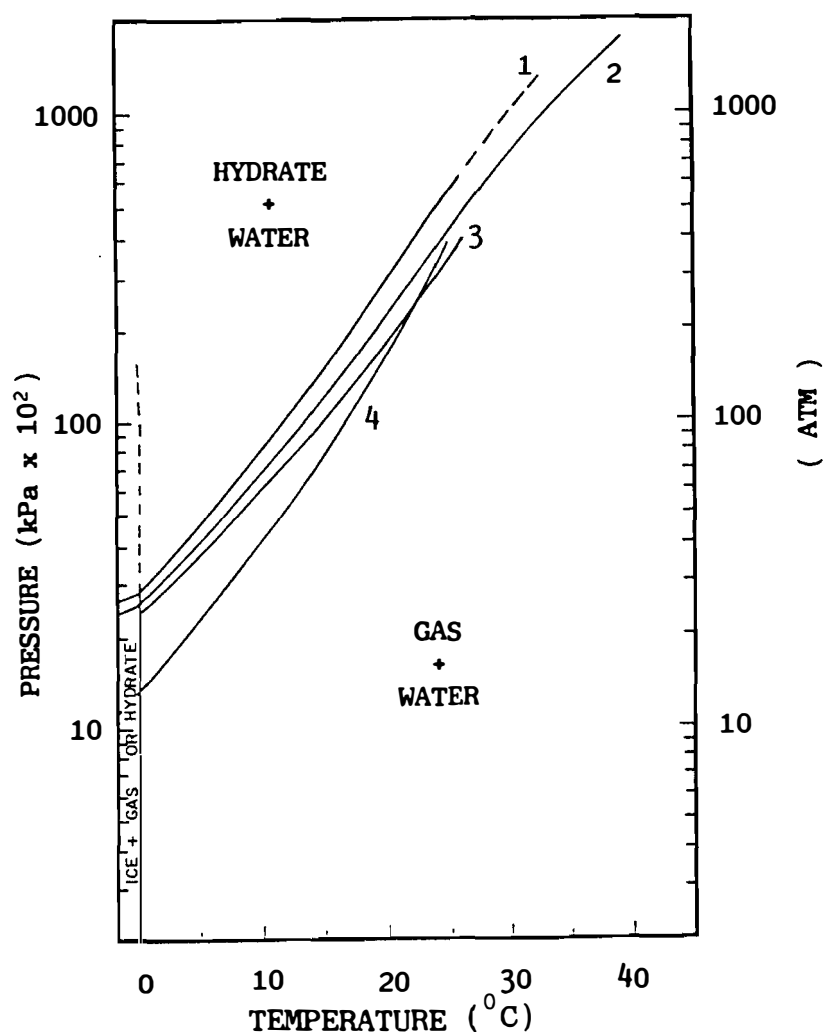
The amount of gas needed for hydrate formation depends on temperature and pressure. In the methane-water system, only methane present in excess of the amount soluble in water is available for hydrate formation. The formula for an ideal stoichiometric methane-water hydrate is $\text{CH}_4 \cdot 5 \frac{3}{4} \text{H}_2\text{O}$. One m^3 of this ideal hydrate would contain the equivalent of about 170 m^3 of methane gas at STP (standard temperature and pressure). However, gas hydrates found in nature will contain less gas than this because the lattice cages are not completely filled (Kvenvolden & McMenamin 1980).

The stability of in situ gas hydrates is influenced by several reservoir and fluid properties; geothermal gradient, gas chemistry, pore fluid salinity, pore pressure, and reservoir rock grain size. The primary factors are the geothermal gradient and gas chemistry, while the other variables are difficult to quantify and may often have

little effect (Collett et al. 1988).

Figure 1.1 shows how the phase boundary for gas and hydrate varies when the gas composition is changed or salt pore water is present. Curve 2 applies to pure methane hydrated in fresh water. Adding slight amounts of other gases, such as ethane or CO_2 , leads to hydrate stability at higher temperatures and lower pressures (curves 3 and 4), and thereby a thicker gas hydrate stability zone. Salt lowers the temperature at which gas hydrate forms (curve 1), leading to a decrease in the thickness of the gas hydrate stability zone (Macleod 1982). The pressure scale can be converted to a depth scale by using a hydrostatic gradient of 10.4 kPa/m. The conversion is based on the assumption that sediments near the seafloor are permeable, and the pressure in the pore spaces will be equal to the hydrostatic pressure (Macleod 1982).

According to Collett et al. (1988), the effects of grain size variations and abnormal pore pressure conditions on gas hydrate equilibrium are unclear. Studies of permafrost have shown that variations in grain sizes and pore pressures affect the freezing point of ice (Anderson et al. 1973; Osterkamp 1975; Osterkamp & Payne 1981). Particles with large surface area relative to grain size, such as clay, can reduce the freezing point of water by several degrees Celsius, apparently because of molecular bonding of the water to the particle (Anderson et al. 1973). A similar relation may exist between grains of high surface area and gas hydrate equilibrium temperatures. Abnormal formation pressures will affect gas hydrate stability conditions in a manner unlike that of ice. High pore pressure conditions increase the stability of gas hydrate, but depress the freezing point of ice (Holder et al. 1975). In general, the higher the pressure gradient the thicker stability zone of gas hydrate (Collett et al. 1988).



CURVE	GAS	WATER
1	100% METHANE	+3.5% NaCl
2	100% METHANE	PURE
3	93% METHANE, 7% CO ₂	PURE
4	90% METHANE, 10% ETHANE	PURE

Fig. 1.1. Pressure and temperatures stability conditions for gas hydrates. Curve 1 show effect of adding salts, and curves 3 and 4 the effect of adding other gases to the methane-pure water system (curve 2). After Macleod (1982), data from Katz et al., (1959).

Subsurface temperature data required to calculate regional geothermal gradients are difficult to obtain. Temperature measurements in wells are often unreliable because the drilling process can disrupt subsurface equilibrium temperatures. The most accurate measurements are obtained from wells that are left undisturbed for a sufficient period of time to allow thermal equilibrium, but such data are not often available.

An alternate method is to use known ice-bearing permafrost depths and regional temperature constants derived from stabilized well-bore temperature surveys to project local geothermal gradients (Collett 1983; Collett et al. 1988). The geothermal gradient changes abruptly at the base of ice-bearing permafrost due to a change in thermal conductivity caused by the transition from ice-filled pores to water-filled pores (Lachenbruch et al. 1982). Due to the freezing point depression of salt water, the equilibrium temperature at the base of the marine permafrost is $-1^{\circ} - 0.5^{\circ} \text{C}$. In Prudhoe Bay, Alaska, Collett (1983) used known permafrost depth from a well (532m), mean annual ground temperature (-10.9°C), lithostatic pressure gradient (9.84 kPa/m) and assumed equilibrium temperature at the base of the ice-bearing permafrost to be -1°C . The calculated geothermal gradient within the permafrost is 19°C/km . Given a regional thermal gradient increase of 1.75 at the base of the permafrost (Lachenbruch et al. 1982), the thermal gradient below the base of the permafrost was calculated to be 32°C/km . The thermal gradients above and below the base of the ice-bearing permafrost zone can be plotted on a methane hydrate stability curve, and the intersection between the gradients and the hydrate phase diagram marks the zone of hydrate stability (Fig.1.2). Collett (1983) estimate that in order to get an intersection between the methane hydrate stability curve and the geothermal gradients in Prudhoe Bay, the permafrost depth have to be a minimum of 290 m.

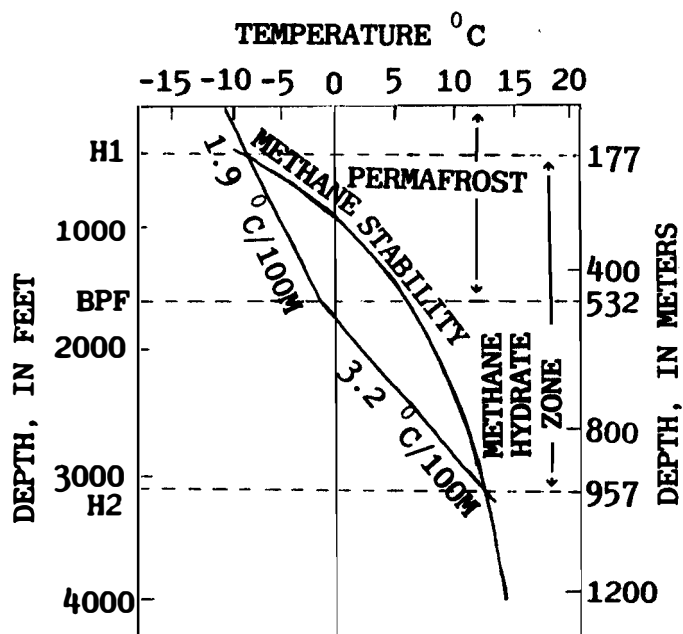


Fig. 1.2. Thickness calculation of the methane hydrate stability zone. See text for discussion (from Collett 1983).

The fact that the temperatures in the sediments increase with depth leads to temperature conditions at which gas hydrates no longer are stable and therefore decompose. The base of the gas hydrate zone follows a pressure-temperature surface that represents the maximum depth at which the gas hydrate is stable. Hydrated sediments are impermeable to fluid flows, thus the gas hydrate zone may overlies accumulations of free gas. The seal at the base of the gas hydrate can trap biogenic methane generated below the gas hydrate or released at the base of the hydrate as it moves downward into unstable regions. Conceivably, the base of the gas hydrate could also form a seal for thermogenic hydrocarbons migrating toward the surface from depth (Kvenvolden & Barnard 1983).

1.1.3 Hydrate-prone physical environment

Natural gas hydrates have generally been found in two different and distinct environments which reflect their dependence on temperature and pressure; firstly, submarine in outer continental margins and ocean basins, and secondly, associated with high latitude regions of permafrost (Fig.1.3).

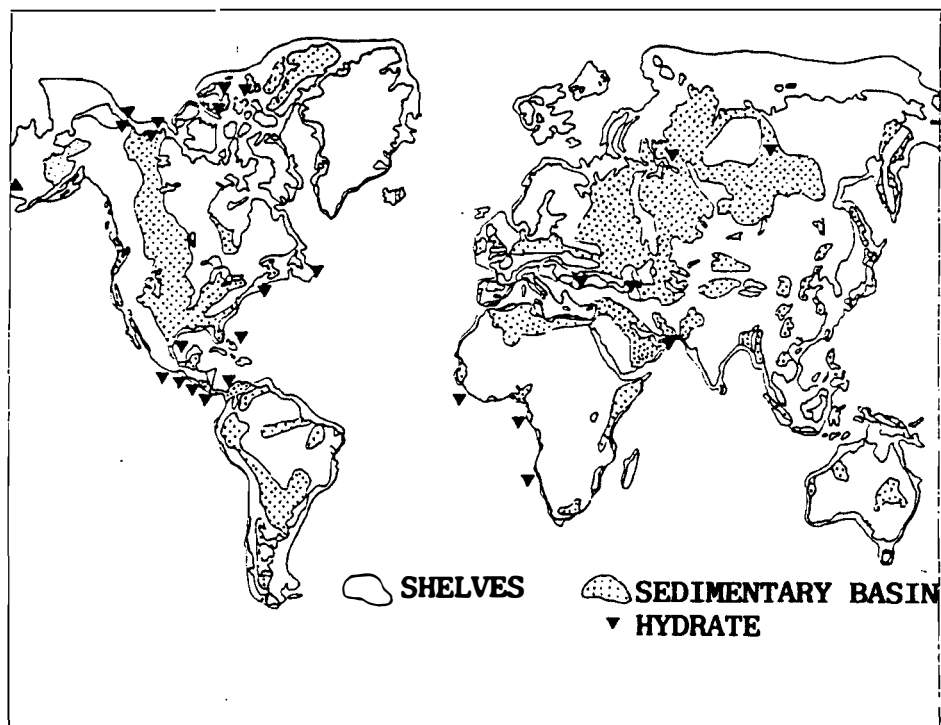


Fig. 1.3. World-wide distribution of gas hydrates as deduced from published accounts (from Judge 1982)

Gas hydrates can occur both within the permafrost layer and below the base of permafrost at temperatures above the freezing point of water (Katz 1971). The presence of gas hydrates in permafrost regions has been established in western Siberia (Messoyakha gas field), in the Mackenzie Delta of Canada, and on the North Slope of Alaska. Estimates of worldwide gas hydrate resources in permafrost regions range from $140 \cdot 10^{11}$ to $34 \cdot 10^{15}$ (STP) m^3 of methane (Potential Gas Agency 1981). The broad range of the estimates demonstrate a general lack of knowledge pertaining to actual gas hydrate occurrence and distribution. The total methane resources in gas hydrates of the oceans are estimated at more than $85 \cdot 10^{15}$ m^3 of gas (Panayev 1987). These estimates can be compared to the proved recoverable world resource of conventional natural gas of $680 \cdot 10^{11}$ m^3 (Parent 1984).

Figure 1.4 shows hydrate-prone zones in different water depths based on a typical bottom-water temperature (0°C) and geothermal gradient ($20^\circ\text{C}/\text{km}$) for arctic shelves (Scotia and Labrador). In general, hydrates will not be found in sediments beneath water depths less than 150 meter unless temperature gradients are depressed in the sediments. Beneath water depths of 300 to 400 m, hydrates may occur in the sea-floor sediments and extend to depths of 600 m (Judge 1982). The maximum reported subbottom depth to a bottom simulating reflector, indicating the presence of gas hydrates, is 1100 m (in water depth exceeding 4000 m) (Shipley et al. 1979).

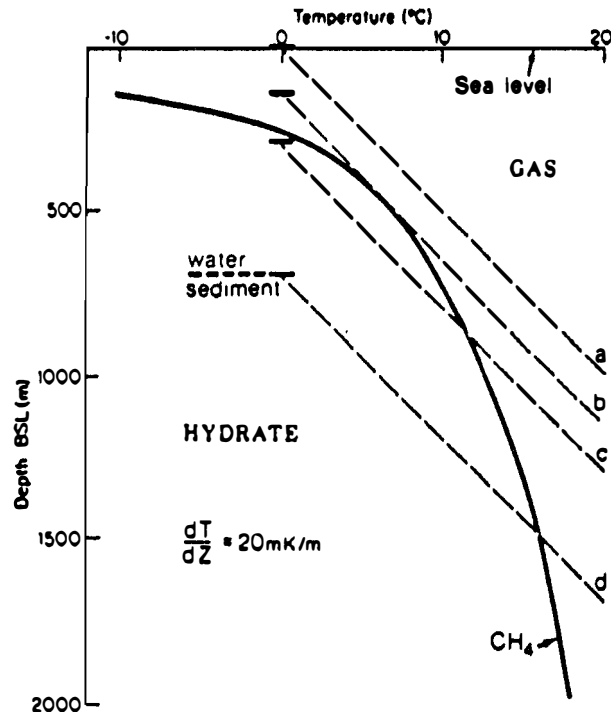


Fig. 1.4. Hydrate-prone zones in different water depths based on a typical bottom-water temperature (0°C) and geothermal gradient ($20^{\circ}\text{C}/\text{km}$) for Arctic shelves (after Judge 1982).

Most of the marine gas hydrates that are not associated with permafrost areas, will be found in continental slopes and rises. Because of the requirement for high concentrations of methane, the occurrence of gas hydrates in sediments of the abyssal basins is not likely even though conditions of temperature and pressure are satisfied (Kvenvolden 1982).

1.1.4 Gas hydrate sampling

A number of gas hydrate studies have been carried out under the Deep Sea Drilling Project (DSDP) and the Ocean Drilling Program (ODP), and marine gas hydrates have been recovered from continental margin sediments in several wells. During DSDP Legs 66 and 67 in the Pacific Ocean offshore Mexico and Guatemala, gas hydrates were recovered on 5 sites in water depths ranging from 1780 to 5490 m. Evidence for gas hydrates was based on observations that high gas pressure was present and that decomposition of the suspected hydrates produced greater quantities of gas than are soluble in water at in-situ pressures and

temperatures. The gas consisted mainly of methane (Kvenvolden & Barnard 1983).

During DSDP Leg 76, Site 533 was drilled in 3184 m of water on the Blake Outer Ridge offshore southeastern United States. The principal object was to recover samples of gas hydrates and to measure the pressure, volume, and composition of gas released during hydrate decomposition. The presence of gas hydrates had been predicted based on a strong seismic reflection and previous results from DSDP Leg 11, showing high concentrations of methane in the sediments. A pressure core barrel (PCB) was developed to recover sediments containing gas hydrates at in-situ pressures (Kvenvolden et al. 1983). Within the PCB a recovered gas hydrate can be decomposed under controlled conditions and samples of gas obtained for analysis. The results from the PCB, together with pressure-volume measurements, visual observations, and chemical analysis confirmed that gas hydrates were present at site 533 (Kvenvolden & Barnard 1983b).

Gas hydrates recovered on Legs 66, 67, and 76 did not occur in massive, thick units but rather in a few thin layers which usually, but not always, were associated with higher porosity intervals. On Legs 66 and 67 the gas hydrates were associated with sands. The single occurrence of solid gas hydrate noted on Leg 76 was in hemipelagic sediment not unlike the rest of the cored sediment (Kvenvolden & Barnard 1983).

DSDP Leg 84, drilled offshore Guatemala and Costa Rica, recovered gas hydrates at 3 sites. The hydrates appeared as solid pieces of white, icelike material occupying fractures in mudstone or as coarse-grained sediment in which the pore space exhibited rapid outgassing. On one site a 1.05 m long core of massive gas hydrate was obtained. Downhole logging showed that this massive gas hydrate was 3-4 m thick at this location. The log provided the first in situ measurements of the physical properties of a gas hydrate: sonic velocity = 3.3 - 3.8 km/s; density = 1.024 - 1.045 g/cm³; resistivity = 200 ohm-m (Kvenvolden & McDonald 1985).

During ODP Leg 112 on the Peruvian continental margin, gas hydrates were found at 2 sites (Kvenvolden & Kastner 1988). The recovered gas hydrates occurred in very fine-grained sediment (Pleistocene mud), in contrast to previous observations where the hydrates appeared to occupy the pore spaces of coarser-grained lithologies.

Although several samples of gas hydrates have been successfully recovered, it is likely that gas hydrates were present in more of the sediment column and at other well sites also. The reason that more gas hydrates are not observed is that they are unstable at shipboard

conditions and are destroyed during the coring process (Kvenvolden & Kastner 1988).

In the permafrost region of Alaska, near Prudhoe Bay, one sample of gas hydrate was successfully obtained from a depth of 666 m in a well. The presence of gas hydrate was confirmed by a pressure test while the core was maintained in the core barrel (Collett et al. 1988). The pressure dropped as gas was withdrawn from the core barrel, increasing to hydrate equilibrium pressure when the system was closed. If the core barrel had contained only free gas, the pressure would not have increased when the system was closed. Collett et al. (1988) interpreted the distribution of gas hydrates on the North Slope of Alaska by using well log responses calibrated to the response of the interval in the well where gas hydrates were recovered. Gas hydrates were identified in 34 wells, mostly occurring in six laterally continuous sandstone and conglomerate units of Upper Cretaceous and Lower Tertiary age. The thickness of the identified individual gas hydrate-bearing intervals range from 2 to 28 m, and the volume of gas within the identified gas hydrates was estimated to approximately 2.4 to $2.9 \cdot 10^{11} \text{ m}^3$ (STP), or about one-third of the volume of conventional gas in the Prudhoe Bay field. However, because of low drilling density outside the Prudhoe Bay area, more gas hydrate occurrences may exist (Collett et al. 1988).

1.1.5 Origin of gas hydrates and hydrate-forming gas

The gases associated with the sampled marine hydrates generally contained more than 99% methane. Other hydrocarbon gases such as ethane and propane were present in parts per million concentrations. This mixture is a very dry natural gas with composition that suggests either a biogenic or metagenic source (Hunt 1979). Because the gas occurs in shallow sediments far from heat sources capable of generating metagenic methane, the methane found is most likely biogenic (Kvenvolden & Barnard 1983b). Other lines of evidence for a biogenic origin include light values for the carbon isotopic composition of the methane gas. Besides, the carbon isotopic composition of CO_2 subparallels that of methane, suggesting that CO_2 is the main precursor of methane (For a more thorough description of the gas analysis see Kvenvolden & Barnard 1983b; Kvenvolden & McDonald 1985; Kvenvolden & Kastner 1988).

The formation and occurrence of gas hydrates on the Blake Outer Ridge and in the Middle America Trench can be explained at least

partly by the model proposed by Claypool and Kaplan (1974) (Kvenvolden & Barnard 1983b; Kvenvolden & McDonald 1985). In this model methane is produced within the sediments by microbial processes, concurrently with sedimentation. When the amount of methane exceeds its solubility in water, and the pressure-temperature conditions are correct, gas hydrates form. The gas hydrate zone will continue to thicken as sedimentation proceeds. When the base of the gas hydrate zone is buried to a depth where temperatures are too high relative to pressure to stabilize the hydrate, the gas hydrate will decompose. However, the formation of the massive gas hydrate found during DSDP Leg 84 can not be explained by this model (Kvenvolden & McDonald 1985).

The most likely explanation for the origin of the gas hydrates of the North Slope of Alaska includes migration of thermogenic solution- and free gas from deeper reservoirs along faults into the overlying sedimentary rocks. As the gas migrated into the upper horizons it was either directly converted to gas hydrate or first concentrated in existing structural/stratigraphic traps and later converted to gas hydrate. Major climatic changes may have influenced the depth limits of the gas hydrate occurrences (Collett et al. 1988).

Based on seismic interpretation and analysis of well log data, several authors indicate that gas hydrates mainly occur in areas of structural anomalies, such as tilted fault blocks, anticlinal folds, dipping beds or adjacent to shale diapirs (Shipley et al. 1979; Katz 1982; Collett 1983). The preferred occurrence of hydrates in these places suggests that the gas was not generated in situ, but had migrated from deeper levels until it reached the stability field of hydrate formation (Katz 1982).

The only known, existing gas field that produces natural gas from gas hydrate zones is the Messoyakha in the West Siberian Basin. The reservoir is a 76 m thick Cretaceous sandstone sequence lying at about 800-900 m depth. The permafrost layer is about 450 m thick in the area. The fields consists of both natural gas hydrates and deeper free natural gas. The productivity of gas from the gas hydrate zone is increased by one order of magnitude by injections of methanol, which serves as a hydrate inhibitor. The parts of the Messoyakha field containing gas hydrates are calculated to have 54% more reserves than would be expected in an equal volume of reservoir rocks filled with free gas (Hitchon 1974).

1.2 Acoustic and thermal properties of gas hydrates

Stoll (1974) and Stoll & Bryan (1979) formed specimens of pure gas hydrates and gas hydrates in sand in the laboratory, and measured acoustic wave velocity and thermal conductivity. Pure water and water-bearing sediment are converted to a stiff elastic mass by the formation of hydrate, resulting in a marked increase in acoustic wave velocity. For unconsolidated sediments (sand) filled with hydrate, the velocity was found to increase from 1850 m/s to 2700 m/s (Stoll 1974). In a massive gas hydrate found during DSDP Leg 84, the sonic log showed a velocity between 3300 and 3800 m/s (Kvenvolden & McDonald 1985).

Laboratory measurements showed that the thermal conductivity of pure hydrate is about 30% less than water. When the water in a sediment is replaced by gas hydrate, the result is a decrease in the overall thermal conductivity (about 23% in the case of sand at 40% porosity filled with propane hydrate). This is contrary to what had been expected on the basis of an analogy with the thermal response of frozen and unfrozen soil. Freezing tends to increase the thermal conductivity of a saturated sediment. In a sediment column containing gas hydrates the changed thermal conductivity would tend to modify the thermal gradient expected for a given type of sediment and heat source (Stoll & Bryan 1979).

1.3 Geophysical and geochemical evidence for gas hydrates

1.3.1 Seismic evidence

Seismic methods may give an indication of the presence of in-situ gas hydrates. The velocity contrast between gas hydrates and the unconsolidated sediments below, and the possible trapping of free gas in these sediments, may cause a strong reflection. Because of the velocity inversion, this boundary will not be registered as a refractor.

a) Reflection seismic

Anomalous, high-amplitude reflections in marine seismic reflection data from continental margins are often correlated with the base of gas hydrated sedimentary rocks (Bryan 1974; Shipley et al. 1979; Katz 1982; Kvenvolden & Barnard 1983). The reflector, commonly called a

"Bottom Simulating Reflector" (BSR), approximately subparallels the seafloor and intersects bedding reflectors (Fig.1.5). Criteria used to characterize these anomalous reflections include:

- a large reflection coefficient
- increasing subbottom depth with increasing water depth
- reflection polarity reversal

The high reflection coefficient and the reflection polarity reversal are most likely related to a fairly thin interval of low density and velocity below the gas hydrate zone. This would be consistent with the hydrates acting as a barrier to gas or water migration and the formation of free gas or high pore water pressures (Shipley et al. 1979). The increasing subbottom depth with the increasing water depth is predicted from the pressure-temperature relations (Fig.1.1). Increasing hydrostatic pressure and decreasing bottom water temperature will make gas hydrates stable to greater depths in the sediments.

Not all bottom simulating reflectors can be directly related to the presence of gas hydrates. The diagenesis of fine grained silica-rich sediments, may cause an acoustic impedance boundary. The change from opal-A to opal-CT causes a marked porosity reduction, which results in increasing density and velocity. The diagenesis is dependant on temperature (burial depth), and the resulting reflection tends to parallel the sea floor. Opal-CT eventually changes to quartz, and the associated diagenesis front may also form a reflection (Badley 1985).

b) Refraction seismic

Sonobuoy seismic velocity measurements can be used to indicate the presence of gas hydrates. High velocities in the sediments above the bottom simulating reflector have been observed on the Blake-Bahama Outer Ridge. A velocity in excess of 2 km/s is unusually high for the hemipelagic mud encountered in boreholes (Bryan 1974).

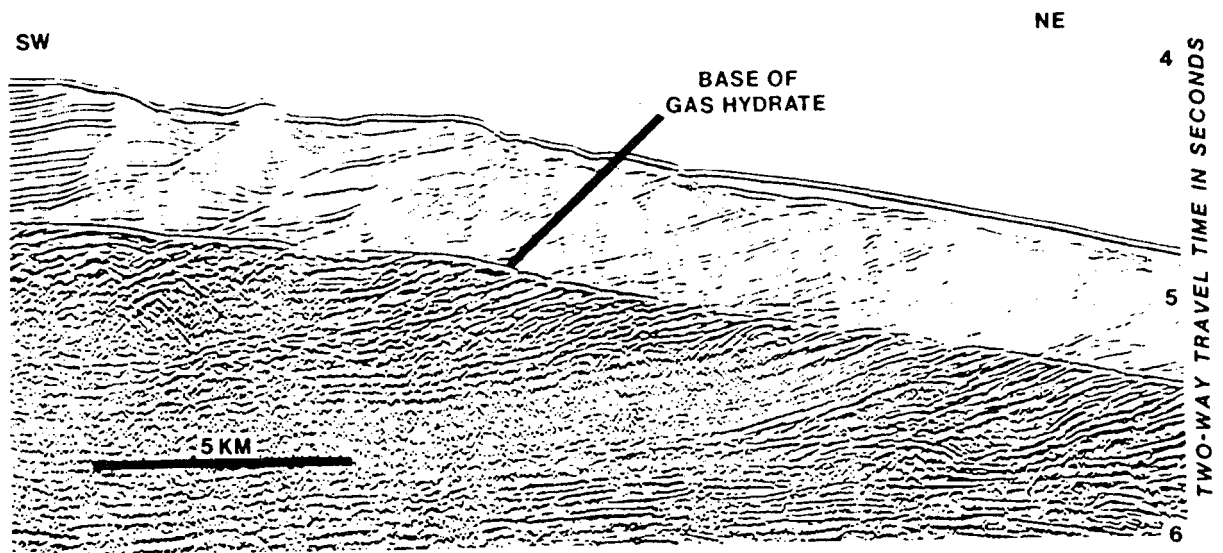


Fig. 1.5. Multichannel seismic reflection profile from Blake Outer Ridge showing Bottom Simulating Reflector (BSR) (from Shipley et al. 1979).

1.3.2 Log evaluation

The recognition of gas hydrate in well log data is not straightforward, and often the zones of potential hydrate occurrence are not logged, or the quality of the logs may be poor. Furthermore, there is a lack of quantitative work. Another problem is that gas hydrates possess physical and electrical properties similar to those of ice, resulting in approximately the same responses as for permafrost in conventional electrical, sonic and nuclear logs (Davidson et al. 1978).

Figures 1.6 and 1.7 present down-hole records in two wells in the Beaufort Sea. High resistivities and acoustic velocities and low mud-gas readings indicate the presence of permafrost in the upper 600 to 800 m (Fig.1.6). High values of resistivity, acoustic velocity, and formation gas below this depth are interpreted to be in situ gas hydrate (Weaver & Stewart 1982).

The following summarizes various log responses, indicating the ability of each log to distinguish gas hydrates from ice-bearing permafrost and free gas (Collett 1983; Collett et al. 1988):

a) Mud log

There is a pronounced gas kick associated with hydrate, due to decomposition during drilling. However, if cold drilling fluid is used there may be minimal decomposition of the gas hydrates and little free gas liberated.

b) Dual Induction Log

There is a relatively high resistivity deflection on the dual induction log in a gas hydrate zone, in comparison to that in a free gas zone. The long normal is separated from the short normal due to thawing next to the bore hole (Fig.1.7). If a unit were gas hydrate saturated within the ice-bearing permafrost sequence, the resistivity response on the dual induction log for the gas hydrate would not be significantly different from that in the surrounding ice-bearing permafrost. Below the base of the ice-bearing permafrost, however, the high resistivity deflection associated with gas hydrate is distinct from the surrounding non ice-bearing permafrost.

c) Spontaneous Potential (SP)

There is a relatively lower (less negative) spontaneous potential deflection in a hydrate zone when compared to that associated with free gas. The frozen hydrate limits the penetration of mud filtrate, hence reducing the negative spontaneous potential. The spontaneous potential curve for a gas hydrate saturated unit within the ice-bearing permafrost sequence would be similar to that in the surrounding ice-bearing units where the mud filtrate penetration is similarly limited.

d) Caliper Log

The caliper log in a hydrate zone usually indicates an oversized well bore due to spalling associated with the decomposition of a hydrate. Because the caliper log also indicates an enlarged bore hole in ice-bearing permafrost, it is only useful in detecting hydrates below the base of the ice-bearing permafrost.

e) Velocity tools

Acoustic velocities in a gas hydrate zone are relatively high. However, the sonic log does not usually perform well as there is poor coupling with the sidewall of the wellbore. Another problem is the thawed zone - the sonic log does not have a deep zone of penetration. Vertical Seismic profiling (VSP) or crystal cable log are better tools because they do not have the problem with coupling. But it is to notice that there should be a close spacing of the detectors for definition of thin beds (S.Blasco 1988).

f) Neutron Porosity

In a hydrate zone there is an increase in the neutron porosity; this contrasts with the apparent reduction in neutron porosity in a free gas zone. Collett et al. (1988) discuss the neutron porosity response to gas hydrate and other pore space constituents in detail.

g) Density Log

Within a gas hydrate there is a decrease in density in comparison to a unit saturated with water. Because the density of ice is similar to that of gas hydrate, the density log cannot be used independently to identify a gas hydrate within ice-bearing permafrost.

h) Drilling Rate

The relative drilling rate decreases, due to the cemented nature of the hydrate. There is a similar drilling rate response within ice-bearing permafrost, and, therefore, drilling rate change is not useful as a hydrate-detector within permafrost.

i) Cross Correlations

Cross correlations between different logs can enhance the log interpretation, yielding definite evidence for gas hydrates. Goodman et al. (1982) present 5 log correlation techniques for application to hydrates:

- density/neutron porosity crossplot
- apparent resistivity and water saturation
- SP/resistivity ratio crossplots
- Dual temperature logs and hydrate equilibrium
- Temperature difference plot

For interpretation of the cross correlations with example applications, see Goodman et al. (1982).

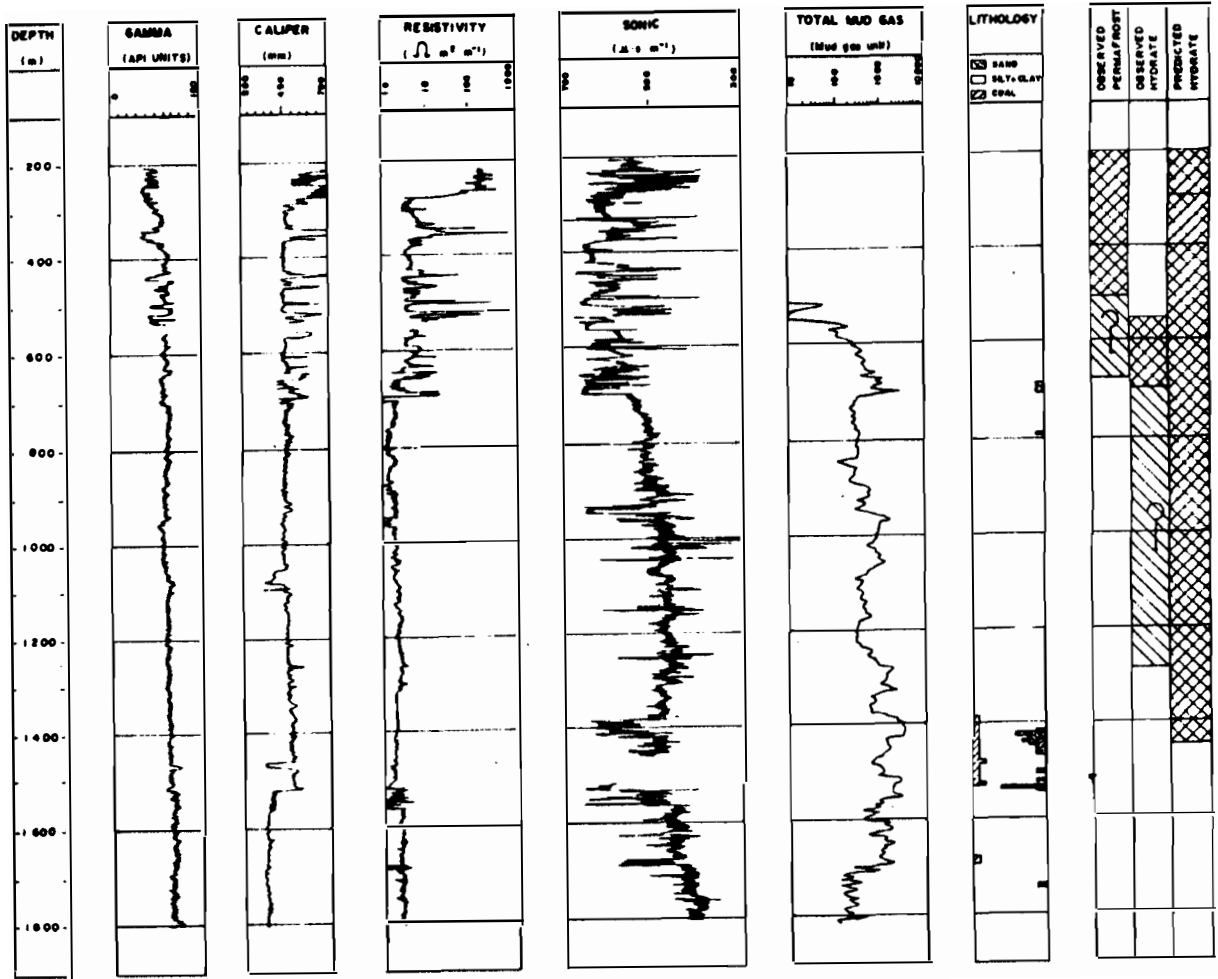


Fig. 1.6. Wire-line and mud-gas logs for the Nerlerk-well on the Beaufort Sea shelf (From Weaver & Stewart 1982).

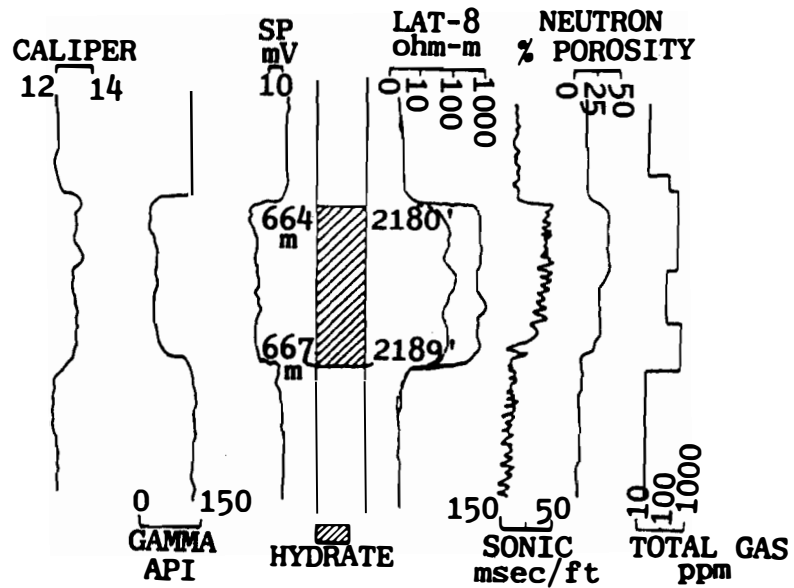


Fig. 1.7. Hydrate characteristics in well log data from Northwest Eileen State. No. 2 well in Prudhoe Bay, Alaska (from Collett 1983).

1.3.3 Sediment sampling and geochemical analysis

Sediment sampling and geochemical analysis from DSDP and ODP well sites show the following lines of evidence for the presence of gas hydrates (Kvenvolden 1982; Kvenvolden & Barnard 1983b; Kvenvolden & McDonald 1985):

1) High gas pressure

2) Volume measurements show that the volume of gas released from sediment samples was many times greater than the volume of pore fluid in the samples, thus exceeding the amount of gas soluble in water at in-situ pressure and temperature.

3) The gas released consists mainly of methane; in general more than 99 %. Concentrations of gases larger than isobutane abruptly decrease to trace amounts. Gas samples taken from sediments lacking obvious gas hydrates often showed another molecular fractionation.

4) Pore-fluid analysis; the presence of hydrates influences pore-water chemistry, leading to a depletion of salinity and chlorinity. During gas hydrate formation, water molecules will be withdrawn from solution to form the water clathrate. This process should lead to increased chlorinity and salinity in any water not involved in hydrate formation. If this water is free to migrate towards the sediment/water interface and escape into the seawater, the water remaining in the sediment will be a mixture composed in part of fresh water (Kvenvolden & Barnard 1983b).

5) Visual observations; recovered samples of gas hydrates can appear as solid pieces of ice-like material occupying fractures and porespace in the sample, exhibiting rapid outgassing. Sometimes, the pressures generated can be sufficient to extrude cores from the barrel and rupture sealed containers.

1.3.4 In-situ testing of gas hydrates

Field testing is needed to determine hydrate decomposition response, thermodynamic behavior, and pressure buildup around a wellbore. For hydrate resource evaluation, testing is needed to define gas composition, reservoir extent, and productivity. The most

practical and economical approach is to test during drilling. Goodman et al. (1982) considered several testing methods, and found that a downhole heater in conjunction with drill stem testing (DST) can be used for field evaluation of in situ hydrates.

1.3.5 Sediment mass movements

Gas hydrates may become unstable and decompose as a result of natural geological processes, including sea level lowering, continuing sedimentation and deeper burial, or by local operations such as drilling. The gas and water volume released by the decomposition, exceed the volume occupied by the gas hydrate itself. The decomposition may cause a rising internal pressure, and the once rigid sediment can be converted to a gas- and water-rich, relatively low density mud. If the internal pressure gets sufficiently high, the overlying sediment may be lifted and/or breached, and the less dense, gas-cut mud may break through. Such hydrate-related phenomena may cause mud diapirs, mud volcanoes, mud slides, or turbidite flows, depending on the sediment configuration and bottom topography (McIver 1982).

Reflection seismic data recorded on several continental margins indicate a possible connection between gas hydrates and sediment mass movements. Off the east coast of the United States, Carpenter (1981) revealed sediment mass movements (slumps) which appear to occur above gas hydrate accumulations. The gas hydrates are identified by reflection anomalies. The slumping is believed to be related to the liberation of free gas by gas hydrate decomposition and the resulting destabilizing of unconsolidated sediments above the gas hydrates. The Storegga Slide on the Norwegian continental margin is suggested to be triggered by a combination of earthquakes and decomposition of gas hydrates (Bugge et al. 1987).

A bottom simulating reflector is observed within the Amazonas Fan (Manley & Flood 1988). Migration of the hydrate phase boundary during sea level fluctuations and diapiric activity are suggested mechanisms for initiating widespread debris flows.

1.4 General aspects of submarine permafrost

1.4.1 Introduction

The original definition of permafrost is based upon temperature alone, and requires only that the sediments remain at temperatures below 0 °C for two years or more (New Permafrost Dictionary, National Resource Council of Canada. 1987). Onshore, and in areas with fresh interstitial water, this normally leads to freezing. However, in marine sediments the saline interstitial water cause a depression of the freezing point. Commonly the temperature in subsea soil in shallow Arctic shelves is around -1.6 °C, while in coastal areas and deltas the temperature is slightly higher. In general, subsea ice-bearing sediments are far less common than in onshore regions with similar temperature regimes.

In recent literature the following nomenclature has been used to describe specific subsea permafrost properties (Sellmann & Hopkins 1984; Hunter 1984):

- Acoustic permafrost (APF) - defined from the acoustic properties of sediments alone. Unlithified sediments with ice-bonded permafrost have abnormally high seismic velocities when compared with similar, unfrozen sediments. High amplitude events, due to high impedance contrast caused by the increased velocity, indicate APF.
- Ice-bearing sediments - 1) a general term to indicate that ice can be expected to occur or does occur, or 2) ice quantity or bonding is not sufficient to influence strength properties or seismic velocity.
- Ice-bonded sediments - material containing ice that has sufficient bond with soil particles to cause a noticeable increase in strength properties and significant increase in seismic velocity.

Where adequate information is available, more specific qualifications of bonding could include "well-bonded" or "partially bonded". The more general term "ice-bearing" is used when nature of soil-ice interaction is unknown. The term "warm permafrost" has been applied for the transition zone between frozen and unfrozen ground.

Submarine permafrost, identified in the near-shore areas of the Arctic Ocean, formed mainly by subaerial exposure to cold surface conditions during periods of lower sea level, e.g. the Quaternary glacial maxima. Available and detailed literature on subsea permafrost is limited to North American high Arctic shelves, particularly the Beaufort Sea shelf. Sparse literature also exists for the nearshore area of the Soviet Arctic.

The shallow Canadian and Alaskan Arctic shelves were exposed down to the present day 100 meter isobath about 18 000 years ago (Osterkamp & Harrison 1982; Hill et al. 1985). Increasing relative sea level until 3000 to 4000 years ago, inundated the subaerially exposed permafrost, replacing the cold onshore surface temperature condition with warmer, marine conditions. During the past 3000 to 4000 years, the shore-lines have continued to recede by thermal and hydrological erosion of ice-rich permafrost. Along the Beaufort Sea coast, shore-line erosion has been rapid, averaging more than a metre per year with short-term rates as great as 30 m/y, creating larger areas of submarine permafrost (Sellmann & Hopkins 1984).

Even though most offshore permafrost is relict and originated subaerially prior to submergence, permafrost may form under present day conditions where fresh water percolates close to ice-bonded sediments (O'Connor 1981). The formation of such permafrost has not yet been proven, and have to be regarded as a hypothesis.

According to seismic studies, borehole and probe data from the Beaufort Sea, the general distribution of ice-bonded sediments follow a patchy and irregular pattern closely related to the geological history of the area. Three types of ice-bonded sediments are identified (Neave & Sellmann 1984)(Fig.1.8):

- Shallow ice-bonded permafrost - observed close to the seafloor and may extend several km off the coastline.
- Deep ice-bonded permafrost - identified at depths down to 200 m below sea-floor, can be traced into shallow, firmly ice-bonded material near the shore.
- Layered ice-bonded permafrost - consist of two or more separate permafrost layers. This type seems to be rather common in areas where detailed data are available.

The formation of the layered permafrost seems to be related to two different sedimentary processes (Sellmann & Hopkins 1984):

- 1) River deltas where stratified sand, silt and clay have accumulated. Fresh water may penetrate the most permeable strata and freeze. Additionally, the fresh groundwater may dilute the saltwater, increasing its freezing point.
- 2) Migrating barrier islands and shoals can leave a trail of recently formed permafrost.

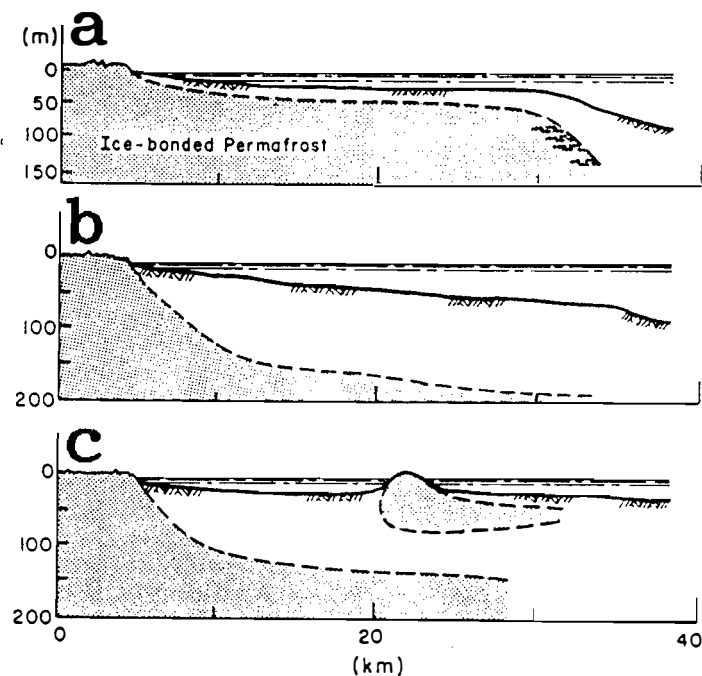


Fig. 1.8. Three distribution patterns suggested for ice-bonded subsea permafrost based on borehole and seismic data: (a) shallow ice-bonded, (b) deep ice-bonded, and (c) layered ice-bonded materials (from Neave and Sellman 1984).

Permafrost on land is relatively stable; natural changes and modifications being associated either with slow climatic changes or with local phenomena. Offshore, the permafrost is more dynamic, particularly in the coastal zone where active coastal retreat is common.

Lachenbruch et al. (1982) have estimated the geothermal conditions beneath a recently submerged portion of the continental shelf at Prudhoe Bay, Alaska. If the inundated terrain initially had a thermal regime like that present on land today, it will generally take about 2000 years after rapid submergence for the entire thickness of the initially cold permafrost to approach near-melting seabed temperature (Fig.1.9). During this time interval, the permafrost, initially

extending to a depth of about 600 m, will thaw only about 10 m from below. Thereafter the base of the permafrost will rise about 15 m/1000 years. Hence, even after 8000 years of submergence, ice-rich permafrost would extend to a depth of about 500 m, and after 15 000 years to about 400 m. Thus deep ice-rich permafrost at near melting temperatures is expected throughout extensive near-shore regions on shallow shelves.

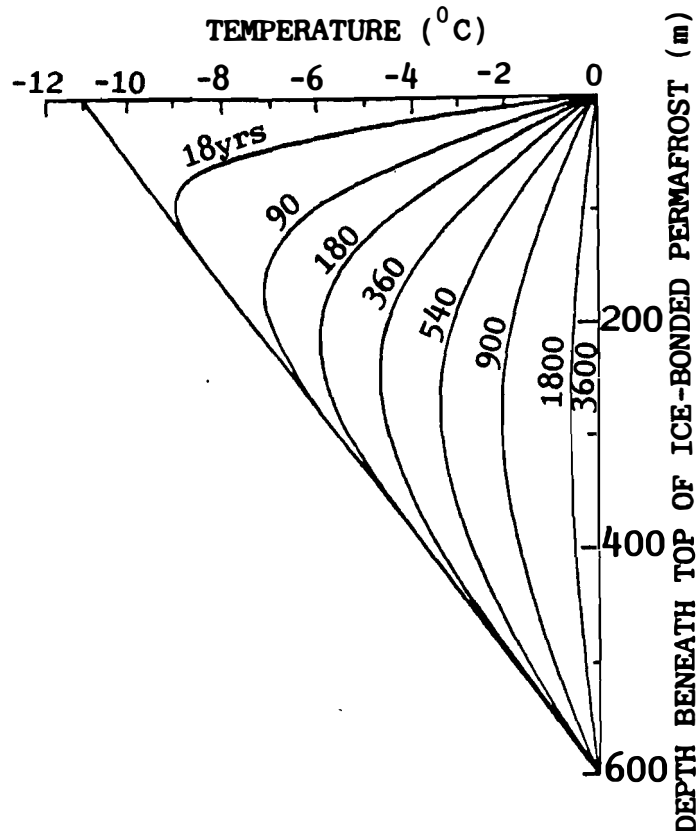


Fig. 1.9. Marine temperature profiles for the Prudhoe Bay region from a tentative model proposed by Lachenbruch et al. (1982). The profiles denoted by time in years, indicate anticipated temperature modification caused by marine conditions over an area for the denoted period of time.

1.5 Physical properties of frozen sediments

The physical properties of offshore permafrost are similar to those measured in onshore permafrost; the slight differences observed are attributed to the more saline pore fluid contained in the offshore permafrost (King et al. 1982).

1.5.1 Acoustic properties

Acoustic velocities of water-saturated material increase with decreasing temperatures below 0°C responding to the increase in interstitial ice-content. Beside temperature, the velocities depend on lithology, porosity and salinity of the porefluid.

King (1977) measured acoustic velocities in the laboratory at permafrost temperatures on a number of samples of sandstone and shale recovered from boreholes in the Arctic. The velocities of frozen sandstones were strongly dependent on temperature in the range $-17 - 0^{\circ}\text{C}$, with a reduction in value as the temperature rises to 0°C . The acoustic velocity of certain shales of low porosity were relatively insensitive to changes in temperature in the range $-17 - +4^{\circ}\text{C}$.

Figure 1.10 shows compressional wave velocities in frozen and nonfrozen material, illustrating that in order to detect submarine permafrost, it is not sufficient with the velocity data alone. Information about the type of material being investigated, particularly whether it is coarse or fine grained, is also required. It is important to notice that correlation between velocity measurements and the conditions of the material, requires direct observation by drilling or probing (Rogers & Morack 1980).

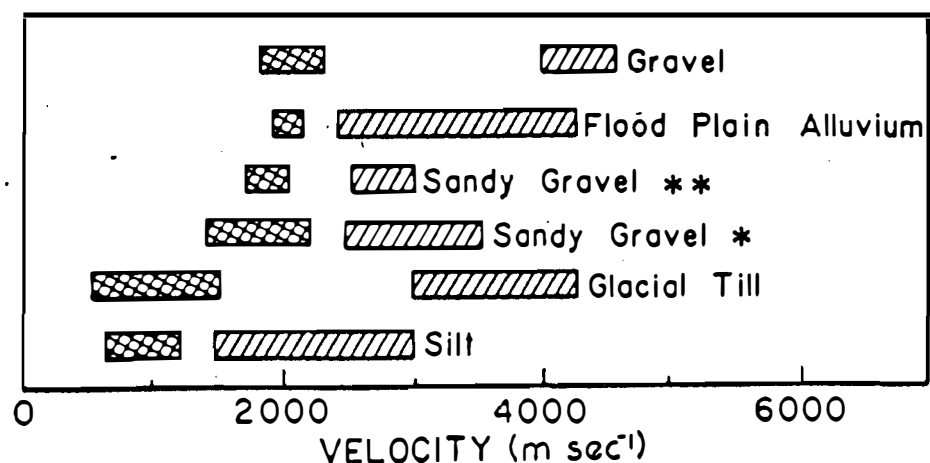


Fig. 1.10. Compressional wave velocities in unbonded (cross-hatched) and ice-bonded (slashed) materials. The data are from Roetlisberger (1972) except those marked * and **, which were measured by Morack & Rogers, 1983 on five offshore islands near Prudhoe Bay and near Point Barrow, respectively (from Morack & Rogers 1983).

Figure 1.11 shows a set of theoretical curves from King (1984), relating compressional wave velocities, porosities, and fraction of ice in the pores of unconsolidated material. It shows a possible linear correlation between velocity and the remaining water-filled porosity. Notice that for the range of porosities given, the "non-ice-bearing" condition is less than about 1650 m/s. The threshold velocity of 2400 m/s used in early refraction interpretations to indicate ice-bonded material can be related to 21 - 33% ice-filling of the pore spaces. This diagram gives a framework for interpretation, but should be extensively tested (Hunter 1984).

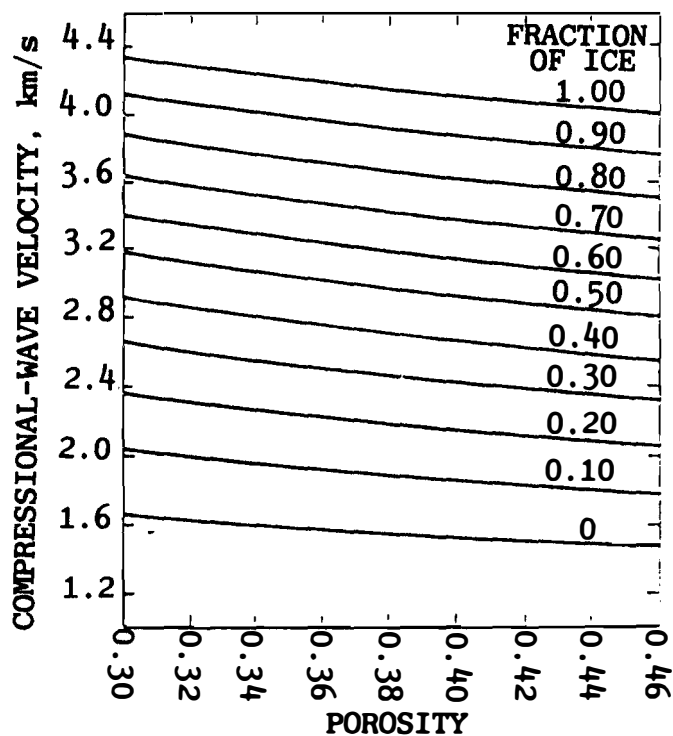


Fig. 1.11. Theoretical curves relating compressional wave velocities, porosities, and fraction of ice in the pores of unconsolidated material (from King 1984).

1.5.2 Electrical properties

The electrical resistivity of sediments is strongly affected by changes in temperature, with a reduction value as the temperature rises to 0°C (Fig.1.12). The change in resistivity depends on the porosity, lithology and salinity of the porefluid. It is to be noted that the salinity of interstitial water can be 25% higher than that of normal sea water (Harrison & Osterkamp 1982). Fine-grained material shows lower resistivity and is more insensitive to changes in temperature than coarser grained material (King 1977). Most measured values of the ratios of frozen to unfrozen resistivity fall in a range between about 5:1 and 100:1 (Corwin 1983).

1.5.3 Thermal properties

Freezing tends to increase the thermal conductivity of a saturated sediment. Kersten (1948) reported an increase in conductivity of 26-57% depending on the porosity, when freezing a "sandy soil".

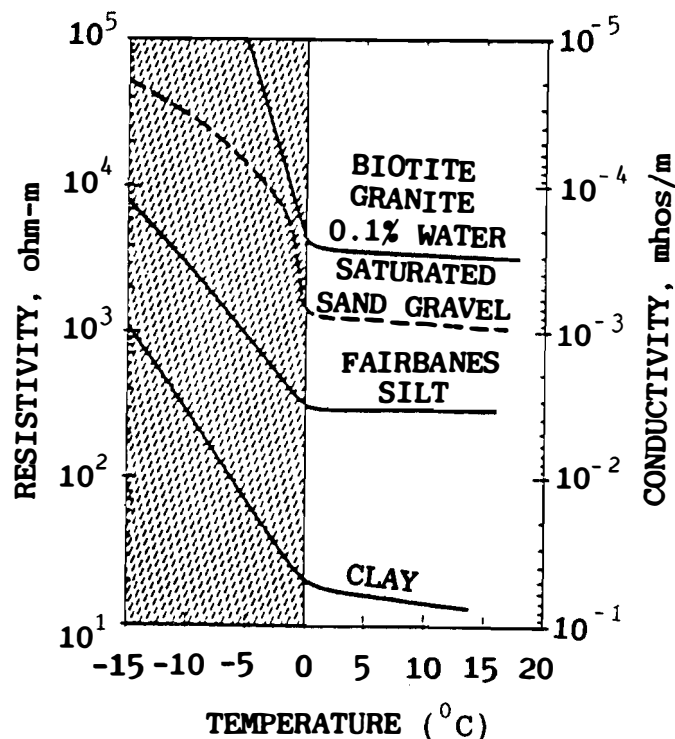


Fig. 1.12. Conductivity versus temperature (from Sartorelli & French 1982).

1.5.4 Mechanical properties

In frozen soil the ice forms a bond between the mineral particles. As this bond can carry stress, the strength of a frozen soil is much higher than that of an unfrozen soil.

The strength behaviour of frozen ground is, however, determined by many factors, among the most important are:

- temperature
- soil type
- water content
- salinity
- rate of stress application

a) Temperature

In frozen ground the effect of temperature on the mechanical properties is particularly important in the range of naturally encountered temperatures (at 0 to -10°C) i.e. Tsytoich (1975) determined the increments in the short term compressive strength of frozen clays per 1°C . He found between -0.3 and -1.0°C a value of $960\text{ kPa}/^{\circ}\text{C}$, between -1 and -5°C $450\text{ kPa}/^{\circ}\text{C}$ and between -5 and -10°C $380\text{ kPa}/^{\circ}\text{C}$. Similar results were obtained for a frozen sandy loam. The reason is that temperature changes not only the interaction of water with soil, but also the ratio of the amount of liquid water to ice. Strength increment of frozen soil with a fall of temperature can also be related to an increment in cohesive strength of the unfrozen water film separating mineral particles and ice (Hoekstra 1969).

b) Soil type

Figure 1.13 illustrates the effect of both temperature and soil type well. Unconfined compressive strength values are plotted against temperature for three different samples (strain rate for these curves was 0.2"/min). It should be noted that the strength values continue to increase even at very low temperatures (-25 to -75 °C).

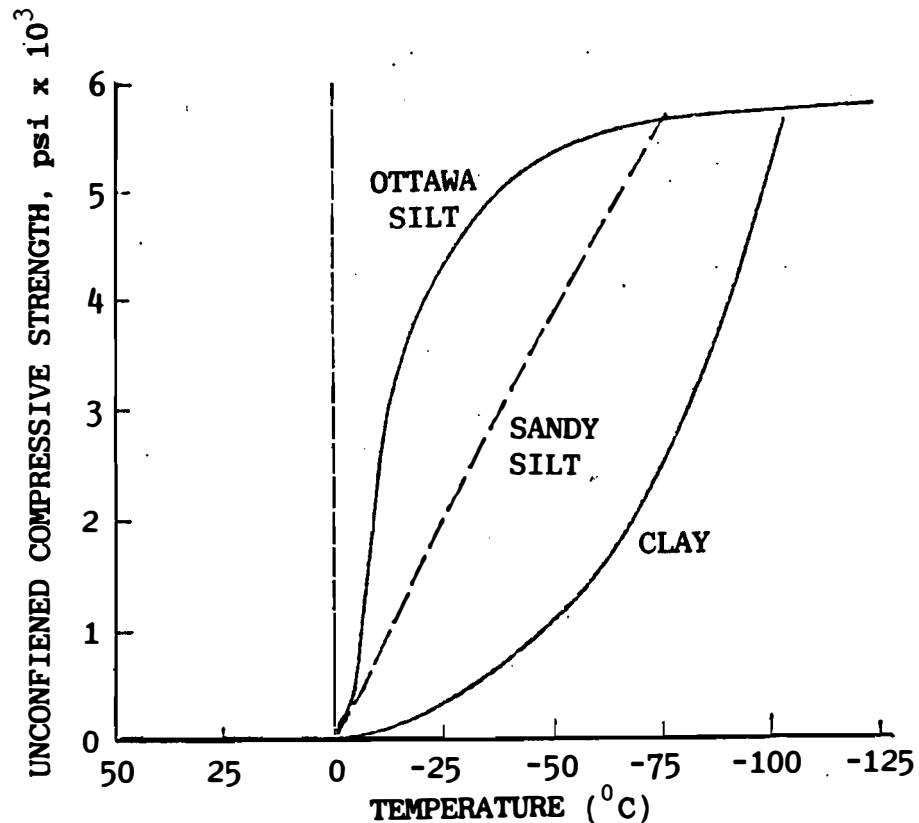


Fig. 1.13. Ultimate compressive strength of three soils as a function of temperature (after Sayles 1966).

c) Water content

Unfrozen water plays an important role in creep. The amount of unfrozen water increases with pressure. Creep is most likely the result of transport of water under stress gradients (Hoekstra 1969). At constant temperature and total water content the creep rate increases as the soil type contains more unfrozen water. This amount of unfrozen water increases from sand to silt to clay and reflects the increase in specific surface areas of the soil.

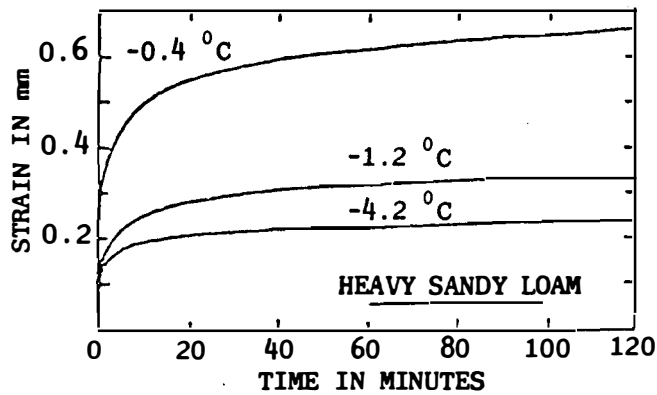


Fig. 1.14. Strain as a function of time at constant load for a heavy sandy loam at several temperatures (after Vyalov 1965).

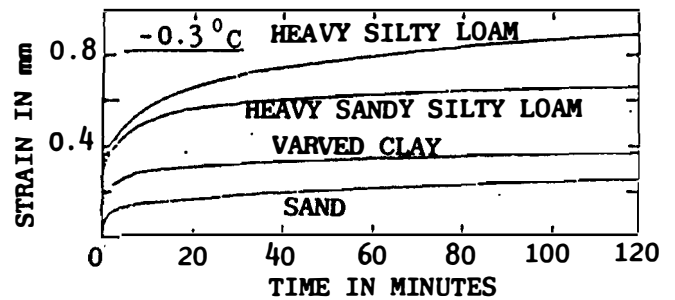


Fig. 1.15. Strain as a function of time at constant load for several soils at a temperature of -0.3°C (after Vyalov 1965).

Figures 1.14 and 1.15 illustrate the effect of both temperature and soil type on the steady creep rate; both reflect the effect of unfrozen water content. In contrast to Hoekstra (1969), Tsytoovich (1975) attributes much of the creep of frozen soil to visco-plasticity of ice. This is why he recommends that the stress strain rate relation for steady state creep of frozen soil should be described with the following power law:

$$\dot{\epsilon}_t = \frac{1}{\eta_{t,\theta}} (\sigma - \sigma_0)^n$$

where

- $\dot{\epsilon}_t$ = strain rate
- σ = normal stress
- σ_0 = creep threshold
- $n \geq 1$ is a dimensionless parameter
- $\eta_{t,\theta}$ = a time and temperature dependent non-Newtonian viscosity

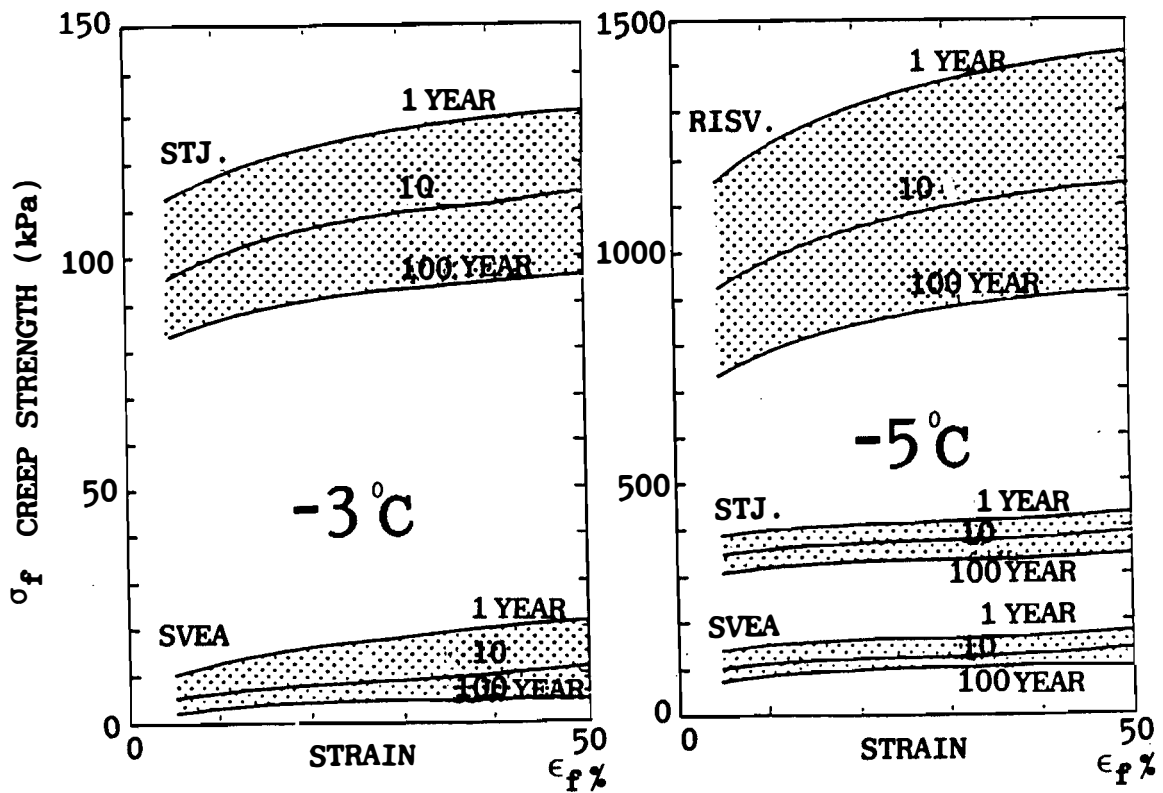


Fig. 1.16. Creep strength as a function of strain and temperature, -3°C and -5°C .

d) Salinity

The freezing point of the pore water in a saline soil is lower than that of a fresh water soil. The freezing of saline soils gives fresh ice, resulting in increasing salinity and hence stronger depression of the freezing point of the remaining unfrozen pore water.

The amount of unfrozen water in a saline soil can be calculated from the following formulae (Banin & Anderson 1974):

$$\frac{W_U}{W} = 6.367 \cdot 10^{-2} \frac{z}{\theta}$$

where W_U = unfrozen water content (g/g soil)
 W = water content (g/g soil)
 z = salt content (g/l)
 θ = number of degrees below 0°C ($^{\circ}\text{C}$)

Test data on frozen saline soils are relatively few in international literature. Some work has, however, been carried out in Norway during the last decade. Figure 1.16. shows the relationship between creep strength and strain for three different clays,

from Svea, Svalbard, Risvollan, Trondheim and Stjørdal, respectively. The data are collected from laboratory tests run at -3°C and -5°C . The difference in strength behaviour is due to salinity and distribution of ice. The Risvollan clay is a leached marine clay, the Stjørdalen clay has a salt content of 33 g/l and the Svea clay has an overall salt content of 30 g/l, distributed with 50 g/l in pore water and zero in ice lenses.

e) Rate of stress application

With increasing rate of load application, higher ultimate strength values are observed. Hoekstra (1969) gives the following equation for Ottawa sand:

$$\sigma_{\max} = A(\dot{\sigma})^B$$

where

σ_{\max} = unconfined compressive strength

$\dot{\sigma}$ = time rate of load application

A and B are empirical constants

This variation in strength values with rate of load application, is due to the time taken for reestablishment of equilibrium between the phases after changes in pressure.

Figure 1.17 shows the behaviour of the strain with time at different load levels. Three stages in these curves can be recognized:

1st: instantaneous elastic strain

2nd: constant strain rate: period of steady creep by visco-plastic flow

3rd: progressive flow, leading to plastic loss of stability or brittle failure

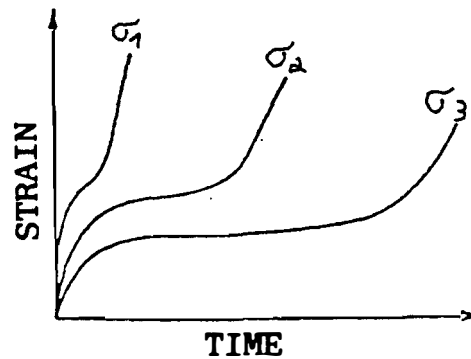


Fig. 1.17. Behaviour of strain as a function of time at different load levels.

To these curves one can add another for the critical load, below which the 3rd stage is absent. In this respect Tsyrovich (1975) distinguishes two types of creep:

sustained creep, pertaining to the above mentioned 3-stage behaviour

decaying creep, below the critical load, stage 2 ending in zero strain rate

Steady state creep arises only when the frozen soil is subjected to stresses exceeding its long-term strength (the creep threshold). Stage 2 usually occupies the longest time and is of greatest interest for practice.

1.6 Geophysical methods for detection of submarine permafrost

The geophysical methods for detection of subsea permafrost are sensitive to the differing properties between the frozen and unfrozen sediments. Seismic methods have been the most successful in locating subsea permafrost, and these methods will be emphasized here. However, electrical methods have also been applied, and will be briefly discussed. These geophysical methods only yield values of different parameters and their distribution. The final step required in the subsea permafrost interpretation is correlation with sediment core and drilling data, i.e. temperature measurements and well log interpretation.

1.6.1 Seismic methods

a) Refraction

Seismic refraction profiling requires underlying layers that are continuous and have increasing seismic velocity with increasing layer depth. Ice-banded permafrost overlaid by unbanded sediments generally satisfies these conditions. The refraction readings yield the depth to the ice-banded permafrost and the refraction velocities in the layer. However, the bottom of the ice-banded permafrost will not be detected because the transition from high-velocity to lower velocity materials at that boundary precludes refraction. It should also be noted that presence of gas limits the use of the refraction method, because of low velocities associated with the gas. In the case of dipping strata, the requirement of plane, homogenous layers, implicate errors in velocity- and depth determination from single-ended refraction records. To get correct values, two refraction profiles should be shot in opposite directions (reversed profiles).

Different techniques for acquiring and processing of refraction data for detection of subsea permafrost have been employed. Hunter et al. (1978) interpreted the refraction arrivals from oil exploration reflection records to determine depth and velocity of ice-banded sediments. The records were obtained from seismic hydrophone arrays designed for reflection profiling, hence refraction arrivals were often preferentially attenuated, and the resolution was limited.

Rogers & Morack (1980) used an airgun source and a short hydrophone cable (480 m) with 24 channels, and increased the signal/noise ratio by stopping the ship's engines during the 30 sec interval needed to shoot one spread. The profiles were not reversed, and the data were recorded in analog form, scaled and reduced to time-distance plots. Straight lines were fit to the plots, and the inverse slopes of these lines were used to determine seismic velocities. The velocity data were then used to determine whether or not the materials were frozen. Where available, drilling information was correlated with the velocities. It is important to remember that frozen and unfrozen materials can generally not be separated using velocities alone, particularly when the ice content of the sediment is low.

Morack & Rogers (1982) developed a reversible refraction system by towing an additional airgun from a small boat at the streamer end, fired by radio link. The data reduction techniques are similar to

refractor.

MacAulay & Hunter (1982) and Morack et al. (1983) used high-resolution reflection data for the refraction interpretation of ice-bonded sediments. The data were acquired using airgun arrays, short hydrophone cables (600-700 m), few hydrophones per trace (16) and high source frequencies. Figure 1.18 is a manually interpreted record showing three refractors.

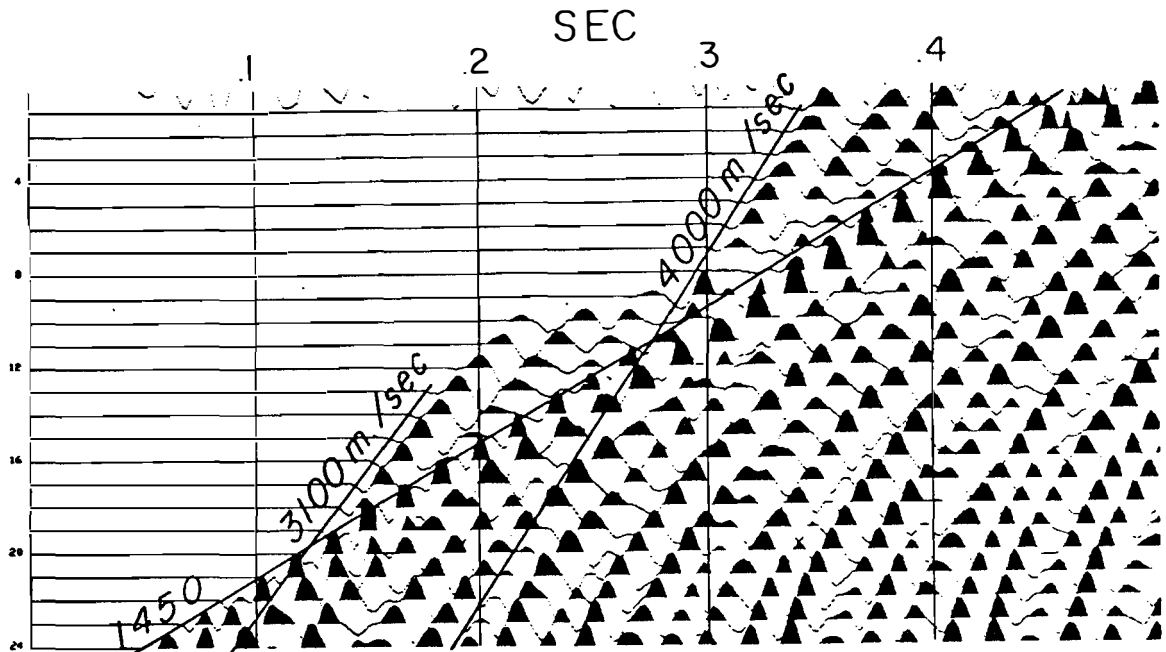


Fig. 1.18. A seismic refraction record from the Beaufort Sea showing a thin, ice-bonded, high-velocity (3100 m/s) layer. Rapid attenuation of first arrival amplitude with increasing shot-receiver distance indicates a thin layer. Below, a thicker, ice-bonded layer (4000 m/s) is indicated. 1450 m/s belongs to the water layer (from MacAulay & Hunter 1982).

Morack et al. (1983) displayed the records in a format termed "Iso-offset time section". This is a plot of shot point locations along the horizontal axis and first arrival time in the downward direction. Arrival times at a given hydrophone group for each of its shot point locations are then connected by straight line segments (Fig.1.19). The vertical spacing of the connected lines decreases as the seismic velocity increases due to shorter interval time. Thus, a sharp velocity contrast is indicated by a change in the density of the connected lines; areas underlain by high velocity material appear as areas of closely spaced lines on the plot. The iso-offset displays can be compared to reflection profiles to confirm high velocity events usually occurring as bright spots on the reflection sections.

Neave & Sellmann (1984) used seismic data acquired by the petroleum

industry, and played back the first two seconds of the tapes with expanded gain to improve the quality in the shallow part. This type of data may provide good regional coverage, but may also suffer from effects that are avoided by use of specially designed permafrost surveys.

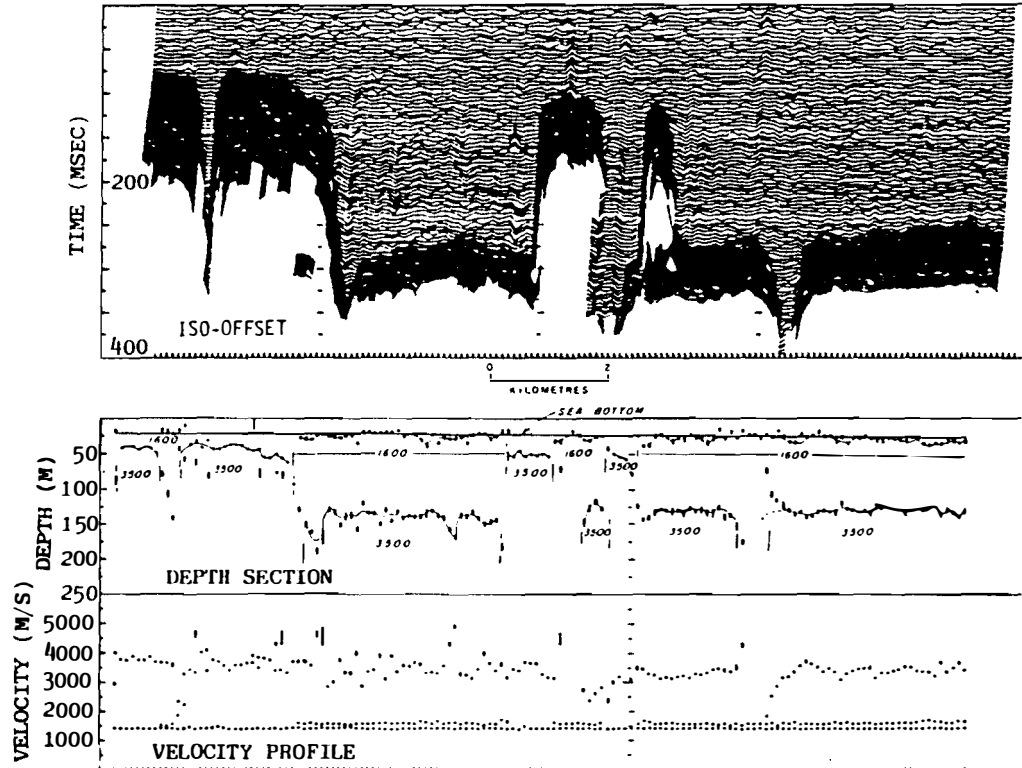


Fig. 1.19. Iso-offset section and velocity-depth section. The numbers shown beneath the depths are the corresponding approximate refractor velocities in m/s (from Morack et al. 1983).

b) Reflection

Seismic reflection profiling may give a continuous coverage of the depth to the ice-bonded permafrost. However, without velocity information from refraction data, acoustically defined permafrost (APF) must be confirmed by ties to boreholes. Three types of shallow acoustic permafrost have been identified using high resolution reflection data correlated with borehole information (Blasco 1984) (Fig.1.20):

Hummocky APF - is recognized by strong amplitude anomalies which exhibit a characteristic hummocky shape on the seismic sections. These "bright spots" always show normal polarity, and are commonly associated with diffractions, or more often half diffractions, at

their ends. The hummocks may occur as sporadic "islands" or in close proximity to one another, and vary from a few tens of metres to several kilometres in extension. Each may be surrounded by zones of no apparent permafrost. The smaller APF "islands" are believed to be limited in thickness, but the larger ones may be connected to deeper, thicker ice-bonded permafrost at depth.

Stratigraphically controlled APF - the occurrence of ice is controlled by the bedding. In many cases the APF reflector appears to be coincident with a change in lithology from a fine-grained soil above the reflector, to a coarser grained soil below. In some cases the actual permafrost boundary may lie above the reflector in the fine-grained material, but the degree of ice-bonding was either insufficient, or occurred too gradually to be detected using the reflection seismic techniques. Lateral lithological changes may enhance or reduce the impedance contrast, and the reflector may disappear or increase in strength along the line.

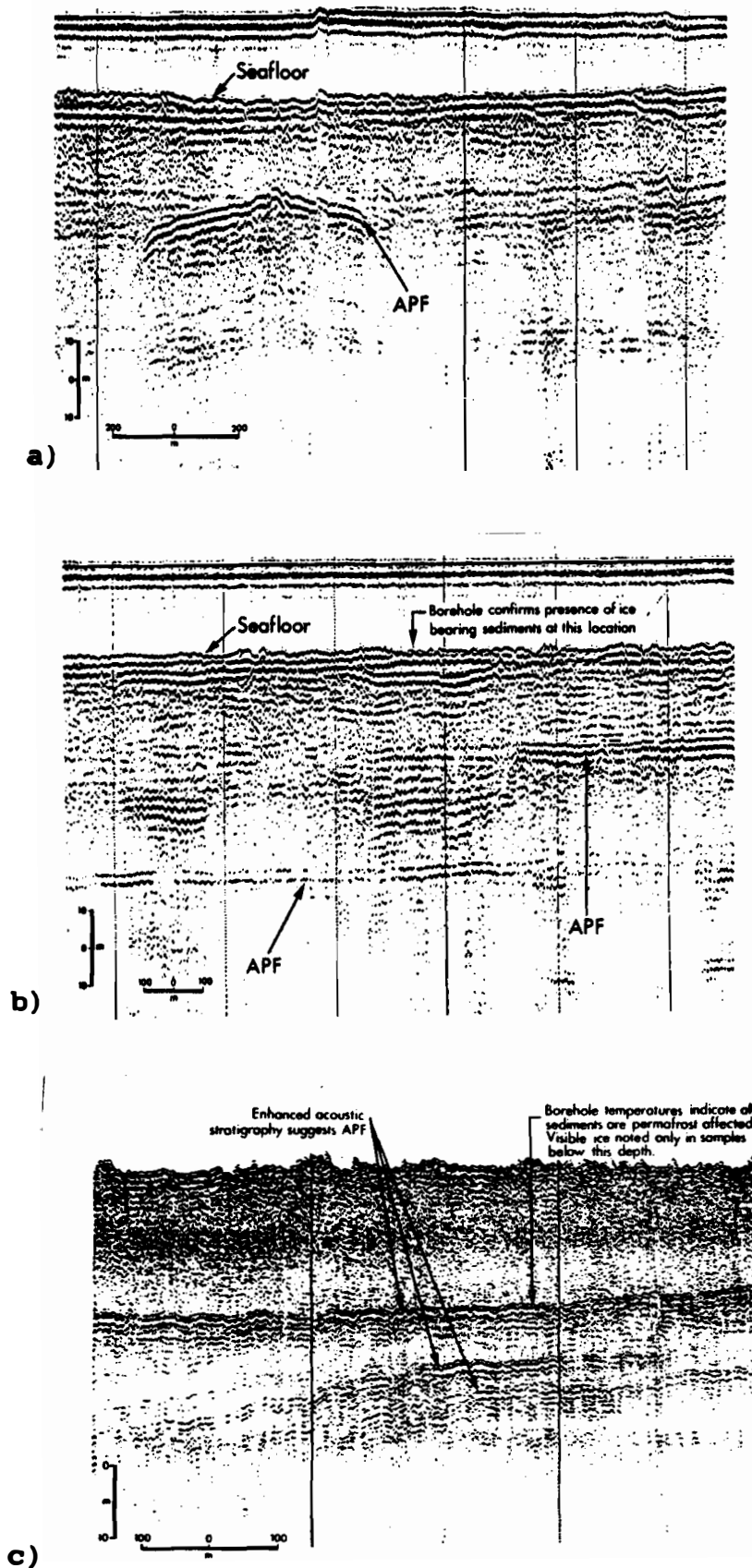


Fig. 1.20. Different types of acoustically defined permafrost (APF):

a) Hummocky APF.

b) Stratigraphically controlled APF.

c) Typical seismic signature where shallow sediments are marginally or partially ice-bonded.

(from Blasco 1984).

Marginally ice-bonded APF - is associated with the coarser fraction of fine grained sedimentary sequences. The distribution of ice within the sediments is so limited spatially and volumetrically that regional mapping of discrete horizons is difficult.

1.6.2 Electrical methods

Because of the different electrical properties of ice-bonded and unfrozen sediments, electrical methods can be used to detect submarine permafrost layers. The vertical distribution of resistivity in the earth may be measured directly by lowering an appropriate instrument into a borehole, or indirectly by means of measurements taken at or above the earth's surface. To make measurements from the surface, an electrical current must be forced to flow through the earth. This can be done by means of two different techniques: 1) galvanic methods or 2) electromagnetic induction.

The galvanic measurements, in which a steady current is injected directly into the earth through two or more electrodes, are capable of determining the depth below the sea-floor, as well as the thickness, of a permafrost layer (Corwin 1983). This is in contrast to the seismic refraction method, which only determines the top of the ice-bonded sediments. Furthermore, the method is applicable in acoustic anomaly areas, i.e. gassy sediments, where seismic data cannot be obtained, and in shallow water where air gun sources are not effective due to multiples. Thus, this method can be a useful supplement to seismic techniques for marine permafrost investigations. However, the method can only provide spot soundings, and no continuous registration can be obtained. Furthermore, it is only applicable in shallow waters. The method is also used for identification of the ice content in the sediments. For further information about the operating principles of the method, together with a case study from Prudhoe Bay, Alaska, see Corwin (1983).

Electromagnetic induction has been widely used for mapping onshore permafrost (Sartorelli & French 1982), but few reports exist from the low resistivity marine environment. Ehrenband et al. (1983) made measurements from the sea-ice in Prudhoe Bay, and were able to map the top and bottom of deep (200-500 m) subsea permafrost in water depths exceeding 200 m. However, their instrumentation involved a 500 m x 500 m square transmitter loop and was operated from the sea ice, and the method is not convenient to use from ships at the present stage.

Furthermore, the method provides poor lateral resolution due to the spot sounding principle (500m or more apart) (Blasco pers. comm. 1988).

1.6.3 Well log evaluation

Ice and gas hydrates possess similar physical and electrical properties, resulting in similar responses in conventional electrical, sonic and nuclear logs (Davidson et al. 1978). In chapter 1.3.2 the ability of the different logs to distinguish ice-bearing permafrost from gas hydrates is discussed. The following is a short description of well-log responses within and below the ice-bearing permafrost (Fig. 1.21) (Collett et al. 1988):

a) Resistivity log

The method provides a good tool because ice exhibits relatively high electrical resistivity compared to water, 200m and 3 m, respectively. The base of the ice-bearing permafrost is commonly marked by a substantial drop in resistivity.

b) Sonic log

Ice is characterized by higher acoustic velocities than water. However, the method has restricted value due to the limited zone of penetration. In addition, the method requires a good coupling between the side-wall and the recording tool, a situation which is normally not met (S.Blasco pers. comm. 1988).

c) Caliper log

The caliper log commonly indicates an enlarged borehole within the permafrost horizon, which can be attributed to caving associated with thawing. The method is particularly good if sand is present.

d) Spontaneous potential

The SP log generally shows a drift from negative in ice-bearing permafrost to positive below the base, attributed to an increased concentration of salt. In general, the method is a weak tool, and is most useful when significant salinity changes are involved (S.Blasco 1988).

e) Drilling rate

The base of the ice-bearing permafrost is often marked by an increased drilling rate.

f) Density log

The density log shows lower density values for ice compared to water. However, density changes are hard to detect unless high ice content is present.

g) Neutron porosity log

The neutron porosity log often indicates small to no reduction in apparent porosity below the base of ice-bearing permafrost.

h) Gamma log

The gamma ray log shows a small deflection from lower to higher values at the base of ice-bearing permafrost. This is apparent when the lithology is well defined.

i) Crystal cable log

The method provides good results. The detector spacing should be short, giving a sufficient resolution.

In general, the tool responses are clear if sediment types are well defined, e.g.; massive sand, fine clay. However, interbedded and mixed soil types will reduce the effect on the logs and make permafrost detection difficult. Due to the similar physical properties of gas hydrates and frozen sediments, the available logging tools do not permit an adequate differentiation, which should rather be based on temperature. The development of a "thermal conductivity log" is highly needed for this purpose (S.Blasco pers. comm. 1988).

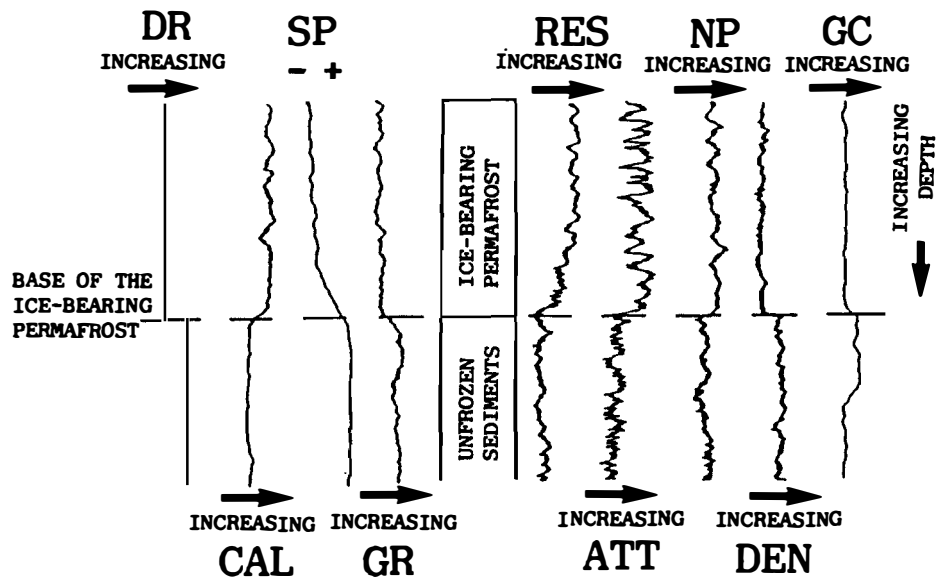


Fig. 1.21. Idealized log responses at the base of the ice-bearing permafrost assuming uniform sandstone lithology (from Collett et al. 1988).

2. PHYSICAL AND GEOLOGICAL SETTING OF THE WESTERN/NORTHERN BARENTS SEA

This chapter gives an introductory overview of the physical and geological conditions in parts of the Barents Sea. Besides a general introduction to the area, the purpose is to focus on conditions relevant for the occurrence of gas hydrates and submarine permafrost. Of particular interest is the Quaternary development of the area; the glaciation history, the extension of the ice caps, the temperature conditions at the base of the ice, and the isostatic rebound. Furthermore, the present day hydrographical setting, particularly the bottom-water temperatures, plays an important role with respect to the preservation of possible gas hydrates or subsea permafrost. Paragraph 2.1 deals with the conditions in the western/northern Barents Sea in general, while paragraph 2.2 focuses specifically on three selected study areas. Based on this chapter, an evaluation of the possibilities for the occurrence of gas hydrates and subsea permafrost in the Barents Sea will be discussed in chapter 3.

2.1 General overview

2.1.1. Physical setting

a) Physiography

The Barents Sea, which forms the largest present-day epicontinental sea (1.2 mill. km²), is bounded by the Scandinavian peninsula to the south, the Svalbard archipelago to the west, and Frans Josef Land and Novaya Zemlya to the east.

The sea floor morphology in the western Barents Sea is an expression of the underlying geology, characterized by parallel, broad trough-structures (Storfjordrenna, Bjørnøyrenna and Frans Viktoriarenn) running northeast-southwest, and shallow banks (Spitsbergenbanken, Sentralbanken and Storbanken) (Fig.2.1). Basins are rarely deeper than 300 m, and the banks are typically 50-150 m deep. The average water depth is 230 m, which is significantly deeper than most of the present day high Arctic shallow (10-100 m) shelves outside North America and the USSR.

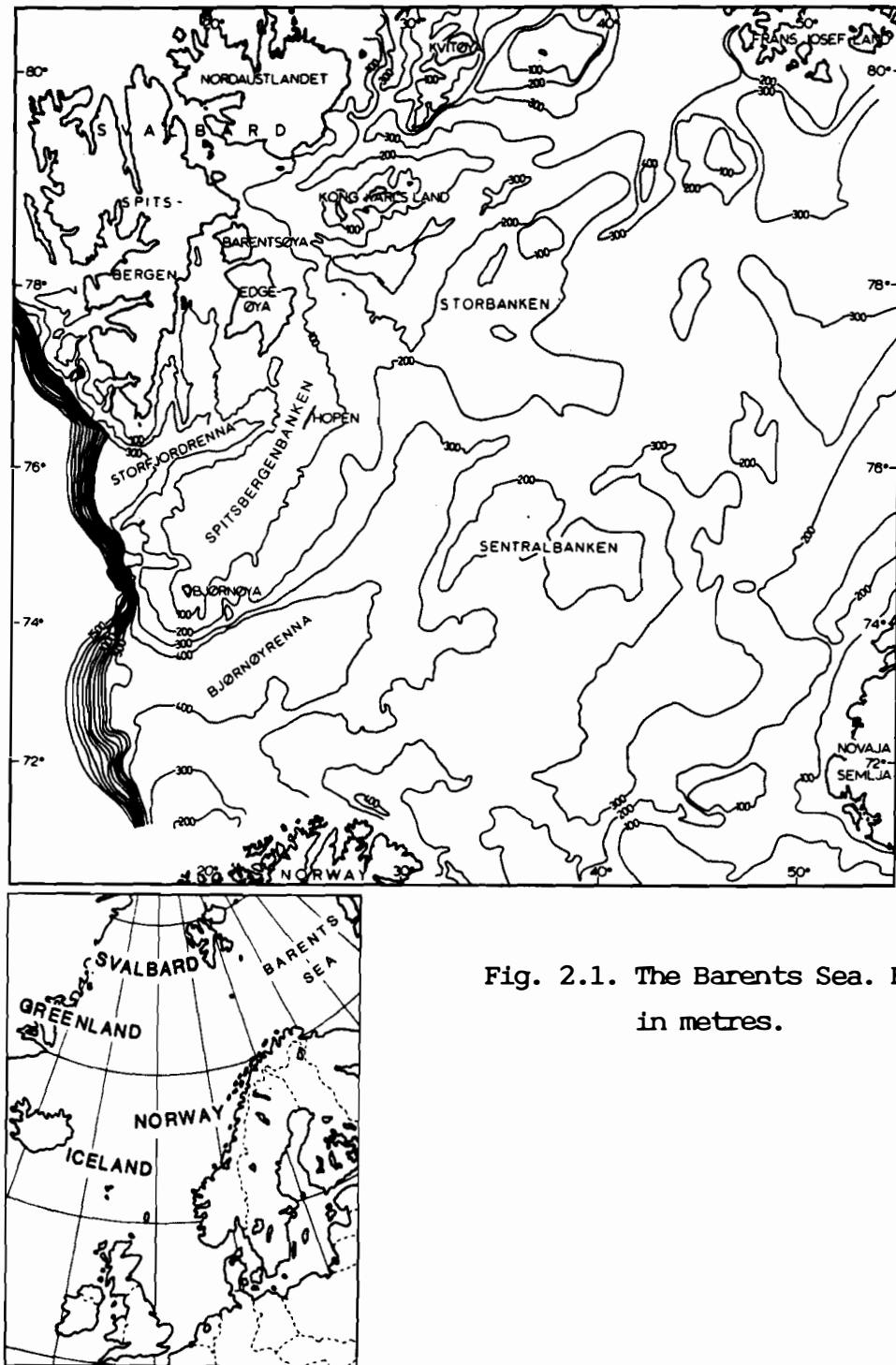


Fig. 2.1. The Barents Sea. Bathymetry in metres.

b) Hydrography

The Barents Sea is influenced by two different types of water masses: Atlantic Water and Arctic Water. Atlantic Water is defined by $T > 0^{\circ}\text{C}$ and $S > 34.7^{\circ}/_{00}$, and Arctic Water by $T < -1^{\circ}\text{C}$ and $S = 34.2 - 34.5^{\circ}/_{00}$ (Pfirman 1985).

Atlantic Water enters the area from the south, and splits up in two currents off the coast of northern Norway (Fig.2.2). One branch flows northward along the west coast of Svalbard as the West Spitsbergen Current, while another part continues into the Barents Sea as the North Cape Current. At about 30°E , the North Cape Current splits into three major routes. One arm turns northwards between Hopen and Storbanken where it submerges under the lighter Arctic Water. The second branch continues eastwards in the deeper area between Storbanken and Sentralbanken. The third part turns south of Sentralbanken, continuing into the Novaya Zemlya Current (Fig.2.2).

The West Spitsbergen Current mainly follows the shelf break, sometimes entering the shelf proper. The inner shelf water may not be classified as Atlantic Water. However, the temperature is well above the freezing point; $+1$ to $+3^{\circ}\text{C}$ (Gammelsrød & Rudels 1983). Sub zero temperatures have been recorded in Raudfjorden and in Van Mijenfjorden (Schei et al. 1979; Gammelsrød & Rudels 1983). Atlantic Water also enters the Barents Sea from the north by the West Spitsbergen Current, continuing eastward along the northern coast of Spitsbergen and southward into the area between Nordaustlandet and Frans Josef Land.

Cold Arctic Water is transported into the Barents Sea by the East Spitsbergen and Persey Currents west and south of Frans Josef Land (Fig.2.2). The Persey Current splits north of Sentralbanken. One branch turns southwards to Sentralbanken, but this part is probably small. The main branch flows southwestwards along the eastern slope of Spitsbergenbanken as the Bjørnøya Current. This current turns around Bjørnøya and flows northeastwards around Storfjordrenna (Midttun & Loeng 1987) (Fig.2.2).

The boundary between the cold Arctic Water and warm Atlantic Water to the south is a strong temperature gradient known as the Oceanic Polar Front (Fig.2.2). In the area west of Sentralbanken, the Polar Front is distinct and follows the bathymetry. The surface expression is located above the 100 m isobath north of Bjørnøya (Johannessen & Foster 1978). In the eastern Barents Sea the front area is less distinct, and a mixed water mass covers great areas (Midttun & Loeng 1987).

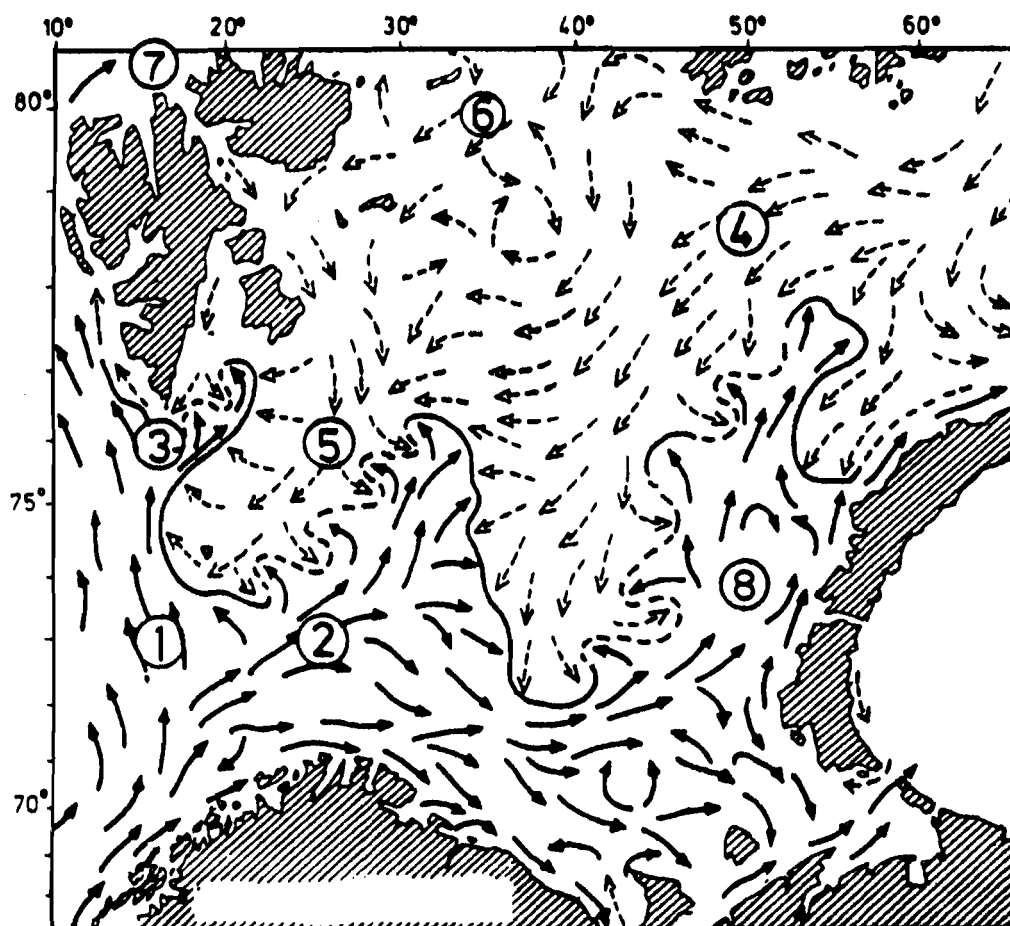


Fig. 2.2. General circulation map. Solid arrows denote warm water, broken arrows denote cold water. Heavy lines indicate the Oceanic Polar Front. From Pfirman (1985). (Data from Tantsiura 1959.)

Labelled currents are:

- | | |
|-----------------------------|----------------------------|
| 1. West Spitsbergen Current | 5. Hopen-Bjørnøya Current |
| 2. North Cape Current | 6. East Spitsberg Current |
| 3. South Cape Current | 7. Arctic Atlantic Current |
| 4. Persey Current | 8. Novaya Zemlya Current |

In the southern Barents Sea the Atlantic Water fills the entire water column, whereas north of the Polar Front the water masses are stratified. Figure 2.3 shows a profile from a station east of Kong Karls Land, and the following stratification of the water column is apparent (Pfirman 1985):

- Surface Water forms during the summer as sea ice melts and

retreats. The layer normally extends to a depth of 20-30 m, but may extend down to 50 m on shallow banks. The Surface Water is bounded downwards by a strong pycnocline (Fig.2.3). Temperature and salinity of the Surface Water generally decrease northwards, from 5 °C and 34.0‰ at 75°N to less than -1 °C and 32.0‰ near Kong Karls Land.

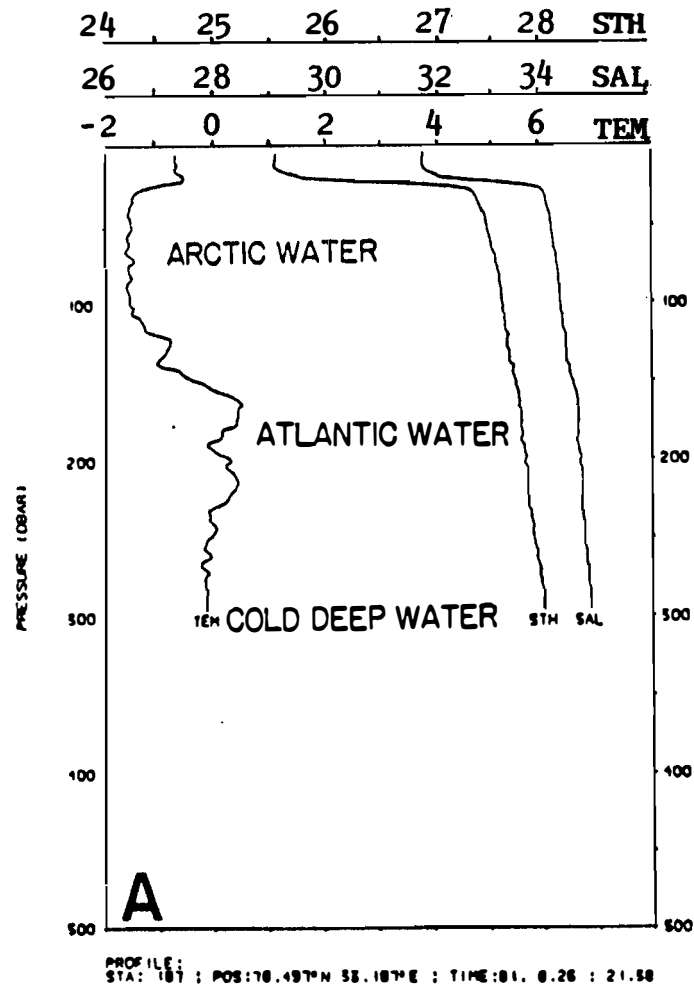


Fig. 2.3. Hydrographic station cast showing typical Barents Sea water masses north of the Polar Front. From Pfirman (1985).

- Arctic Water is defined by $T < -1$ °C and $S < 34.5$ ‰, and is located beneath the surface layer. Minimum temperatures typically occur near 75 m water depth, but can vary between 20-150 m. These cold water masses probably originate from a deep convection layer developed during sea-ice formation at the sea surface in the Arctic Ocean, the Barents Sea, and the Kara Sea (Eilertson et al. 1981).

- Atlantic Water is defined by $T > 0$ °C and $S > 34.7$ ‰, and usually identified as a temperature maximum at a depth of 200-250 m (Fig.2.3). The temperature decreases northward, and maximum values for the northern Atlantic Water are 1.0 - 1.5 °C. Atlantic Water is present in Storfjordrenna and the deep basins. In large areas of the northern Barents Sea these water masses do not occur.

- Cold Deep Water has temperatures lower than 0°C and salinities higher than $34.7^{\circ}/_{\text{oo}}$. The cold water mass may form by cooling of Atlantic Water near shallow banks (Loeng 1980), or may be due to modification of Arctic Water by brine rejection during sea-ice formation (Midttun 1985). The Cold Deep Water is the densest water mass in the Barents Sea (Fig.2.3), and has a limited distribution. It occurs beneath Atlantic Water west of Sentralbanken and Storbanken.

The winter and summer situations differ most clearly in the vertical structure of the water masses. During summer, warm Surface Water is formed by ice melting and usually reaches down to 15 m. However, on shallow banks such as Spitsbergenbanken, the melt layer and the Arctic Water mix, and the whole water column may be warmed up to temperatures as high as 3°C (Loeng & Skjoldal 1987). During autumn, the surface water is cooled, and stable temperature and salinity conditions are established on the banks. The temperatures will be just above freezing point, i.e. -1.5 to -1.8°C . In the deeper areas, the water masses may be homogeneous down to 200 m (Midttun & Loeng 1987).

In conclusion, the bottom water temperatures in the northern and central Barents Sea are characterized by sub zero conditions except for limited areas. Figure 2.4 shows the summer temperatures of the bottom water. Warm water covers the whole of Spitsbergenbanken. This condition lasts for approximately two months; throughout the rest of the year the bank is covered by sub zero water. On the eastern slope of Spitsbergenbanken, the cold southerly flowing Bjørnøya Current keeps the temperatures below -1°C . On Sentralbanken, Storbanken and south of Kvitøya, the bottom water temperature is less than -1°C , while Atlantic Water in the areas between generally has temperatures higher than 0°C (Fig.2.4). In Bjørnøyrenna, south of the map, the bottom water temperature is more or less constant around 2°C .

During the Holocene, the water depth has changed, mainly due to isostatic rebound. In the early Holocene (8-9000 BP), the water depth in the central Barents Sea may have been 100 m deeper than at present. The Polar Front is strongly confined by the bathymetry. Accordingly, the distribution of the water masses may have varied considerably. The apparently deeper early Holocene Barents Sea may have experienced intrusion of Atlantic Water over the entire area

c) Sea ice conditions

Sea ice covers large parts of the Barents Sea most of the year. The

interannual variation of the sea ice extension is very large (Fig.2.5). The outer ice edge in winter usually follows the Oceanic Polar Front with maximum ice extension (about 73 - 75°N) occurring in March-April. During the melt season, the ice edge usually retreats as far north as 79°N. The recession of the ice front occurs mainly between June and July. The minimum ice extension occurs in August - September (Loeng 1979; Vinje 1985).

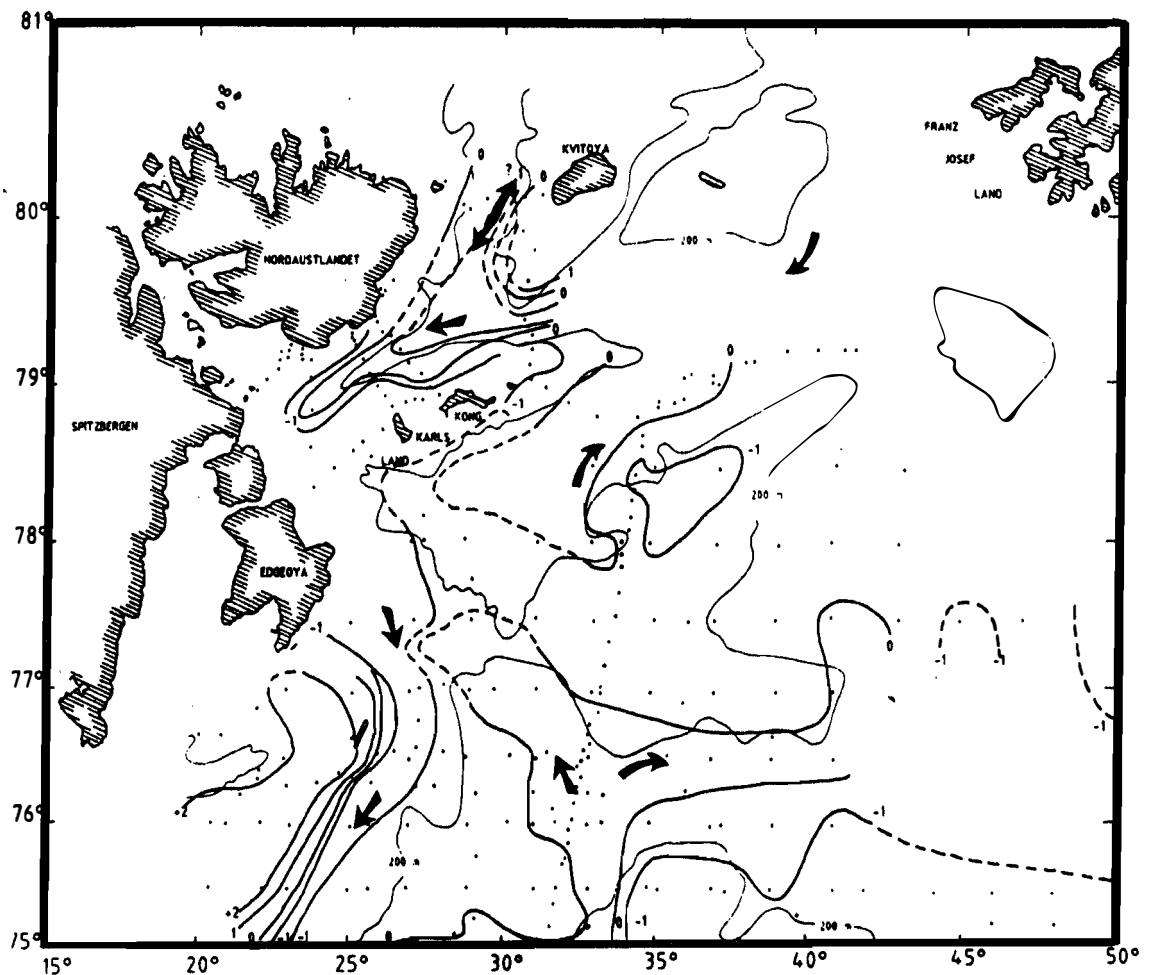


Fig. 2.4. Schematic bottom water circulation pattern and bottom water temperature in the Barents Sea (measured during summer).
From Elverhøi et al. (1989)

The greater part of the ice in the Barents sea is formed locally, while multiyear ice from the Arctic Ocean may pass through the straits east of Svalbard for shorter periods. The ice drift pattern is generally towards the south, and wind is the dominant driving force (Vinje 1985). In the southern part, between Bjørnøya and Hopen, the ice thickness is generally about 40 - 150 cm. At the latitude of Kvitøya it is estimated to average 165 cm at the end of the freezing season (Vinje 1985).

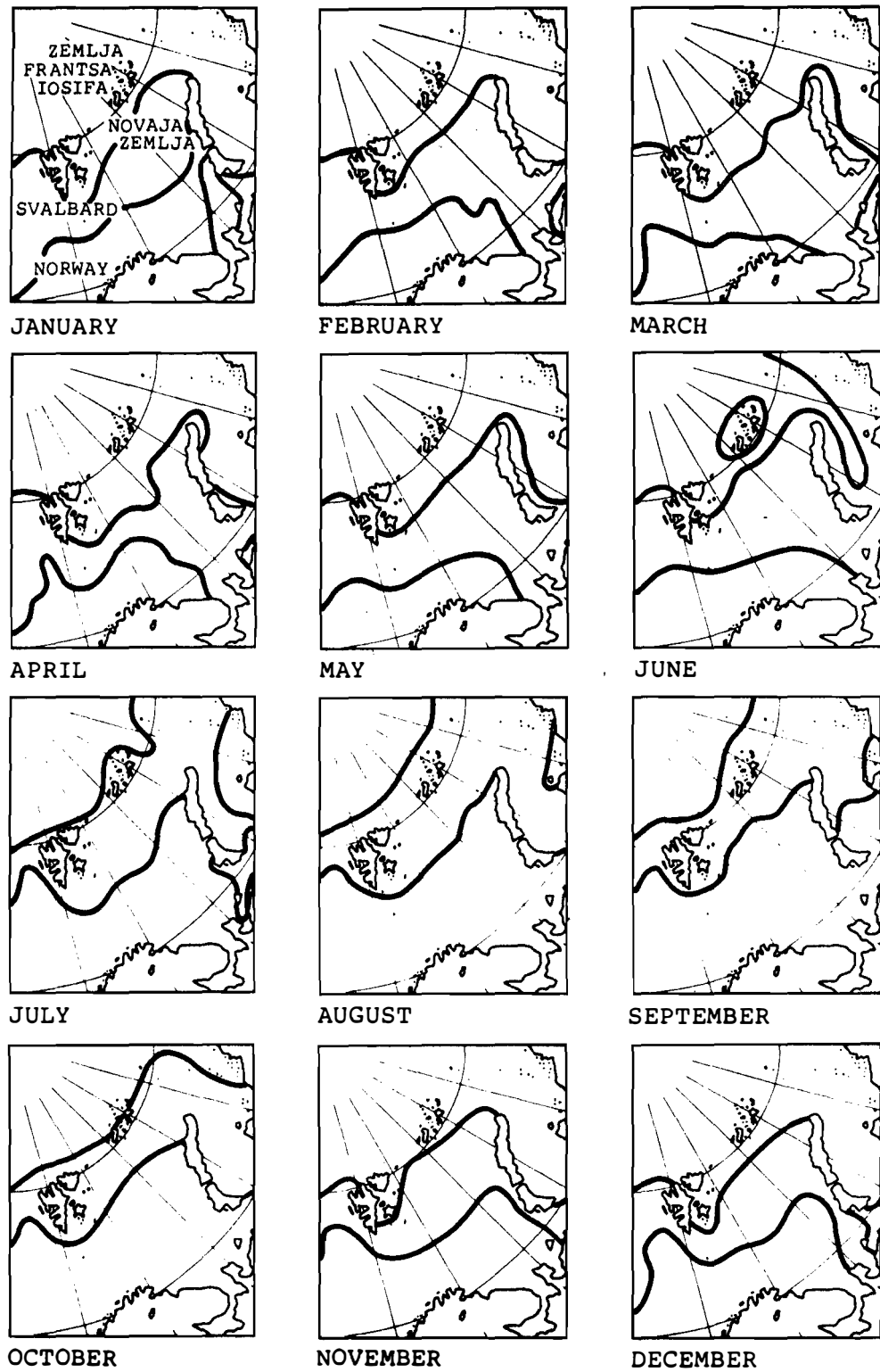


Fig. 2.5. Maximum and minimum extension of sea ice in the Barents Sea.
From Vinje (1985).

2.1.2 Geological setting

a) Pre-Quaternary history

The pre-Quaternary of the Barents Sea can be summarized as follows (Faleide et al. 1984; Rønnevik & Jacobsen 1984; Gabrielsen et al. 1984; Gabrielsen et al. in prep.):

- The Caledonides, most likely constituting the metamorphic basement in the southwestern parts of the Barents Sea and in Svalbard (Faleide et al. 1984; Steel & Worsley 1984), were consolidated during the Late Silurian to Early Devonian Caledonian Orogeny. In the central and northern Barents Sea the basement is suggested to be of Baikalian age, although the platform probably was partly reactivated during the Caledonian Orogeny (Ulmishek 1985). Aeromagnetic studies undertaken by the Geological Survey of Norway (NGU) and deep seismic studies by (IKU) suggest that the basement of the central and southwestern Barents Sea is constituted by the "Norwegian branch" of the Caledonian orogen, and the basement of Spitsbergen and the northwestern parts of the Barents Sea are constituted by another "Svalbard branch" of the orogen.
- The Late Devonian to Early Carboniferous was characterized by graben formation and large sedimentation rates within the basin. The subsidence of the basins terminated in the middle Carboniferous, and thick evaporites were then deposited in some of them (e.g. Nordkapp and Tromsø Basins).
- In middle Carboniferous to Late Permian, the Barents Sea was a platform area with deposition of carbonates and evaporites. Basin margins were situated to the west and south.
- In the Late Permian, clastic input from the basin margins increased. Approximately at the Permian-Triassic boundary, regional carbonate deposition terminated.
- During the Triassic and Early Jurassic, thick clastic shelf sequences were deposited during tectonic quiet conditions.
- In the Mid Jurassic to Early Cretaceous, the area was affected by several tectonic phases which caused the area to be broken up into different tectonic blocks, mainly by reactivation of older lineaments. Lower Cretaceous sequences of great thickness were

deposited in the rapidly subsiding basins to the west.

- In the Late Cretaceous, tectonic activity at the western margin of the Barents Sea caused local compression and uplift, and condensed sequences were deposited in most of the Barents Sea. Thick Upper Cretaceous sequences are found only in local subsiding basins at the western margin.
- In the Palaeogene, most of the area subsided, while tectonic activity along the western margin caused uplift of the northwestern area between Bjørnøya and Spitsbergen. The compressional deformation affecting the northern platform areas probably took place at this time (Eocene-Oligocene?), and therefore it is possible that these areas were uplifted relatively to the platform south of 75°N.
- In the Neogene, the Barents Sea shelf was strongly eroded, and the erosional products were deposited in large fans along the western and northern margin of the Barents Sea.

b) Bedrock geology

The knowledge of the bedrock geology in the northern Barents Sea is generally poor. Current information is essentially based on geophysical investigations combined with correlations to the adjacent islands and exploratory wells in the southern Barents Sea (Rønnevik et al. 1982; Faleide et al. 1984). In the area north of 74°N and west of 35°E, Elverhøi et al. (1988) presented a revised subcrop map (Fig.2.6) based on single channel sparker profiles, in combination with data from the Late Quaternary unlithified sediments, which are suggested to be of semilocal origin. From the area east of 35°E, only few reflection seismic lines have been published so far, and the geological interpretation of these areas is largely based on extension of the onshore geology combined with seismic refraction measurements (Murzin et al. 1984; Verba 1984; Ulmishek 1985).

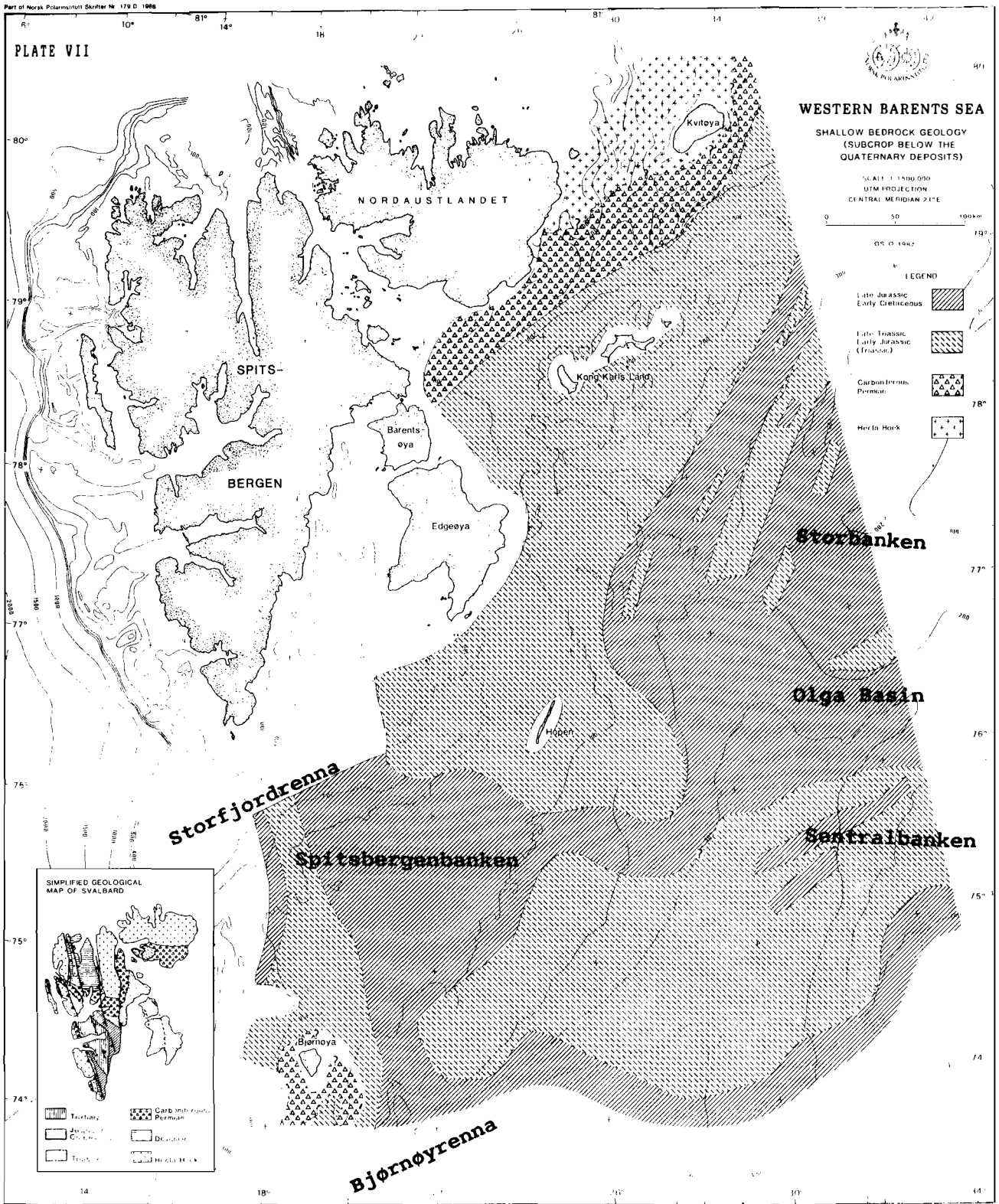


Fig. 2.6. Shallow bedrock geology. Subcrop below the Quaternary deposits. From Elverhøi et al. (1988).

The main elements of the shallow bedrock geology of the western Barents Sea north of 74° N are (Fig.2.6)(Elverhøi et al. 1988):

Pre-Devonian Hecla Hoek rocks subcrop between Kvitøya and Nordaustlandet. South of this area, carbonates of Carboniferous - Permian age are localized in an east-northeast striking zone. Permian sediments are also found south and southeast of Bjørnøya (Fig.2.6).

In the rest of the study area (north of 74° N and east of Knølegga Fault), Mesozoic rocks of various age subcrop. Samples of Early Triassic age were not recovered, a fact attributed to 1) no or very limited exposure, or 2) the combination of fine-grained composition and glacial comminution may cause under-representation of Lower Triassic clasts in the Quaternary sediments. Recent investigations in the central Barents Sea seem to support explanation 1 (Antonsen et al. in prep.).

The Upper Triassic - Lower Jurassic rocks show a wide distribution. South of the Permo - Carboniferous outcrop in the Northern Barents Sea, a southwest-northeast trending area with Upper Triassic - Lower Jurassic rocks extends to south of Hopen (Fig.2.6). To the south, the Sentralbanken High has mainly Triassic rocks, except for scattered Jurassic samples, coinciding with synforms. A minor window of Upper Triassic - Lower Jurassic rocks is also present on the southern part of Storbanken, and in areas north and southeast of Bjørnøya (Fig.2.6).

Upper Jurassic - Lower Cretaceous rocks are suggested to subcrop on the main part of the Storbanken High, and in a southwestern extension, indicating a connection with the Upper Mesozoic rocks in the Olga Basin. A continuous subcrop of Upper Mesozoic rocks across the inner part of Bjørnøyrenna is also indicated. Upper Jurassic - Lower Cretaceous rocks most likely subcrop in the Sørkapp Basin on central Spitsbergenbanken, in a southern corridor east of Bjørnøya, and in a narrow corridor west of 18° E (Fig.2.6).

On the basis of shallow seismic profiling, the northwestern Barents Sea is characterized by gently dipping or flat lying layers. However, northeast of Hopen a north-northeast - south-southwest trending, tectonically disturbed zone is present. The zone is characterized by antiforms/synforms, but faults have also been observed. Typical of this zone is a subcrop of Upper Jurassic-Lower Cretaceous rocks within the synforms, while Upper Triassic-Lower Jurassic rocks are found within the antiforms. The thickness of the Upper Jurassic-Lower Cretaceous sequence is estimated to less than 400 m, while in the Olga Basin (Fig.2.6), the thickness may exceed 1 km.

c) Sediments above bedrock

In the southwestern Barents Sea, the thickness of the Quaternary sediments is generally between 50 and 100 m, increasing to more than 200 m in depressions (Fig.2.7). North of 74°N the Quaternary cover is thinner, averaging < 15 m, with the exception of locally thicker accumulations fringing banks and in troughs. Larger sediment accumulations are present in the western part of the major troughs (Bjørnøyrenna and Storfjordrenna). Near the shelf edge in Bjørnøyrenna the thickness exceeds 500 m (Fig.2.7) (Solheim & Kristoffersen 1984). The boundary between the bedrock and the unlithified sediments is usually seen in the seismic profiles as a well-defined angular unconformity (Upper Regional Unconformity, URU). However, in areas of flat-lying bedrock layers the unconformity may be difficult to detect (Solheim & Kristoffersen 1984).

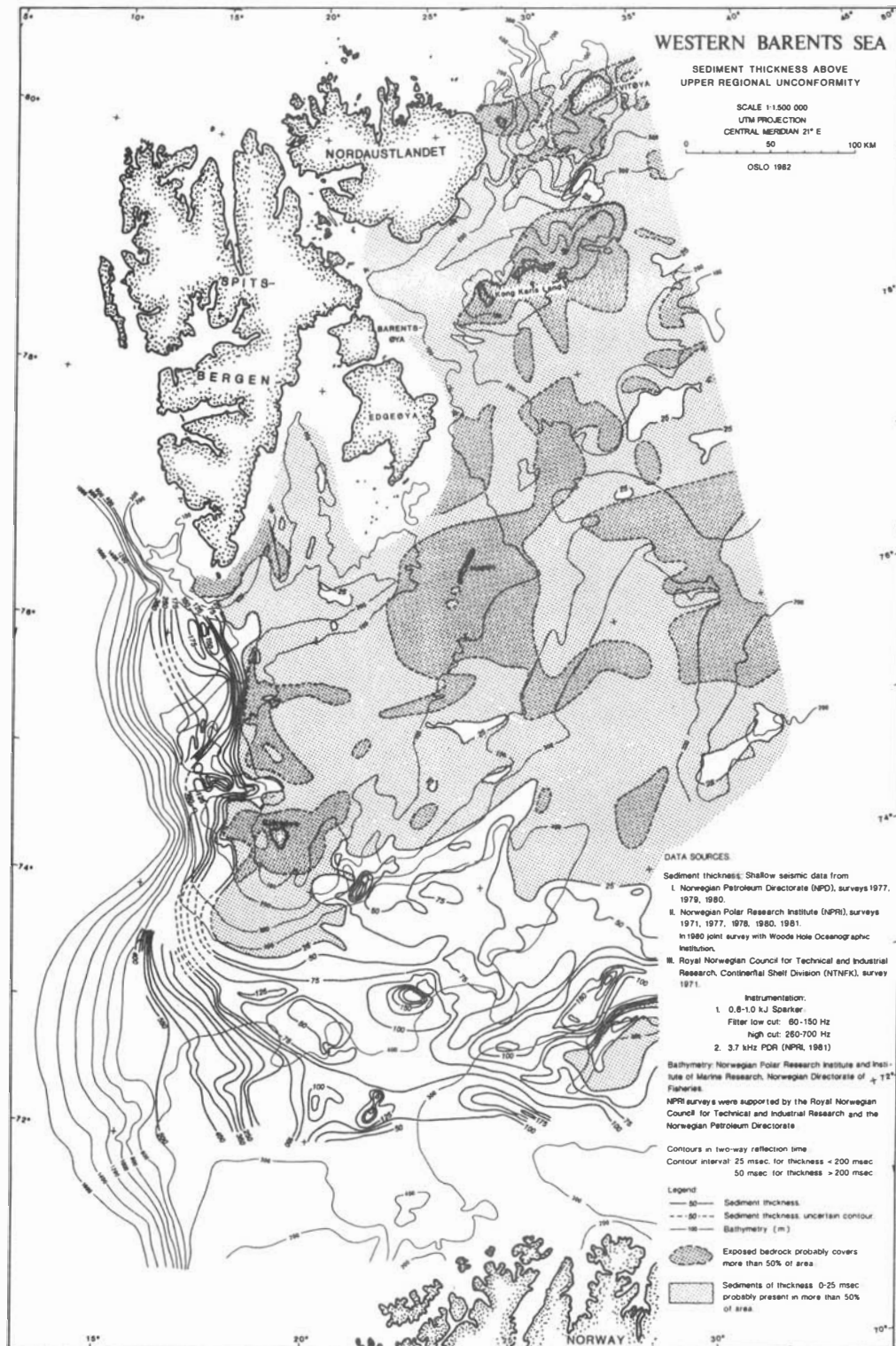


Fig. 2.7 Thickness of unconsolidated sediments. From Solheim & Kristoffersen (1984).

The sediment type and thickness can be summarized, from the bottom and upwards (Elverhøi & Solheim 1983)(Fig. 2.8):

A: Stiff, pebbly mud, interpreted as till and/or glaciomarine sediments overrun by a glacier. In areas with water depth less than 300 m, the thickness of the unit is in general less than 15 m.

B: Soft mud with pebbles, interpreted as Late Weichselian proximal glaciomarine deposits. In areas with water depth less than 300 m, the thickness is commonly less than 5 m. Otherwise, the thickness increases to 15 - 20 m.

C: Fine-grained, Holocene mud, with higher content of foraminifera and organic debris. This unit occurs in areas with water depth greater than 300 m, and the thickness is commonly less than 1.5 m. The Holocene mud is also present in shallower areas, particularly in depressions and as infill in iceberg ploughmarks.

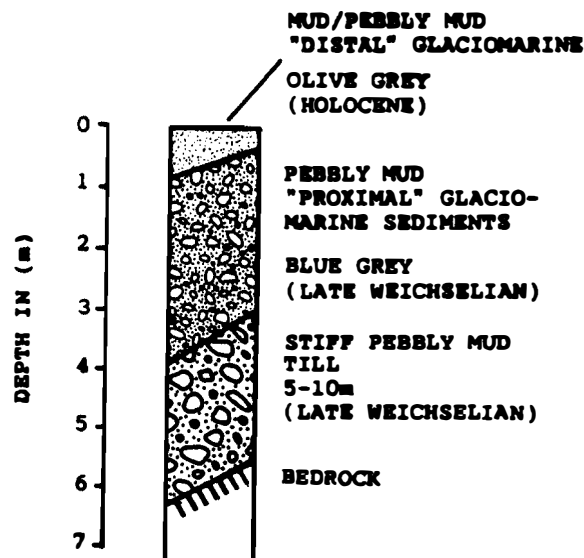


Fig.2.8. Sediment stratigraphy in the northern Barents Sea

d) Arctic silts

Sediments of the Arctic shelves in general contain a larger fraction of silt than their counterparts in more temperate regions of the world. The Arctic silts often overlie relict permafrost, and these sediments have a highly variable nature compared to other offshore deposits. The engineering properties of the Arctic silts are poorly

known. The combination of strong dilatancy and low permeability result in unusually high shear strength values for fast loading (Watt 1982). However, data now exist to conclude that typical undrained triaxial compression tests can overestimate the in situ undrained strength by 75% (Ladd et al. 1984). The behavior of the Arctic silts under cyclic loading (i.e. waves or earthquakes) is very poorly defined. Arctic silts in the Barents Sea have not been identified and their properties are completely unknown.

2.2 Selected study areas

The present project includes seismic interpretation from several areas in the Barents Sea. In this chapter, the geological/geophysical/physical properties in these areas are discussed, and presented in 3 transects. The purpose is to submit data relevant for an evaluation of possible occurrences of gas hydrates or subsea permafrost in the regions. The positions of the transects were chosen in accordance with the areas of seismic interpretation and acquisition presented in chapter 4; Bjørnøyrenna, Sentralbanken and Spitsbergenbanken south of Hopen, respectively (Fig.2.9). Transect 1 extends from the shallow area around Bjørnøya, southwards into Bjørnøyrenna to approximately 72°N. The Polar Front is located on the northern slope of Bjørnøyrenna (Fig.2.9). Transect 2 runs from the southern tip of Hopen, and southwards on Spitsbergenbanken, north of the Polar Front. Transect 3 extends towards the southeast from the southern tip of Hopen, crossing the northeastern part of Bjørnøyrenna, to Sentralbanken. The Polar Front is crossed twice, on both slopes of Bjørnøyrenna (Fig.2.9). Figure 2.10 shows the three transects plotted against depth. The values given for the various parameters are taken from several papers, and are briefly described as follows:

2.2.1 Physical setting

a) Air temperature

Mean temperature for the whole year, measured in the period 1951-80 (Steffensen 1982):

Bjørnøya: -2.1 °C.

Hopen: -6.1 °C.

b) Water temperature and salinity

Typical values for the water temperature are shown on the sections in figure 2.10, based on measurements done in approximately the same area (Eide 1983, Loeng 1983). Most of the observations are from the summer.

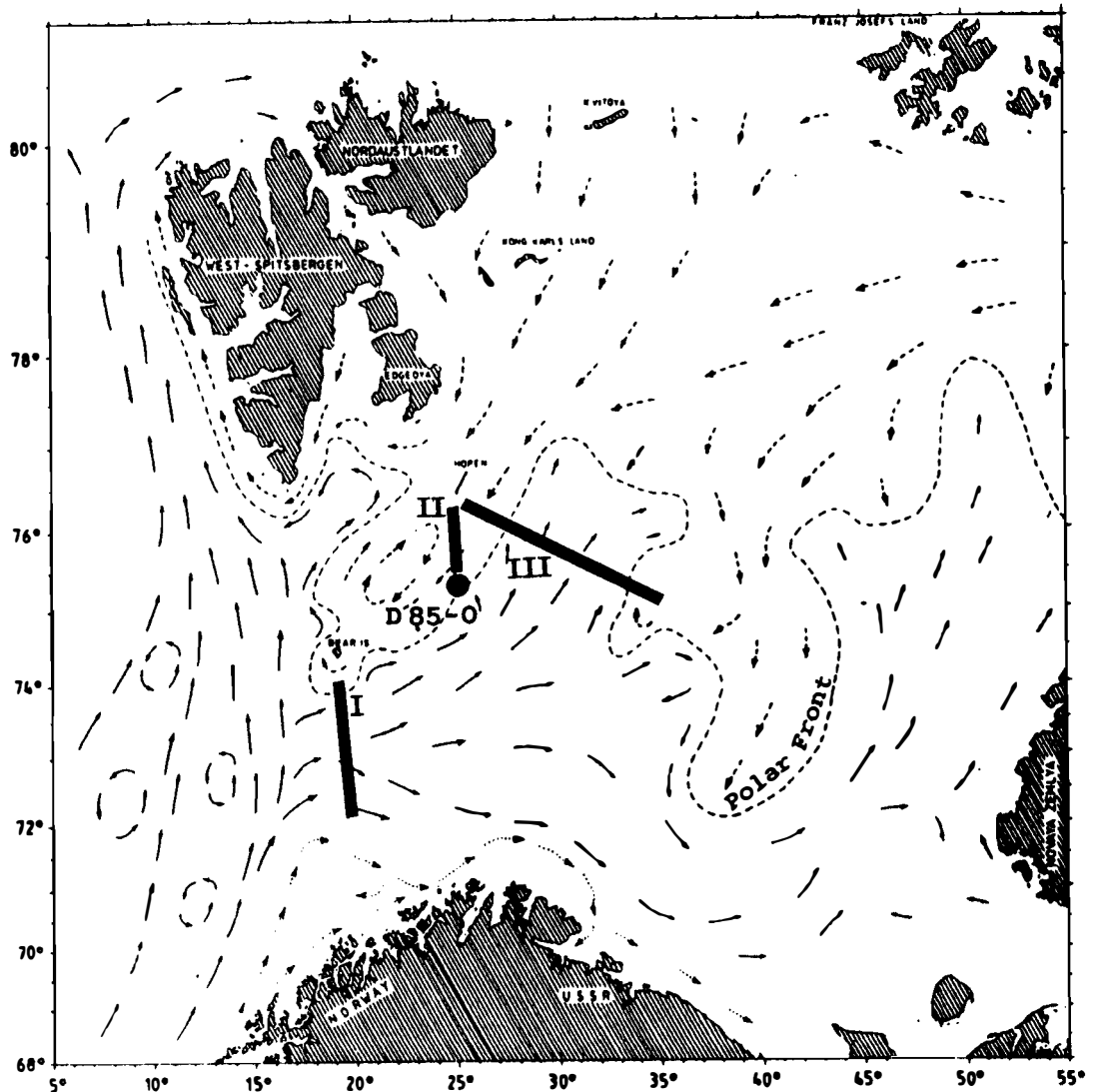


Fig. 2.9. Map showing location of the three transects presented in figure 2.10. ← - - Arctic Water ← — Atlantic Water.

In the Bjørnøya section (I), the Atlantic Water follows the southern slope of Bjørnøyrenna. Colder and fresher water is found on the bottom of the channel and on its northern flank. On Spitsbergenbanken a less saline and somewhat colder water mass is found. The section is based on mean values for observations made in August-September during the years 1966-1977 (Eide 1983). In winter the temperature of the bottom-water at Spitsbergenbanken may approach the freezing point, -1.5°C to -1.8°C (Loeng 1983). Transect II is based on a section showing the temperature and salinity over the slope of Spitsbergenbanken in the middle of the summer (Eide 1983). A shallow

(15 - 30m) layer of meltwater has formed, with temperatures $>0^{\circ}\text{C}$. Below this layer is a vertically well mixed layer with a temperature around -1.5°C .

Measurements on Spitsbergenbanken by the end of the winter show very cold (-1.5°C) water with salinities up to 3.49 ‰ throughout the whole water column. On both sides of the bank, there is warmer and more saline Atlantic Water. Spitsbergenbanken is usually ice covered in the winter, and rejection of salt from the ice increases the salinity of the bank water (Eide 1983). Section III is based on sections from Eide (1983) and Skjoldal (pers. comm. 1988) measured in August-September. The Atlantic Water is completely split at Sentralbanken, and temperatures below -1°C are found. In Hopen-djupet, the minimum temperatures are around 0°C .

c) Water depth

The water depth in the study area varies from 50 m to more than 400 m (Fig. 2.10). The water depth in the rest of the Barents Sea is shown in figure 2.1.

2.2.2 Sediments above Upper Regional Unconformity

a) Thickness

The thickness of the Quaternary sediments in the study area is plotted on the sections in figure 2.10, based on the map by Solheim & Kristoffersen (1984) (Fig.2.7). In the area around both Bjørnøya and Hopen, and in parts of Sentralbanken, they found exposed bedrock to cover probably more than 50% of area. However, newer 3.5 kHz data show most of this region to be covered by a thin veneer (1-5 msec twt) of soft sediments, not resolvable by lower frequency seismic data. To the south and in the area between Hopen and Sentralbanken, somewhat thicker sediments (up to 25 msec twt) are probably present in more than 50% of the area. In central parts of Bjørnøyrenna, the thickness locally exceeds 150 msec twt, increasing westward to more than 500 msec twt near the shelf edge (Solheim & Kristoffersen 1984) (Fig. 2.7).

b) Composition

The type and composition of the unconsolidated sediments are described in section 2.1.2c).

BJØRNØYA

SECTION 1

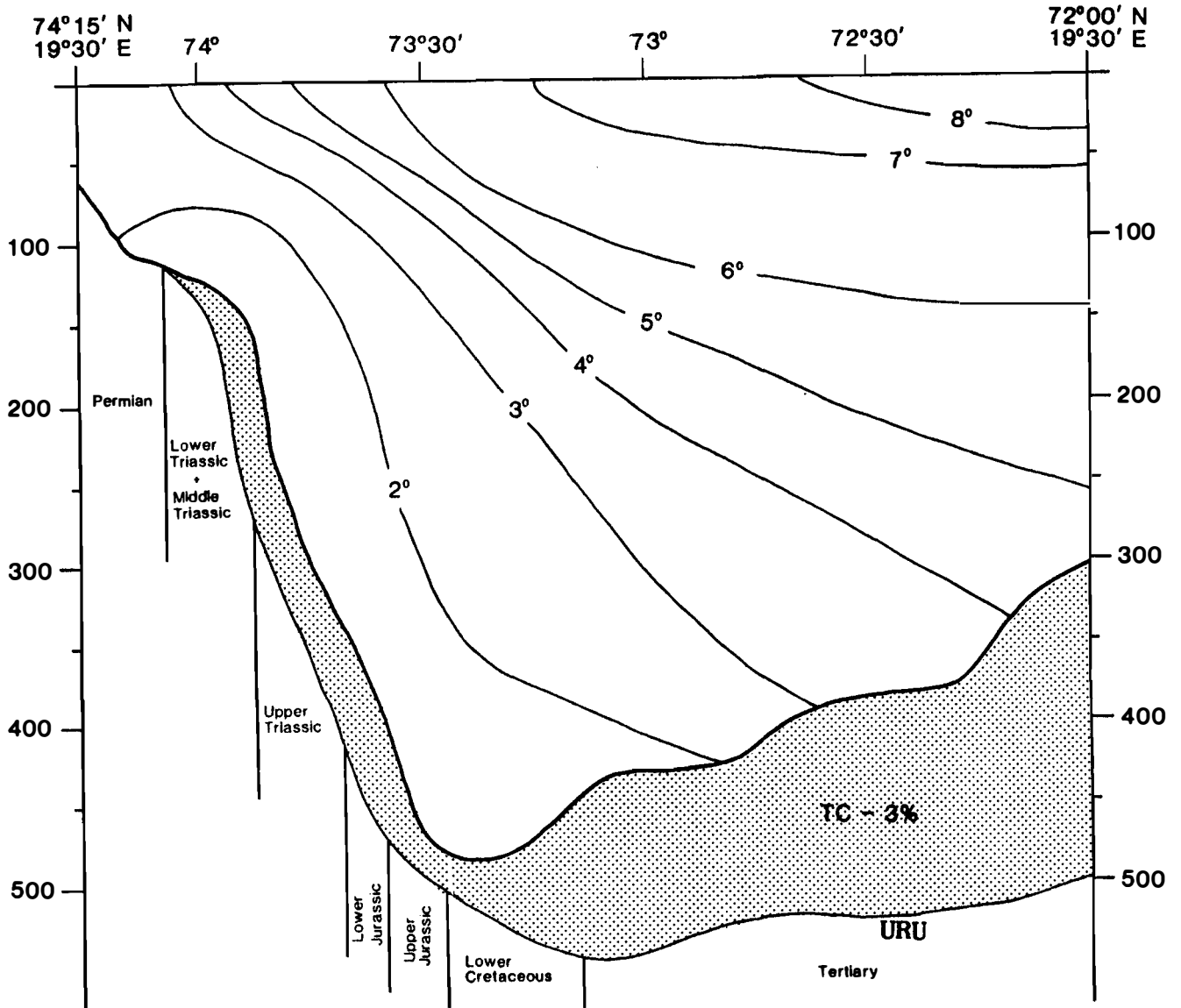
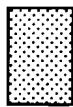


Fig. 2.10. a) Section 1. Mean values of water temperatures measured in August-September. URU marks the upper regional unconformity. Based on Eide (1983).



Quaternary sediments

c) Total organic carbon (TOC) and total carbon (TC) content.

The total carbon (TC) values in the unconsolidated sediments generally varies from 1 to 3 %. In the Holocene sediments, TC is greatest for the clay-sized fraction, with the content decreasing with increasing grainsize. The Late Weichselian deposits all have about the same total carbon content, which is usually lower than that in the Holocene sediments above (Forsberg 1983). TOC values are slightly

lower, up to 1-2%, indicating that the main carbon content is of organic origin (Elverhøi et al. 1988). Palynologic investigations demonstrate that the organic matter is mainly reworked from Mesozoic rocks (Trondsen & Bjærke 1983).

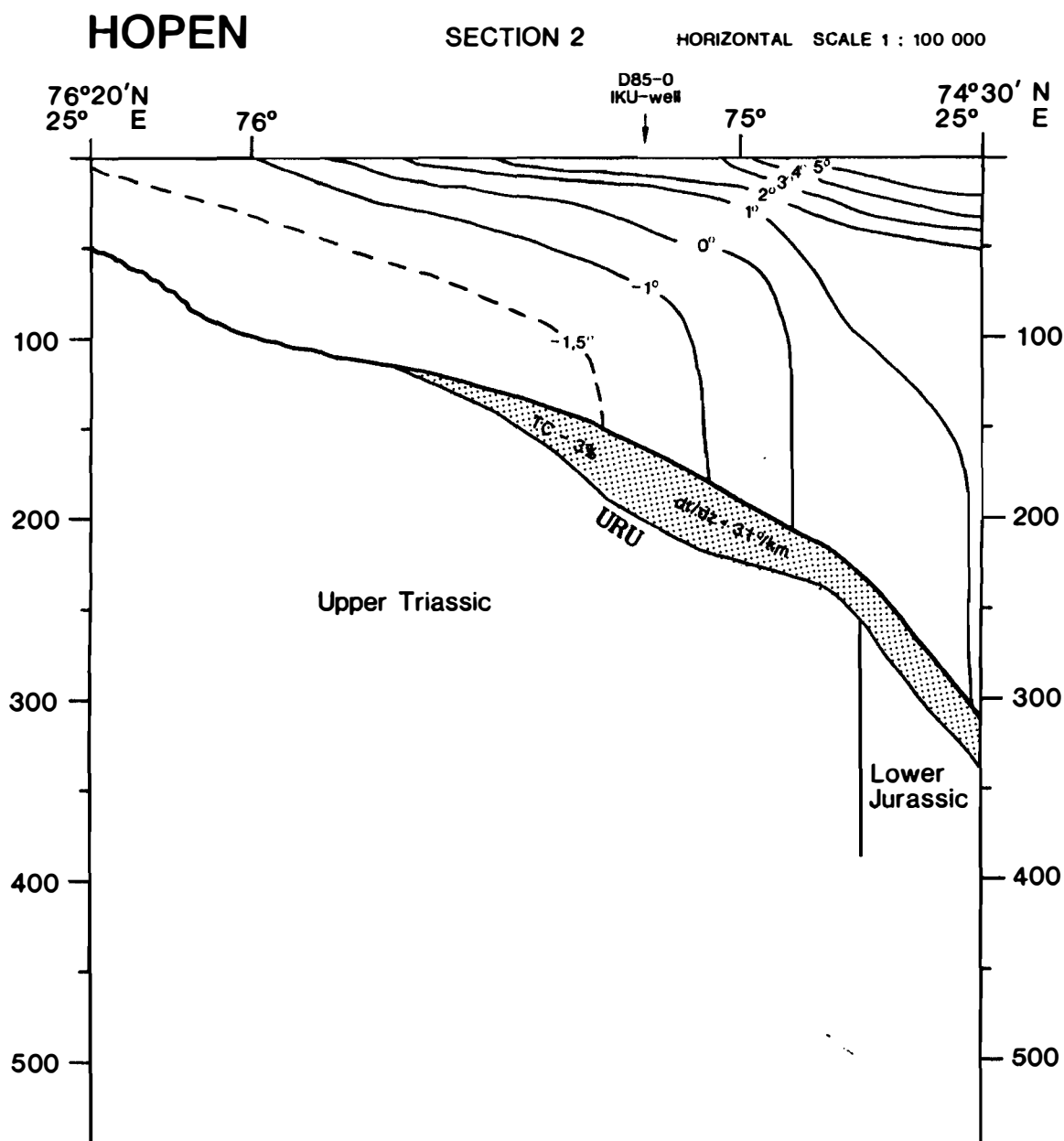
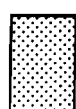


Fig. 2.10. b) Section 2. Mean values of water temperatures measured in the middle of July. Based on Eide (1983).



Quaternary sediments

d) Geothermal gradient

The Continental Shelf and Petroleum Technology Research Institute Ltd. (IKU) has measured temperature and thermal conductivity of

sediment samples in a shallow well (D85-0) of Spitsbergenbanken (Fig.2.9). The measurements were done down to 40 m below the seabed, all in unconsolidated sediments of Quaternary age. Subzero temperatures occurred in a zone down to more than 15 m below the seabed (Fig.2.11). The temperature gradient below the subzero interval was estimated to be $31.0\text{ }^{\circ}\text{C}/\text{km}$ (IKU news 1988).

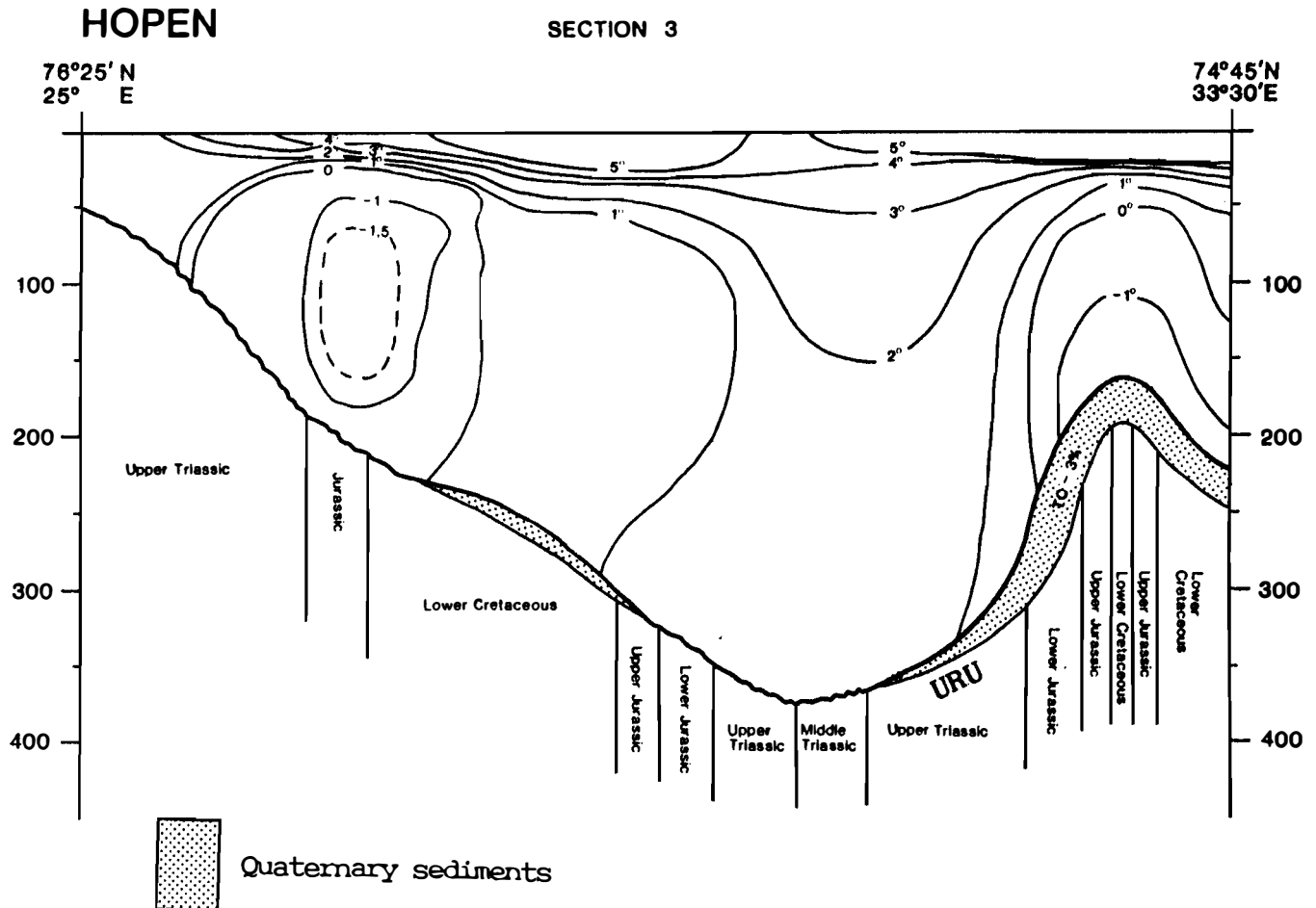


Fig. 2.10. c) Section 3. Mean values of water temperatures measured in August-September. Based on Skjoldal (pers. comm.) and Eide (1983).

e) Seismic velocity

In order to map the seafloor velocity and the velocity distribution in the upper sediments, Beskow et al. (1984) used sonobuoy data, while Berge & Beskow (1983) interpreted non-muted reflection data, using both reflected and refracted waves. The seafloor velocities found along a profile stretching from Spitsbergenbanken, over Bjørnøyrenna to Sentralbanken, varied between 1700 m/s to 2750 m/s. The highest

velocity is found in Bjørnøyrenna where the water depth is greatest. According to Berge & Beskow (1983), the velocity corresponds mainly to the velocity in glacial and postglacial sediments. Houtz (1980) presented a map of seafloor velocities based on sonobuoy data, showing considerably higher velocities than described above. According to Berge & Beskow (1983), these velocities seem to be describing the sediment velocities at same depth below sea bottom.

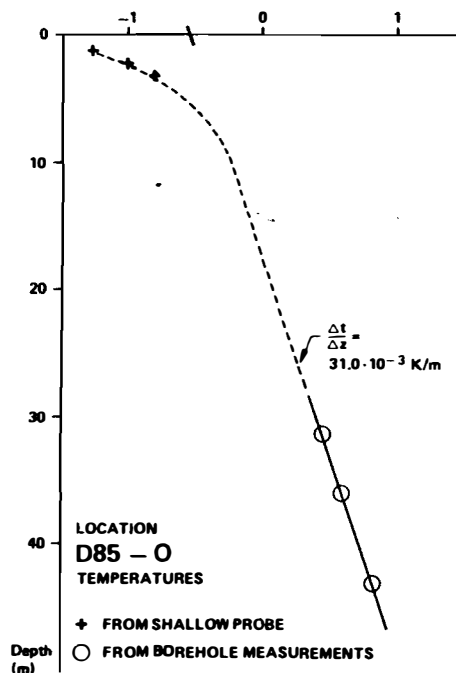


Fig. 2.11. Temperature measurements in a shallow well on Spitsbergenbanken. From IKU news (1988).

f) Pockmarks.

As side scan sonar surveys were not carried out in the northern Barents Sea until 1983, reports on pockmarks are sparse. However, a somewhat restricted data base obtained since then seems to indicate that pockmarks are abundant over large parts of the northern Barents Sea. Solheim & Elverhøi (1985) reported a pockmark field on the flank of Spitsbergenbanken, southeast of Hopen (Fig. 2.1), in waterdepths ranging from 150 to 250 m. In this area, pockmarks covered up to 25 % of the sea floor. They were relatively small, averaging only 10-20 m in diameter, and usually < 1 m in depth. The small dimensions were taken as a function of the thin cover of soft, Holocene mud in which the pockmarks were recorded. In areas of a more reflective, apparently harder sea floor, pockmarks seemed to concentrate in the troughs of iceberg plough marks. Due to the thin cover of Quaternary sediments (generally < 10 m), mainly consisting of

glacigenic sediments with a low content of primary organic carbon, Solheim & Elverhøi (1985) interpreted the pockmarks to be formed by gas seepage from a deeper petrogenic source. The pockmark density also appeared to be highest where dipping layers almost outcropped in somewhat steeper slopes. Based on data acquired during hydrographic surveying in 1984 and 1985, Solheim (1988) reported pockmarks from Erik Eriksenstretet, between Kong Karls Land and Nordaustlandet (Fig. 2.1). The density in this region is low, but the dimensions seem to be comparable with the ones reported from southeast of Hopen. Associated with the pockmarks are also patches of more reflective sea floor, appearing as dark spots of the same diameter as the pockmarks in side scan sonograms. These are preliminarily interpreted as formed by the same process that formed the pockmarks, but with only a sorting effect, causing a more coarse grained sea floor, without producing a noticeable depression. An extensive acoustic survey in 1987 covered the northern part of Bjørnøyna, between Storbanken and the northeastern part of Spitsbergenbanken (Solheim et al. 1988). The side scan records showed pockmarks of similar dimensions as previously reported to be widespread over the entire survey area, but mainly below 150 - 200 m water depth. At shallower depths the sea floor is too disturbed by iceberg plough marks. In conclusion, pockmarks are widespread over the northern Barents Sea. They are generally small (10-20 m diameter) and shallow (<1 - 2 m). Their size and distribution seem to be a function of the distribution of soft, post-glacial sediments. So far, no attempt has been made to relate pockmark distribution to subcrop bedrock geology.

2.2.3 Bedrock characteristics

The approximate subcrop of the main boundaries is shown on the transects (Fig.2.10), based on interpreted seismic profiles.

a) Total organic carbon

Values for the total organic carbon content in the sedimentary bedrock can be estimated by extrapolating from the wells farther south. Spathian and Ladinian (Lower/Middle Triassic) typically have 2-5% TOC, while the Middle/Upper Triassic Ladinian and Carnian contain 0.5-1.5%. In general, the Upper Jurassic rocks may contain 5-7% in the better zones; locally however, the values may be as high as 10-15%. In Lower Jurassic and Cretaceous the values generally are low (0-2%) (F. Riis pers.com. 1988).

b) Porosity

Approximate values for the porosities, estimated from well data in the southern Barents Sea yield 20% for the Triassic sequence in the western areas, increasing to 25% towards the east (35°E). In the Jurassic and Cretaceous, the porosities can be as high as 30% (F.Riis pers.com. 1988). However, measurements in Svalbard indicate lower porosity values. Elverhøi & Grønlie (1981) found porosity values as low as 3-10 % for the Mesozoic and Tertiary sedimentary sequences on Spitsbergen and Edgeøya. Porosity values from Hopen and the Svalbard Platform are not available, but petrographical studies of clast material from the western Barents Sea indicate similarity with the Mesozoic strata in Svalbard (Antonsen & Flood 1987). Therefore it seems reasonable to anticipate porosity values in the same range as that found in Svalbard for most of the transect areas.

c) Seismic velocity

The velocities for the sedimentary layers in the transects are taken from a study by Faleide et al.(1984), based on multichannel reflection seismics and sonobuoy data from the western Barents Sea. They found the following velocities representative for the different sedimentary layers:

Paleocene - Upper Cretaceous:	2.3 - 3.5 km/s.
Lower Cretaceous	: 2.7 - 3.8
Jurassic - Triassic	: 3.7 - 5.4
Permo - Carboniferous	: 5.0 - 6.4

However, on the Svalbard Platform the velocities are slightly higher than those in the same sequences farther south (Eldholm et al. 1984). In this area, Triassic sediments range from 4.3 to 5.5 km/s with sea floor velocities of 4.3-4.4 km/s close to Hopen.

2.3 Late Cenozoic History

The Late Cenozoic is a time interval when the high latitude areas of the northern hemisphere experienced a climatic cooling. Glacial episodes in the areas surrounding the Norwegian Sea are, based on ice rafted detritus, documented as early as late Miocene (5.5 Ma)(Jansen et al. in press). But the most dramatic change is the onset of

the major glaciations in the Pliocene. The exact dating of the development of the major continental glaciations is still under discussion. However, recent data from ODP Leg 104 on the Vøring Plateau suggest that the first major expansion of the Fennoscandian Ice Sheet to the Norwegian coastal waters took place at about 2.6 Ma (Jansen et al. 1988). This is based on the appearance of a large influx of ice-rafted debris and a major change in the oxygen -isotope composition towards heavy $\delta^{18}\text{O}$ -values at that time.

According to Jansen et al. (in press) (Fig. 2.12), the Late Pliocene and Pleistocene can be divided into three periods. The first period, covering the time interval between 2.6 and 1.2 Ma, was characterized by cold surface water conditions in the Norwegian-Greenland Sea, and during interglacial periods there was only a weak influx of Atlantic water, as compared with interglacials towards the end of the Pleistocene (Jansen et al. 1988). The initial part of this first period, until about 2 Ma, was also characterized by severe or extensive glaciations, while in the time interval between 2 and 1.2 Ma, the glaciations in Scandinavia most likely were small. In the second period, from 1.2 Ma to 0.6 Ma, the input of ice-rafted material increases, and is interpreted to reflect intensified glaciations. During this period, there is also a gradual transition towards larger glaciations and warmer interglacials, conditions which characterize the third period spanning the last 0.6 My (Jansen et al. 1988). In this third period, the glacials - interglacials changes show a cyclic pattern of the well known 100, 41 and 21 ka wavelengths.

Drilling on the outer parts of the Norwegian shelf also indicates onset of extensive glaciations in Pliocene. In 1988 the Norwegian Petroleum Directorate carried out stratigraphic studies of two wells in the Senja Ridge, penetrating the eastern part of a sedimentary wedge which is developed along the western margin of the Barents Sea. Foraminifera and in particular Sr isotope values suggest a Pliocene age (ap. 2.5 Ma) for the deepest part of the wedge. Dropstones are found at several levels in the wedge. Rough calculations indicate that the sediment volume in the wedge corresponds to 1000 m of erosion of the central Barents Sea (Vorren pers. comm. 1988). As discussed further in chapter 3, this indicates a very high erosional rate throughout the Late Pliocene/Pleistocene.

Prior to the development of the continental ice sheets, the northern regions most likely developed tundra conditions, and the boundary of boreal and forested conditions were forced to the south (Brigham-Grette et al. 1988). Evidence for the beginning of a cold climate in the Late Cenozoic is also seen from the thick glaciomarine

sediments in Alaska interpreted as depositions from a widespread mountain glaciation as early as 10 Ma (Yakatanga Formation) (Pflaker 1981).

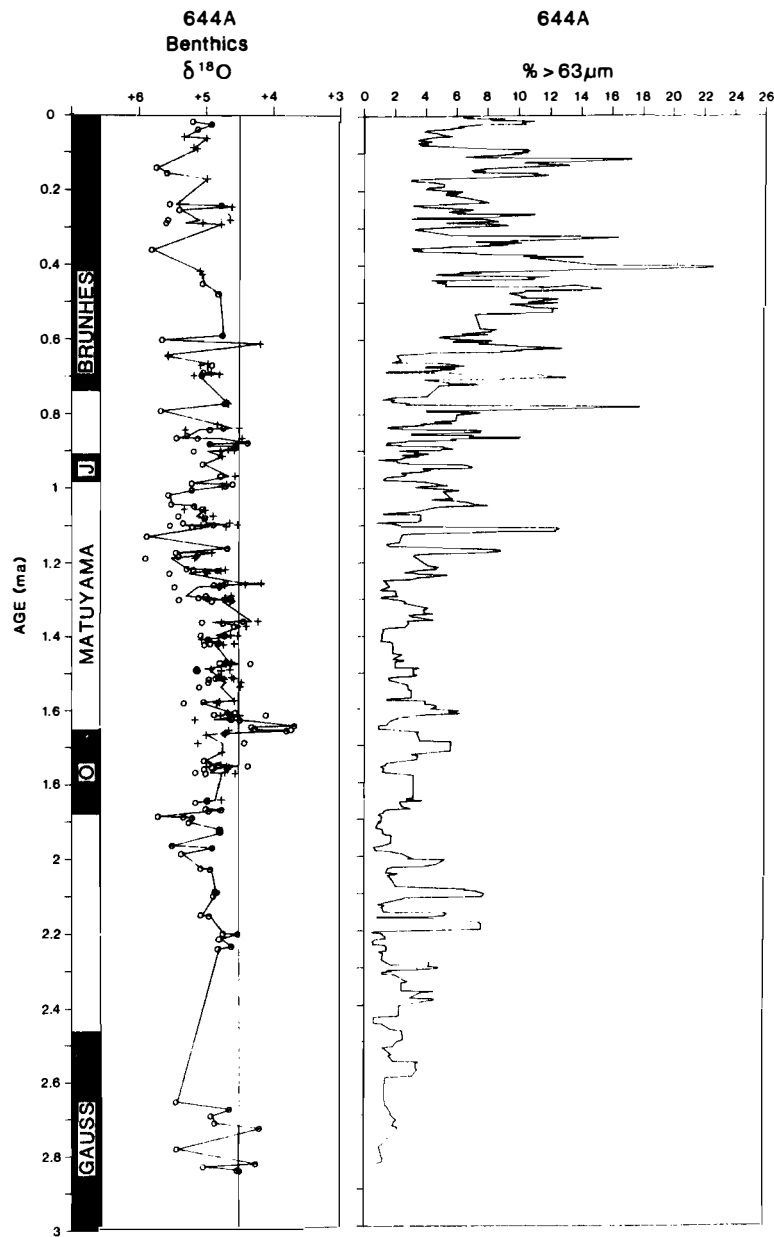


Fig.2.12. Coarse fraction and isotope record of ODP Site 644A, on the Vøring Plateau. The coarse fraction (mainly reflecting ice-rafted debris, IRD) is used as an indicator of the extension and intensity of the glacials. As seen from the figure, the amplitude of the IRD increases in the Brunhes, suggested to reflect increased intensity and extension of the glacials. The time scale is produced by linear interpolation between magnetic reversals. (From Jansen et al. 1987).

Lack of suitable and precise dating methods has led to a number of controversies and apparently contradictory information on the development of the cold late Cenozoic climate. The timing of development of tundra conditions, reflecting sub-zero average annual temperatures, in the high Arctic regions is a highly debated subject (Brigham-Grette et al. 1988). The minimum age for permafrost is probably about 2.4 Ma, but a cold climate may also have existed prior to this. A main topic of discussion is the timing of the development of permanent sea ice cover of the Arctic Ocean (e.g. Clark 1982; Herman & Hopkins 1980; Markussen et al. 1985).

The paleoenvironmental interpretations of the Arctic Ocean have largely been based on lithostratigraphy combined with paleomagnetic data. For a long time it has been suggested that the onset of perennial sea ice conditions in the Arctic Basin took place in the Late Miocene. However, this concept has now been challenged by a revision of the paleomagnetic data, indicating onset of perennial sea-ice cover at the Matuyama/Gauss boundary, at about 2.48 Ma (Jones 1987). It is to be noted that according to results from the ODP Leg 104 from the Vøring Plateau, sea ice and/or minor continental glaciers extending to the sea may have existed prior to 2.5 Ma. So far, thick Late Miocene glacigenic sediment sequences, similar to those in Alaska, have not been found in the European Arctic, indicating that mountain glaciations and the associated climate may have a limited existence and distribution in the European Arctic.

2.3.1 Summary - Late Cenozoic paleoenvironment: Svalbard - Barents Sea

Our knowledge of the Late Cenozoic paleoenvironment in Svalbard and the Barents Sea is very limited. If we apply the general ideas developed for the Late Cenozoic, we can very tentatively outline the following evolution of the Svalbard/Barents Sea Region:

a) Early - Early Late Pliocene (5 - 2.6 Ma)

Initial cooling of the region with possible mountain glaciers in Svalbard. Parts of the Barents Sea may have been submerged and covered by sea ice during wintertime. Towards the end of the period, permafrost and tundra conditions may have developed in Svalbard and subaerial parts of the Barents Sea. However, the extension of the submerged and subaerially exposed areas of the Barents Sea in this period is unknown.

b) Mid/Late Pliocene/Early Pleistocene (2.6 - 1.2 Ma)

This period is characterized by the onset of major glaciations at about 2.6 Ma. The extent and duration of the glacials are not well known. However, judging from the intensity of the ice rafting, glaciations in the first part of the period may have been extensive, while the glaciations towards the end of this period were less severe. Permanent sea ice cover is likely to have developed in the Arctic Ocean. Due to restricted intrusion of warm Atlantic water to the northern shelf regions during interglacials, the submerged parts of the Barents Sea were probably covered by sea ice for long intervals.

c) Pleistocene, pre-Weichselian (1.2 - 0.12 Ma)

This epoch is characterized by glacial - interglacial cycles, and for the last 0.9 Ma, the duration of the major events is approximately 100 000 years. During glacials, the ice cover has, however, not persisted continuously. For example, the Weichselian glaciation apparently consisted of three stadials, interrupted by two interstadials. In general, the interglacials are characterized by warm climate, and Atlantic Water most likely penetrated northward to Svalbard and the Barents Sea.

According to shallow seismic stratigraphy from the outer part of Bjørnøyna, 4 depositional sequences of probable glacial origin have been identified, interpreted to reflect at least 4 major glacial expansions out to the shelf edge (Solheim & Kristoffersen 1984). The age of these stages are unknown, but they appear to be pre Weichselian.

d) Weichselian/Holocene (0.12 Ma - present)

The information on the Early (120 - 75 ka) and Mid Weichselian (75 - 25 ka) glaciations is very limited. However, terrestrial data indicate the existence of a major Early Weichselian ice sheet reaching the shelf edge north and west of Svalbard (Salvigsen & Østerholm 1982, Miller 1982). This Early Weichselian Ice sheet is also suggested to have covered the entire Barents Sea (Elverhøi & Solheim 1983).

There is no evidence for major glacial activity in the Mid Weichselian, but the Mid Weichselian ice margin may have expanded into the fjords on the western coast of Svalbard, and may also have reached almost to the present-day western coast line (Miller et al. 1987). Lindner et al. (1987), suggest two Mid Weichselian glacial advances. This result is mainly based on thermoluminescence dating, which is very uncertain, and further datings have to be carried out before this idea can be proved. No information exists from the Barents Sea, but

due to the lack of evidence for a major glaciation in Svalbard, we suggest that also the Barents Sea was non-glaciated during the Mid Weichselian.

The discussion of the Late Weichselian (25 - 10 ka) evolution of the Svalbard/Barents Sea region has for a long time been characterized by strongly conflicting views. Until recently, only scattered studies of detailed stratigraphy were available from the region. However, during the last 5-8 years, systematic and detailed studies of the terrestrial as well as the marine record have been conducted. Even though disagreement still exists, there now seems to be common consensus on the following points (Lehman & Forman 1987; Mangerud et al. 1987; Elverhøi & Solheim 1987; Vorren et al 1987; Elverhøi et al. in press):

- 1) The margin of the maximum Late Weichselian ice sheet extended almost to the present day coast-line of western and northern Svalbard.
- 2) The Svalbard ice sheet was continuous with grounded ice in the northern Barents Sea, but the question of coalescence with the Fennoscandian Ice Sheet is still under discussion.
- 3) The initial retreat of the Svalbard/northern Barents Sea ice sheet started relatively early, probably at 13 -12 ka, and was completed at least at 10 ka.

For tentative reconstructions, see figure 2.13.

The growth and decay of the Barents Sea ice sheet have been widely discussed, and so far, our knowledge is limited to the withdrawal. The data for our models are mainly from the surrounding deep sea regions, which indicate high influx of: i) meltwater, ii) ice rafting of Svalbard/Barents Sea bedrock clasts and iii) increased sedimentation rate at about 14 - 12 ka.

Sea level curves from western Svalbard may also indicate an early deglaciation of the Barents Sea region (Lehman & Forman 1987). Data from the interior parts of the Barents Sea (Elverhøi & Solheim 1983; Solheim et al. 1988; Elverhøi & Solheim various unpubl. data) indicate that the present day 300 m contour defines a major stage during the withdrawal of the last ice sheet. Alternatively, this limit may also identify the outer boundary of a limited Late Weichselian ice sheet. Accordingly, we have outlined two models: 1) one maximum model covering the entire shelf and 2) a limited model covering the shallower Barents Sea, leaving Bjørnøyna as a calving bay (Fig.2.13).

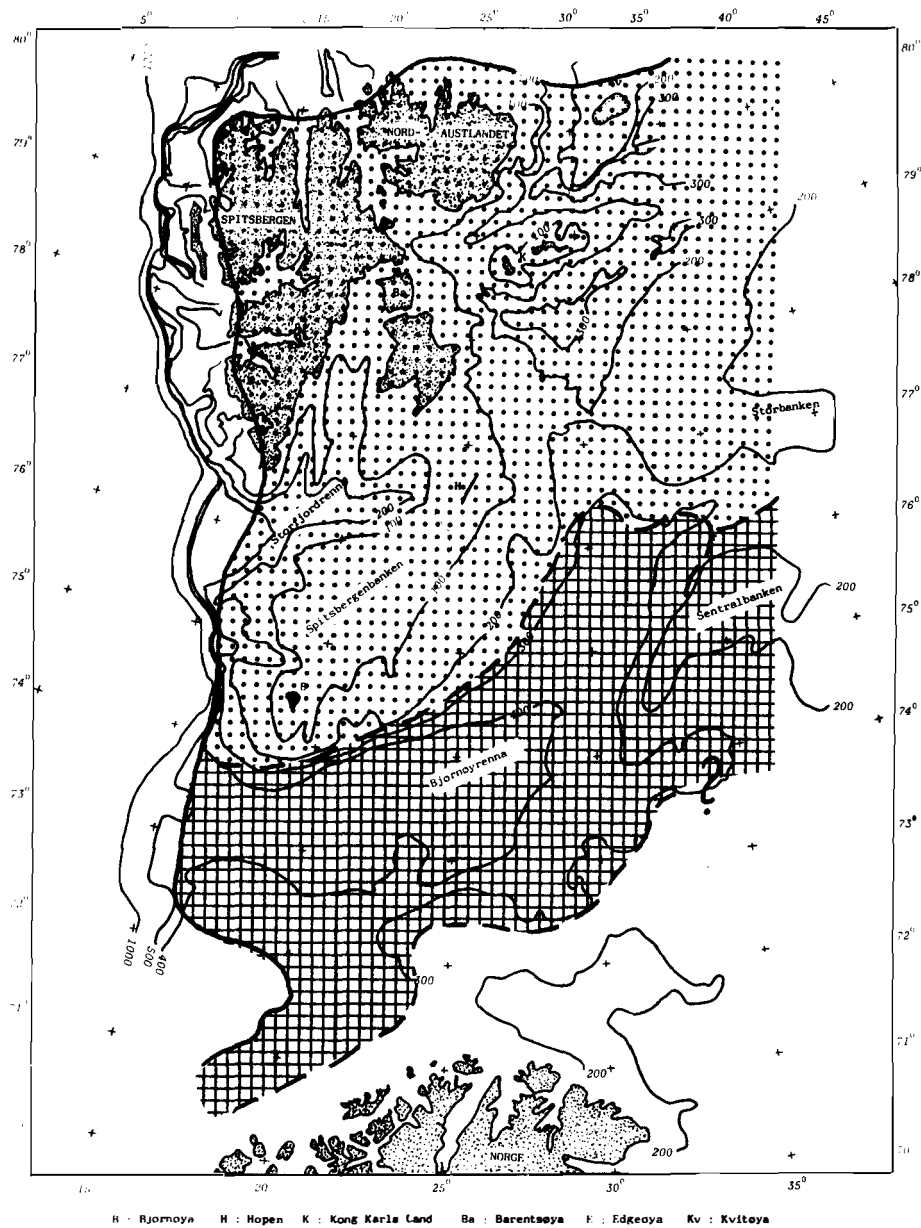
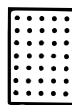
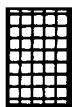


Fig. 2.13. Tentative reconstruction of the extension of the Late Weichselian ice sheet. Two models have been indicated:

- 1) a maximum model extending to the shelf edge.
- 2) limited ice cover extending to the present day 300 m contour.



limited ice cover



extensive ice cover

The Barents Sea Ice Sheet, which was grounded below sea level, is classified as a "marine ice sheet". The stability of such marine ice sheets is strongly controlled by the relative sea level (Paterson 1981), and rise and fall of the sea level will cause ice recession and expansion, respectively. Due to the flat and uniform substratum in the Barents Sea, it is likely that the Barents Sea ice sheet was easily destabilized due to the eustatic sea level rise. A rapid deglaciation is suggested from an extensive meltwater outflow in the Fram Strait at about 15-13 ka (Jones & Keigwin 1988). A rapid deglaciation, at least from the 300 m contour ("limited model"), is also seen from the very thin (<1m) cover of glaciomarine sediments above the Late Weichselian till in the inner part of Bjørnøyna (Solheim et al. in press). We have no information on the early stage of the glaciation of a maximum ice sheet, but we have indicated a withdrawal from the shelf edge to a more limited extension ("limited model") to have taken place at 16 ka.

A well established and classical concept for the growth of an ice sheet is that the ice expands from higher regions (Flint 1957). For a marine based ice sheet where the ice field has to expand into the marine environment or start to grow within the marine environment itself, the ideas are much more complicated. E.g. Denton & Hughes (1981) have argued for a gradually thickening sea ice as one way of formation. However, an alternative idea of initial growth of the Barents Sea Ice Sheet is:

eustatic lowering during glacials caused sub aerial exposure of the shallower banks in the Barents Sea, and considerable parts of Spitsbergenbanken were exposed. Glaciers may have formed at these exposed banks, and later expanded into the marine areas.

The Barents Sea Ice Sheet may then have formed from a number of ice caps, growing into a continuous ice sheet.

This idea implies that the growth of the Barents Sea Ice is delayed compared to the growth of continental based Svalbard and Fennoscandian ice sheets. Furthermore, the duration of a Barents Sea Ice Sheet was relatively limited compared to the Fennoscandian Ice Sheet (Fig.2.14).

Alternatively to this idea of a delayed growth, the Barents Sea Ice Sheet may have grown continuously out from Svalbard and Northern Norway as the sea level dropped in the Late Weichselian. According to this model, the Barents Sea glaciation starts earlier in the Late Weichselian, and the duration of the glaciation increases (Fig. 2.14.). However, as seen from the Fennoscandian glaciation curve, the Mid and Late Weichselian ice sheet did not expand into the marine areas until 30 ka. If we apply this concept to the Barents Sea, the

region remained ice free until the Late Weichselian (Fig.2.14).

In summary, the growth and decay of the Late Weichselian Barents Sea Ice Sheet are suggested to be strongly controlled by the sea level. A relatively early deglaciation, with an ice free Barents Sea during Younger Dryas (11-10 ka), is likely. Two models for the ice growth have been proposed:

- 1) A "delayed" model where the ice sheet forms from ice caps expanding out from sub aerially exposed bank areas during maximum glacioeustatic lowering at 18-20 ka.
- 2) An early Late Weichselian growth, simultaneous to the major expansion of the Late Weichselian Ice Sheet in Scandinavia and Svalbard

These ideas imply that the duration of the glaciation in marine areas is shorter than in the adjacent land areas. The timing of isostatic and geothermal adjustment for the glacially depressed marine areas therefore becomes significantly shorter than what is the case for Scandinavia.

In a long-term perspective, glaciations of the Barents Sea may have been less influenced by the sea level. In the Late Miocene and Pliocene, large parts of the present-day submerged Barents Sea may have been sub-aerially exposed. Thus, the timing of growth and decay of the Barents Sea Ice Sheet, may have been less sensitive to sea level changes. Consequently, the duration of former glaciations in the Barents Sea would have increased, compared to what has been indicated for the Late Weichselian.

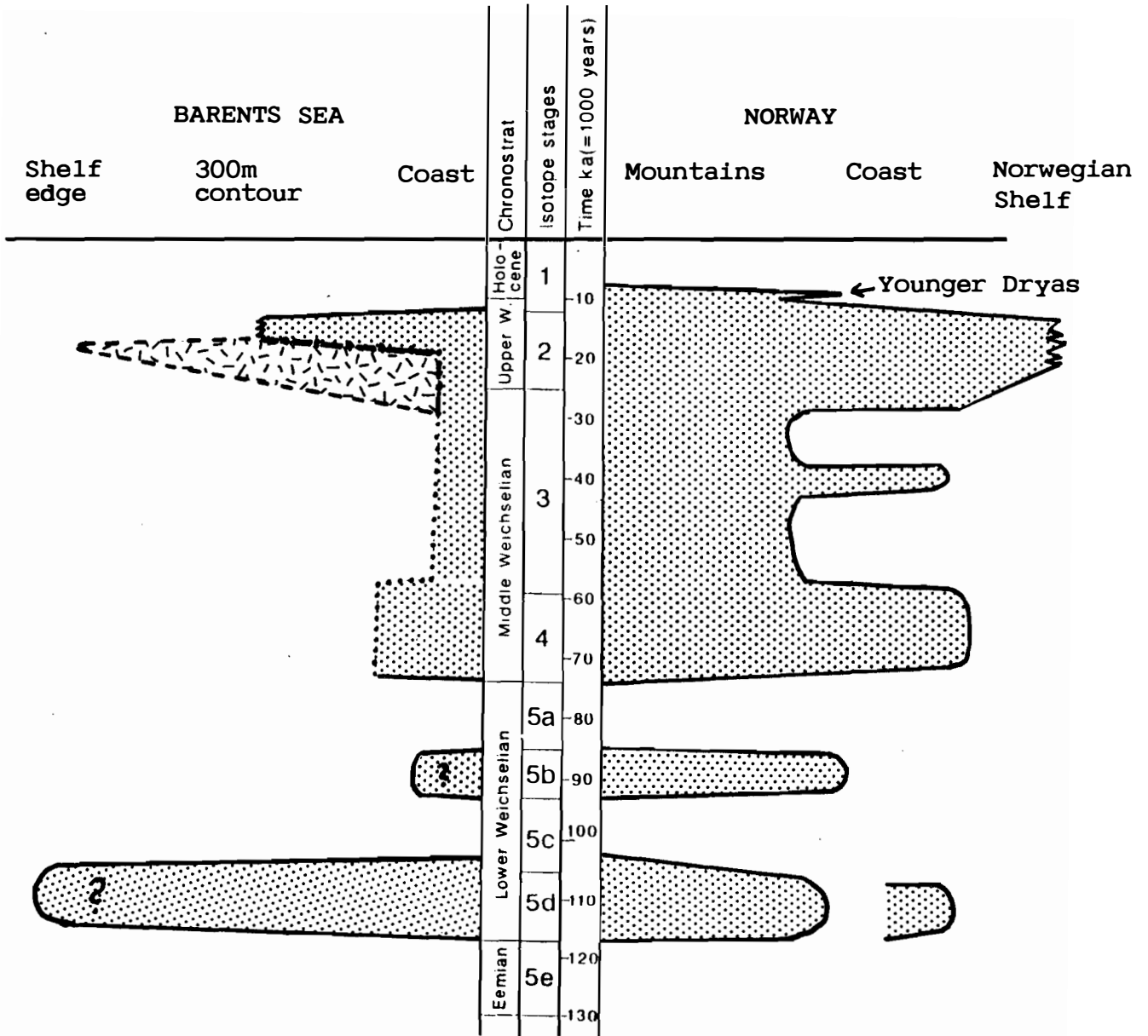


Fig. 2.14. Schematic glacialiation curve for the Weichselian in the Barents Sea (left) and the Fennoscandian (after Mangerud in press).
 - · - · - · - delayed formation
 - - - - early formation

2.3.2 Weichselian sea level changes and paleogeography of the Barents Sea.

Knowledge of the sea level variations is essential for the understanding of the paleoclimate of the Barents Sea. Sub aerial exposure of shallower parts of the shelf associated with low sea level could have provided the proper setting for 1) growth of the Barents Sea Ice Sheet (as discussed) and 2) the formation of permafrost (discussed below). Reliable data on sea level changes during the Late Cenozoic is best documented for the Weichselian and Eemian. Figure 2.15 shows a revised sea level record for the last 140 ka. The record is based both on $\delta^{18}\text{O}$ - isotope data and datings of marine terraces in New Guinea (Shackelton 1987). The maximum Weichselian sea level lowering of 120 m occurred at about 20 ka, while for isotope stage 3 and 4 (Mid Weichselian), the lowering was about 50 m (New Guinea record). During Early Weichselian, isotope stage 5a-5d, the sea level lowering was slightly less, 30-50 m. During the Eemian interglacial, stage 5e, the sea level was approximately the same as at present, while in the Saale glacial, the sea level dropped to nearly the same level as at the Late Weichselian maximum. The discrepancy between the isotope and the New Guinea terrace record, in particular during isotope stages 3 & 4, is not fully understood. Among the various explanations, a lowering of the bottom water temperature is probably the most likely (Shackelton 1987).

In accordance with the sea level record and the Weichselian glacial history (extensive and limited models), the shallower parts, <50 m, of the shelf north and west of Svalbard should have remained subaerially exposed since the Mid Weichselian. The shallower part of Spitsbergenbanken should also have been subaerially exposed since the Mid Weichselian. However, during the Late Weichselian it is suggested that this region was covered with grounded ice. Sea level curves from Hopen and Kong Karls Land indicate that at the end of the Late Weichselian, the water depth was approximately 50 to 100 m deeper than at present in the central and northern Barents Sea. The Weichselian and Holocene sea level record of Spitsbergenbanken is summarized in figure 2.15.

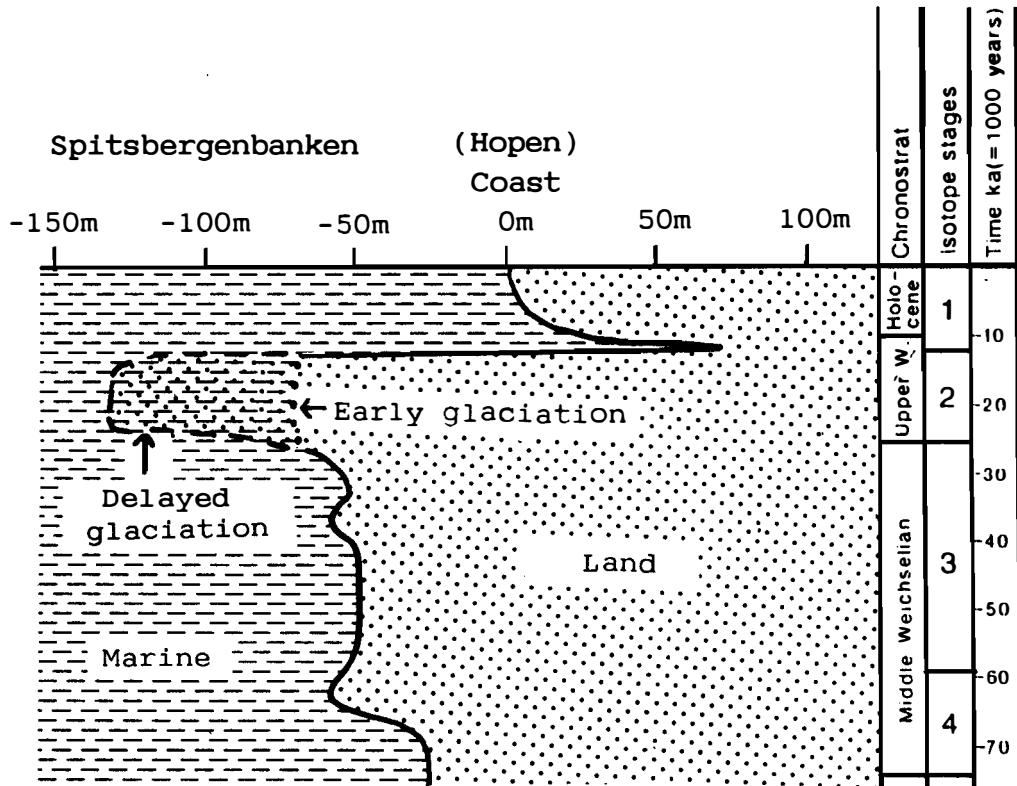
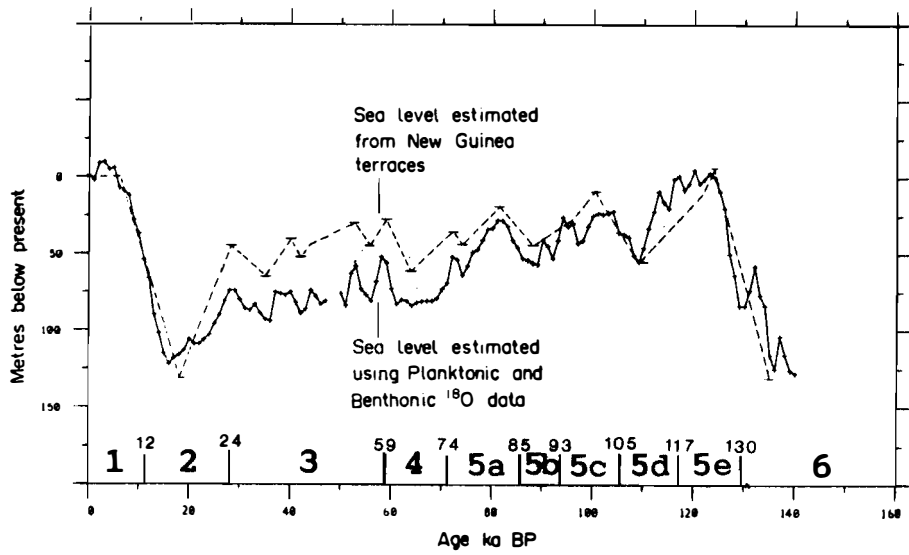


Fig 2.15. Global sea level record (upper) based on marine terraces in New Guinea and ¹⁸O isotope data (Shackelton 1987) and tentative relative sea level curve from Spitsbergenbanken (lower) during the Weichselian and Holocene.

2.3.3. Ice profiles and sub-glacial conditions (Late Weichselian)

Various ice profiles have been indicated for the marine Barents Sea Ice Sheet. If we apply an equation commonly used for terrestrial ice sheets flowing across a rocky substratum (Paterson 1981).

$$h = 3.4 (L - x)^A \quad A=1/2$$

(h is the thickness at distance $L - x$ (in meters) from the ice front, located at the shelf edge), the ice thickness in central areas as Storbanken and Sentralbanken may reach a thickness of more than 2500 meters (Fig. 2.16). However, it has been argued that when a glacier expands across a clayey, deformable substratum, the basal friction is reduced and the ice surface profiles are lowered (Boulton & Jones 1979).

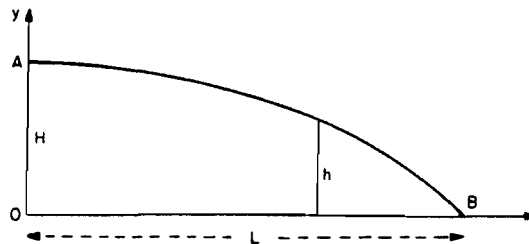


Fig. 2.16. Coordinate system for an ice sheet (from Paterson 1981).

According to the reconstruction by Denton & Hughes (1981), the ice thickness in the central Barents Sea is in the range of 2000 - 2500 m, increasing to > 3000 m at the ice maximum at Novaja Zemlja (Fig. 2.17). The existence of the major European Arctic Ice Sheet, (Fig. 2.17) has not been verified, but it can be used as an illustration of the ice thickness for a covering of the entire Barents Sea. From figure 2.17 the different gradients of the Barents sea and the Fennoscandian Ice Sheet can be seen.

For our "limited ice model", leaving the deeper (>300 m) parts of the Barents Sea ice free, the ice thickness becomes significantly reduced. The distance from the ice margins to a possible centre or ice divide of such an ice sheet in the northern Barents Sea would be in the range of 100 to 150 km. Hence, the ice thickness will vary from 1000 to 1300 m at the centre.

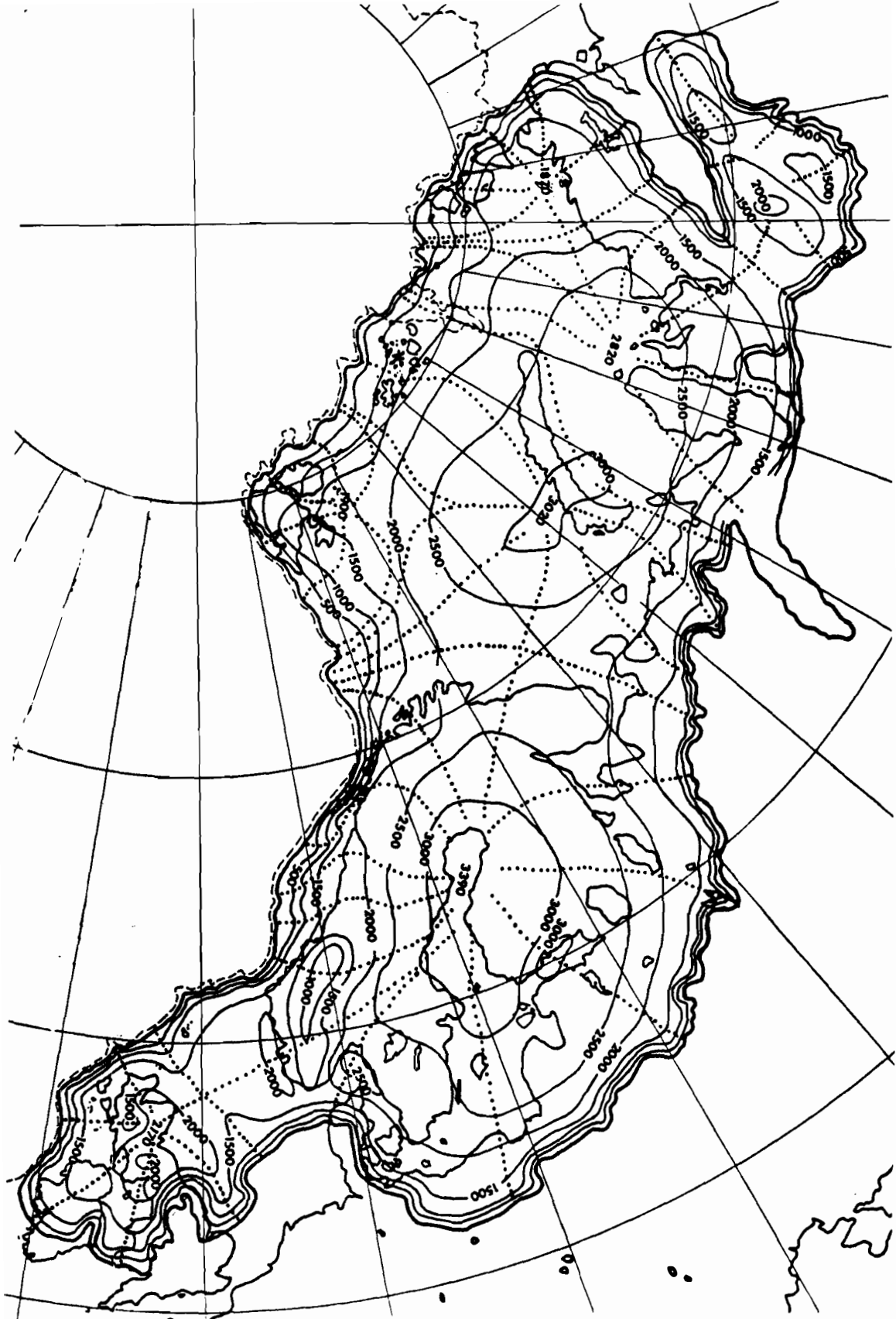


Fig.2.17. Ice thickness of the Barents Sea/Svalbard and the Fennoscandian Ice Sheets according to Denton & Hughes' (1981) maximum model.

However, due to the clayey substratum in the Barents Sea, we suggest a lowered ice profile and we tentatively propose a reduction in the ice thickness of 300m.

The temperature distribution in glaciers results from interaction of a number of processes, such as heat flow both from the bed and the surface, ice movement and water flow within the glacier (Paterson 1981). Due to these factors, the temperature profile differs from the ablation area to the accumulation area. In a simplified way this is illustrated in figure 2.18. In the accumulation area, there is a downward movement of snow/ice, and heat from below is used to warm the downward moving ice. Hence, in the accumulation area, the temperature gradient decreases upward in the glacier. In the ablation area, where there is a net upward flux of ice, the ice is cooled as it rises. Thus, heat is added to the geothermal heat, leading to an increase in temperature gradient with height above the bed.

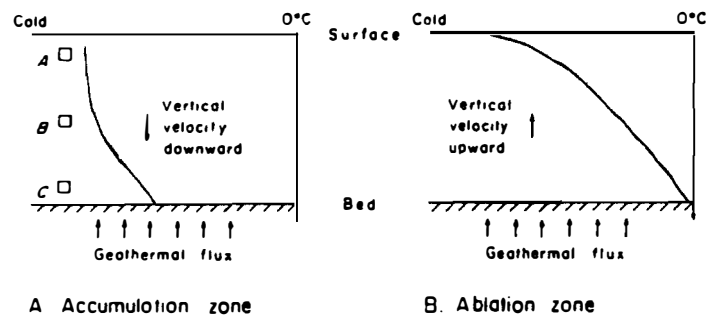


Fig. 2.18. Schematic temperature profiles in polar glaciers (Hooke 1977).

A number of temperature profiles have been calculated, and some measured profiles are also available from various glaciers (Fig.2.18). However, as seen on figure 2.18, the gradient varies throughout the glacier. Hooke (1977) proposed the value of 0.015K/m as an average temperature gradient for polar ice caps. Using this number as a first approximation, we see that an ice sheet with a thickness of 1000 m and annual average surface temperature of -15°C will have a basal temperature at the pressure melting point, approximately -0.7°C at 1000 m ice load.

Available information (drilling and radio-echo sounding) from recent ice sheets (i.e. Antarctica and Greenland) indicates that the basal temperature is at the pressure melting point below the thicker parts of the ice sheets. In the outer part of the accumulation area,

where the ice is thinner, the basal temperature is well below pressure melting point. However, beneath ice streams, e.g. "Byrd 9" (West Antarctica, figure 2.19), the temperature will rise to the pressure melting point because of friction of the moving ice.

For the Barents Sea glaciations one can only speculate and define a set of conditions, and then suggest some scenarios based on different temperature regimes.

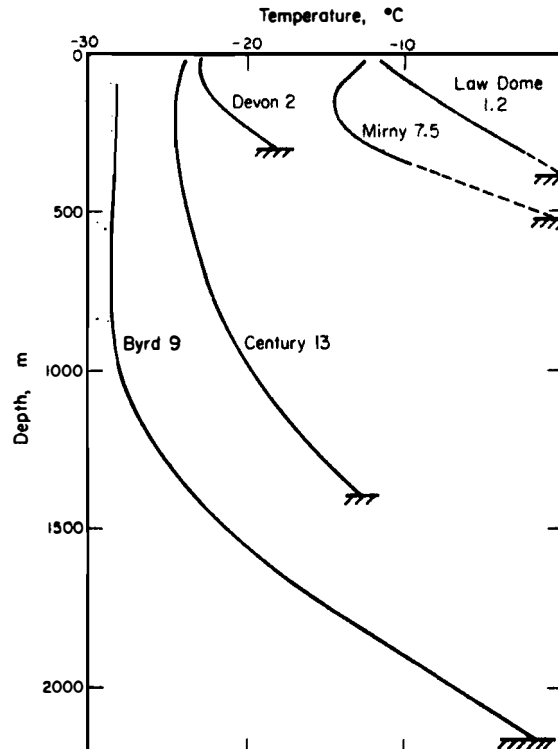


Fig.2.19. Measured temperature profiles in accumulation areas of polar ice sheets (from Paterson 1981).

a) Extensive ice cover

As indicated in the ice profiles for an extensive ice cover of the Barents Sea, a thickness of 2000 - 2500 m is likely for the central parts of the region. Reasonable annual temperatures are in the range of - 25 or 30 °C, and the base of central parts will then be at the pressure melting point. For the marginal areas, the estimation of the basal temperature is not so straightforward. A thinner ice profile as shown for the Barents Sea Ice sheet may favour a relatively higher mean annual temperature than for a "normal" ice profile (e.g. in Greenland). Calculated thickness for areas like Spitsbergenbanken is approximately 1000 - 1500 m. The annual mean temperature can be estimated to - 15 °C and the basal temperature may therefore be slightly below the pressure melting point. In areas with possible ice streams, like Bjornoyrenna and Storfjordrenna, we suggest that the ice

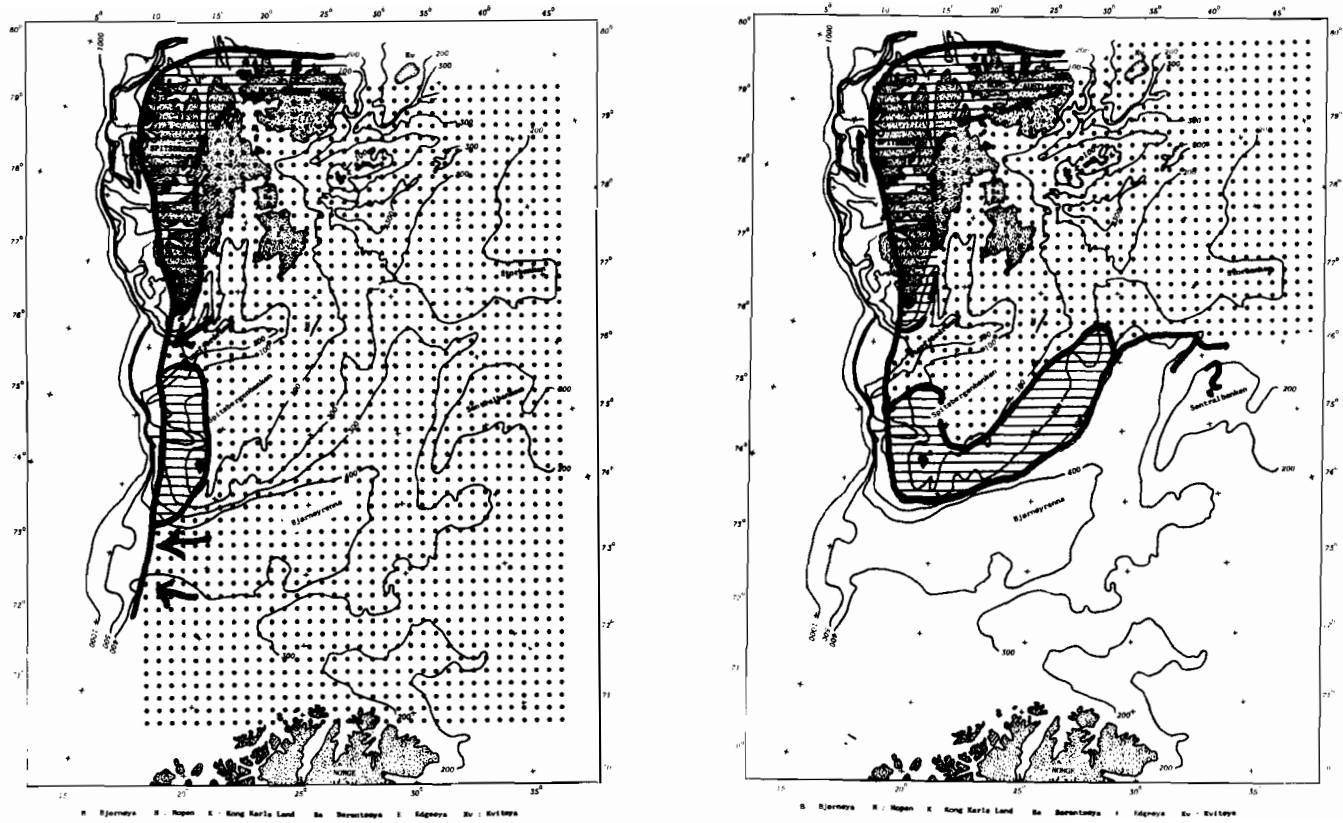
was at the pressure melting point all the way to the margin. Figure 2.20 summarizes the tentative basal temperature distribution for an extensive ice cover.

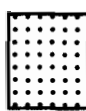
b) Limited ice cover

As discussed above, the ice thickness for our limited model, would have been in the range of 700 to 1000 m at the ice divide. The relatively thin ice combined with severe climatic conditions may have favoured temperatures below pressure melting point at the base of the ice in marginal areas. However, as the case for an extensive ice sheet, the basal temperature may have been at pressure melting point in areas with ice streams, e.g. Storfjordrenna and the inner part of Bjørnøyrenna. The following sedimentological observations indicate pressure melting point conditions in these areas:

- 1) Glacial flutes, located in the inner, northern part of Bjørnøyrenna. Such features most likely form beneath temperate ice (Boulton 1976).
- 2) Thick glaciomarine sediments in the inner part of Bjørnøyrenna, Storfjordrenna and Franz Victoria Renna suggest extensive sub-glacial drainage.

In summary, the basal temperature conditions for a major ice sheet will most likely be at the pressure melting point, i.e. in the range of -1 to -1.5 °C for considerable parts of the Barents Sea. This temperature equals the temperature of Arctic water, presently flooding the shallower part of the shelf. For a limited Barents Sea Ice Sheet, temperatures below pressure melting point may well have existed along the margins. However, for a limited model too, the basal temperature will have been in the range of -1.5 - -1 °C for the internal parts of the ice sheet.



 pressure melting point

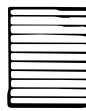
 below pressure melting point (-3 - -5 °C)

Fig.2.20. Speculative basal temperature conditions of an extensive (left) and limited (right) Barents Sea Ice Sheet.

2.4 Glacial erosion and its influence on the Late Cenozoic evolution of the Barents Sea.

The Barents Sea, forming the north western part of the Eurasian shelf, is a typical deep high latitude shelf (average water depth of 230 m). As stated above, the area has been repeatedly glaciated by grounded marine based ice sheets during the Late Cenozoic. In order to understand its present water depth, essential to the stability of gas hydrates, knowledge about the influence of glacial erosion is essential.

Progress in theories of glacial dynamics during the last decades has provided basic understanding of the qualitative aspects of glacial erosion (Glen 1955; Boulton 1974; Boulton & Jones 1979; Hallet 1981). However, existing models do not provide adequate equations for quantification calculation, and still indirect measurements have to be used in quantitative calculations of glacial erosion. For minor modern temperate glaciers, calculations, mainly based on sediment discharge by meltwater rivers, indicate erosional rates in the range of 0.1 - 1 mm per year (recalculated to sediment yield: 270 -2700 tons/km²/year)(Kjeldsen 1983). However, the knowledge of the efficiency of erosion by major ice sheets is very limited, and conflicting views exist. A classical concept is that continental glaciers are ineffective erosional agents, and cumulative erosion by the Laurentide Ice Sheet is suggested to be in the range of 20-40 metres in its central parts (Flint 1971). Alternatively, calculations by White (1972) and Bell & Laine (1985) indicate almost an order of magnitude higher rates. Critical for the indirect calculations of glacial erosion is the knowledge of: 1) sediment volume, 2) drainage area and 3) time. For the Barents Sea and its surrounding areas the broad outline of the Late Weichselian sediment stratigraphy is known, but the Late Weichselian ice extension is not well established. However, the available data can be used to make a first approximation of the amount of the Late Weichselian glacial erosion. These results may then be applied in a general discussion of glacial erosion and the Cenozoic evolution of the Barents Sea.

2.4.1 Glacial erosion

The effect of glacial erosion, which is a combined effect of 1) crushing and fracturing, 2) abrasion and 3) mechanical and chemical erosion by subglacial meltwater streams, is highly debated. Essential

for the crushing and fracturing process is the mechanical removal of weakened rocks. Most likely this occurs as a mixed process of hydraulic jack effect by opening of cavities from high water pressure and detachment of the fragments to the overriding ice from a heat pump mechanism (Rothlisberger & Iken 1981; Drewry 1986) (Fig. 2.21). The crushing and fracturing process is also the mechanism by which fragments are eroded, and the process is also suggested to be of major importance for creating overdeepened features.

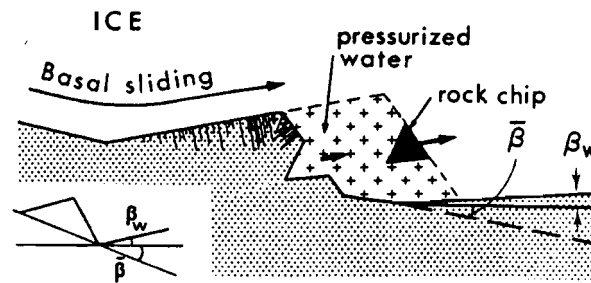


Fig. 2.21. Hydraulic jack effect with removal of fractured bedrock by opening of cavity resulting from high water pressures. Rock fragments are detached by freezing to the ice by the Robin heat pump mechanism. At intermediate water pressures freezing and hydraulic jacking combine to remove rock fragments (from Rothlisberger & Iken 1981).

The glacial abrasion has recently been discussed by Boulton & Jones (1979), Boulton (1981), and Hallet (1979, 1981) and later been extensively summarized by Drewry (1986). Here, we will only very briefly comment on the abrasion. The abrasion rate can be expressed as:

$$A = a \cdot D \cdot F \cdot n \quad (\text{Hallet 1979})$$

a and n , constant, (hardness of the bedrock)

D the number of particles per unit time per areal unit passing the substratum

F effective forces pushing the particle to the ground.

Alternatively, the abrasion can also be formulated as follows (Hallet 1981):

$$A = a \cdot Cr \cdot Vp \cdot F$$

Here, Vp represents particle velocity and Cr particle concentration in the basal zone. According to this equation, the

abrasion rate decreases with increased debris content in the sole (Fig. 2.22). A high content of material in the basal layer will then cause deposition of lodgement till, and hence transition from erosion to deposition.

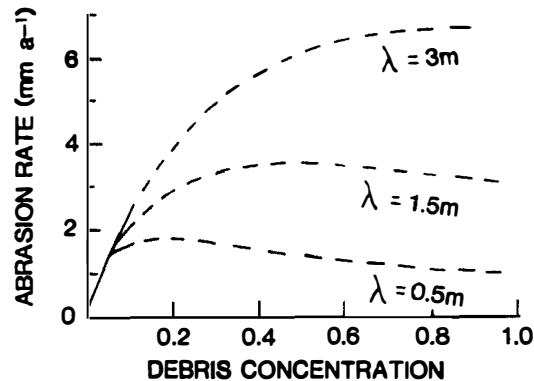


Fig. 2.22. Abrasion rate as a function of the concentration of basal debris, (i.e. proportion of fragments covering the bed) for three different wavelengths of bed undulation (λ). Fragment size = 0.2 m, bed roughness = 0.05 (from Hallet 1981)

The relative importance of the erosional processes is not known, but Drewry (1986) tentatively proposes that crushing and fracturing are most important for a hard rock substratum, while abrasion is the most efficient process for a soft substratum. In case of basal temperatures below the pressure melting point, as in parts of Greenland, it is generally accepted that no or very limited erosion takes place (Shreve 1984; Drewry 1986).

Essential for the erosion by glaciers at pressure melting point is the existence of sub-glacial meltwater. From observations in sub-glacial tunnels the ratio between en-glacial transport and sub-glacial meltwater transport has been estimated to 1 : 9. (Hagen et al. 1983). From figure 2.23 we see that the debris concentration is significantly higher in the basal zone of the ice than in the subglacial meltwater channels.

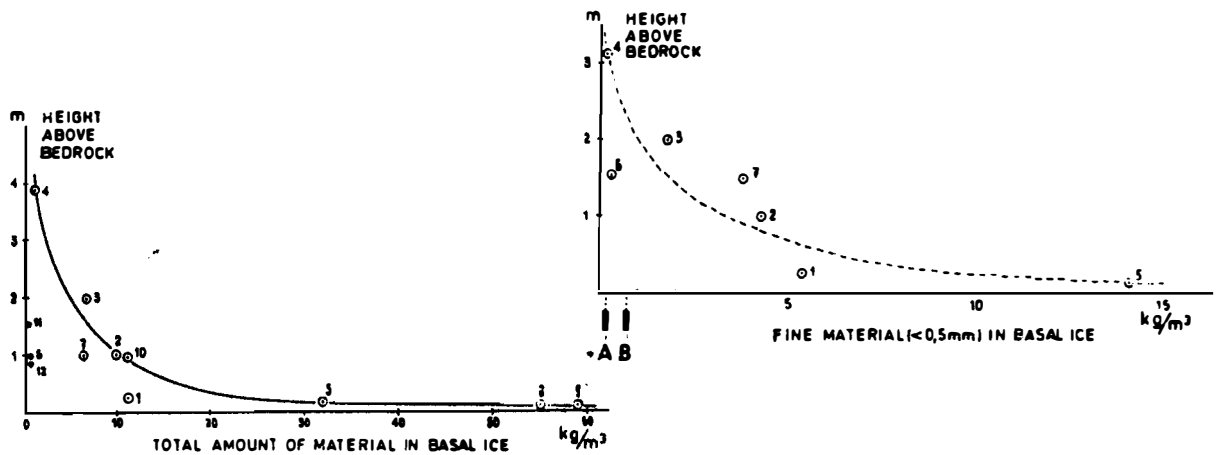


Fig. 2.23. Concentration of englacial sediment transport in Bondhusbreen (Folgefonna) (from Hagen et al. 1983).

A: sub-glacial meltwater discharge (normal)

B: sub-glacial meltwater discharge (flood)

However, the water velocity is much higher than the ice flow velocity, and the sediment flux by subglacial melt water is therefore much more significant than the one by ice. It is to be noted that the origin of debris transported by the melt water is materials produced by the glacier and not by water erosion. The effect of the melt water flow is to evacuate glacially produced debris from beneath the glacier and to deposit the material in proglacial areas. An important conclusion from this is that glaciofluvial or glaciomarine deposits can be used in first approximation of glacial erosion.

a) Indirect measurements of glacial erosion

Overdeepened fjords and large volumes of glacial sediments distal to the possible ice margins indicate extensive denudation caused by the Late Cenozoic ice sheets. Alternatively, reconstruction of the preglacial surface beneath central parts of the Laurentide Ice Sheet indicates a cumulative erosion in the range of 20 - 40 m, or $\sim 0,01$ mm/year if averaged over the entire interval of the Pliocene/Pleistocene glacials and interglacials (e.g Flint 1971). Limited erosion by the Fennoscandian Ice Sheet in its central parts is

also indicated from incorporation of preglacial deep-weathered components into Quaternary tills (Roaldseth & Rosenquist 1971). The sparse amounts of reported data on erosion by the Antarctic Ice Sheet also indicate a limited erosion, in the range of 0,05 mm/year (Wellman & Tingey 1981) .

Support for the idea of glaciers as efficient erosional agents is, however, found from indirect measurements of the erosion by modern temperate and sub-polar glaciers. Long-term measurements (6 to 13 years) of the sediment discharge by meltwater rivers from Norwegian glaciers reflect mean erosion in the range of 0.1 to 0.6 mm/year (Kjeldsen 1983). Similar and somewhat higher rates are reported from glaciers in Svalbard (1.0 mm/a) (Elverhøi et al. 1983), USSR (0.7 - 2.9 mm/a) (Scheglova & Chizov 1981) and Iceland (2.8 - 5.6 mm/a) (Boulton 1974). These values do not truly reflect the total amount of glacial erosion, as the volume of en- and supra-glacial debris is usually not included in the calculations. Sub-glacial measurements in tunnels have, however, indicated that the main part of the erosional products is found in the sub-glacial meltwater (Fig.2.23).

b) Further comments on the recent glacial erosion from Svalbard

60 % of Svalbard is presently covered by glaciers, and most of the glaciers are of a sub-polar type, i.e. the base of the glaciers is at pressure melting point in their higher areas, while frozen in the marginal parts. Similar conditions may also have prevailed for the Late Weichselian Ice Sheet. Hence, despite the fact that the present-day glaciers in Svalbard are much smaller than the Late Weichselian Ice Sheet, erosional values from the modern polar region are probably more applicable to the past for the Barents Sea Ice Sheet than the minor, temperate glaciers in lower latitudes.

In Svalbard the sediment discharge and the sediment thickness above well dated reflectors (40 years old) have been estimated outside a 1000 km² subpolar glacier, Kongsvegen, NW Svalbard (Elverhøi et al. 1980,1983). The erosion is calculated to be in the range of 0.5 - 1 mm, or recalculated to sediment yield: 1400 - 2700 ton/km²/year.

The sediment discharge from eastern Svalbard, in particular the areas outside Nordaustlandet and east of Barentsøya and Edgeøya has also been estimated based on the thickness of the Holocene sediments in the area and averaged over the Holocene (Table I). The calculation is also based on the assumption that the major part (80 - 90 %) of the continental sediment discharge is deposited within this region. Furthermore, the present-day ice coverage has also been applied for

the entire period. Most likely, the ice extent has been much less during the Holocene climatic optimum. The sedimentation rates are shown in Table I, and using a water content of 50% for the sediments, the annual sediment discharge from Nordaustlandet, Barentsøya and Edgeøya is $3.2 \cdot 10^6$ tons. Approximately 70 % of the drainage area is ice covered, and assuming that these areas are the main sediment contributor, this results in an annual sediment delivery of 400 ton/km²/year, or 0.15 mm/year. These values are somewhat lower than those found for the Kongsfjorden area, but the glaciers in the former region are likely to be less active.

In summary, estimates from the present-day Svalbard region indicate an erosional rate in the range of 0.2 - 0.5 mm/year. Even though the glaciers in Svalbard are much less in areal extent than the Barents Sea Ice Sheet, the present-day glaciers in Svalbard and the Late Weichselian Ice Sheet may have had similar dynamic characteristics. Furthermore, the various glaciers have all mainly eroded the same type of fine-grained low-metamorphic/non-metamorphic sedimentary rocks. The values obtained for present-day Svalbard may therefore be similar to those of the Late Weichselian Ice Sheet.

Table 2.1: SEDIMENT YIELD FROM EASTERN SVALBARD: NORDAUSTLANDET, EDGEØYA AND BARENTSØYA

Total marine depositional area:	20,000 km ²
Thickness of Holocene land derived sediments:	1,5 m
Weight of Holocene land derived sediments, total:	$3.2 \cdot 10^{10}$ tons
	annual: $3.2 \cdot 10^6$ tons
Ice covered part of drainage area:	8000 km ²
Sediment yield: Eastern Svalbard:	400 ton/km ² /year
Annual erosional rate:	0.15 mm/year

c) Estimates of glacial erosion in the Barents Sea

Calculation of glacial erosion should be based on:

- 1) The total volume of sediment produced
- 2) The dimension of the erosional area
- 3) The time span of the erosion

For the Late Weichselian, the maximum extension of the ice sheet is

not known; thus, exact information of total sediment volume, dimensions of the erosional area and finally the time of erosion cannot be given. The calculations therefore must be limited to cover the northern Barents Sea, assuming a limited ice cover. The results will therefore be minimum values.

Re.1): In the estimation of sediment volume the glaciomarine sediments and the till deposits will be used (Fig. 2.8).

Based on dating and detailed petrographic studies, the glacial sediments are mainly of a relatively local origin (Elverhøi et al. 1988). The two units of Late Weichselian sediments represent the following types of deposits:

1) Lodgement till from erosion of the underlying bedrock and/or older glacial sediments formed during a former glacial cycle. Even though locally thicker accumulations exist, the unit appears as a relatively uniform sheet-deposit, and the average thickness is approximately 5 m. Recalculating to values comparable to sediment yield and using available data on bulk density and water content, this corresponds to $8 \cdot 10^6$ tons/km². Due to the fact that we find some reworked organic material within these sediments, the till unit may not be entirely formed from erosion of the underlying bedrock, but may also include some older sediments. The volume of primary produced sediments is therefore lowered to $5 \cdot 10^6$ tons/km².

2) The glaciomarine sediments also form a relatively uniform sheet-like deposit. Despite local accumulations also of this material an average thickness of 5 meters is estimated. Recalculating to tons/km², the sediment corresponds to approximately $5 \cdot 10^6$ tons/km². These deposits are also of a semilocal origin, and are suggested to be produced entirely during the Late Weichselian glacial cycle.

In summary, a minimum of $10 \cdot 10^6$ tons of glacial sediments are suggested to have formed during the Late Weichselian glaciation. Furthermore, the sediments are suggested to have been formed relatively locally. The major unknown factor in the sediment budget is the amount of:

- i) glaciomarine sediments transported out of the Barents Sea and
- ii) sediments eroded and transported during a wider maximum extension, probably far out in Bjørnøyrænna.

Re. i): From studies of modern environments we know that the main part of glacially derived sediments is locally deposited. The amount of this part can therefore be neglected.

Re. ii): The amount of these sediments is unknown, but most likely they do not represent a major part of the eroded sediments. This hypothesis is based on the following concept:

When the ice expands into Bjørnøya, or achieves full size and covers the entire shelf, the ice will mainly erode and redeposit soft sediments, originally formed when the ice had a more limited extension. Moreover, data from the Fram Strait strongly support the idea of only short intervals during which the glaciers had a maximum extension. Thus, the time for a fully expanded ice sheet is short compared with the time interval it covered more shallow regions.

According to our calculations, $10 \cdot 10^6$ tons/km² of sediments have been produced during the Late Weichselian glacial event. Using a density of 2.7 g/cm³, approximately 4 m of the bedrock have been eroded. However, as this is a minimum value, we suggest as a first approximation 5 m of erosion per glacial cycle. The timing of the erosional episode, i.e. the time interval when the areas were covered by grounded ice is not known, Most likely the Barents Sea Ice Sheet disappeared in the time interval of 12 - 10 ka, and if the Barents Sea Ice Sheet started to grow at the early stage of the Late Weichselian, 10 000 years can be used as a rough estimate of its life-time. Accordingly, an erosional rate of $10 \cdot 10^2$ tons/km² or 0.5 mm/year is indicated, a value which seems reasonable compared with results from other regions.

2.4.2 Late Cenozoic development of the Barents sea, glacial versus fluvial erosion.

It is accepted that the Barents Sea was subaerially exposed in the Tertiary (Dowdeswell 1988). Fluvial erosion has been suggested as an important process that shaped the main shelf morphology, which later has been modified by glacial erosion. A comparison between the two modes of erosion can be visualized from Table 2 and figure 2.24, where the relative importance of glacial and fluvial erosion has been illustrated on a world basis. The sediment yield from the internal part of Australia is in the range of 10 tons/km², while in fluvially dominated basins like the Mississippi region, a yield of 10^2 tons/km² is estimated. A yield in the range of 10^2 /km² is indicated in glacially drained basins with temperate glaciers, as found in Norway today. Similar or somewhat higher rates are found for glaciers in Svalbard. Calculation of the sediment yield for the Barents Sea also

shows erosional rates within the same range. Similar rates are also found for other glacially influenced drainage basins, as in the Himalayas and the glaciated part of Alaska.

The conclusion from this type of comparison is that glacial erosion is roughly ten times more efficient as an erosional agent than the fluvial system. However, a very important aspect in the calculations is the time interval. The Late Cenozoic glacials have only lasted for a couple of millions years. The number of glaciations is not known, but if we apply the idea of at least 30 major glacial events, and use 5 m erosion per glacial event, 150 m of the bedrock would have been eroded during the Pliocene/Pleistocene glacials. Recent datings of Late Cenozoic sediments from the outer part of Bjørnøyrenna (Senjaryggen) (Eidvin et al. 1989) indicate significantly higher (>1000 m) Pliocene/Pleistocene erosion in the Barents Sea.

Table 2.2: Sediment yield from selected areas

AREA	T/KM/YR	TYPE OF EROSION
	270 T/KM/YR = 0.1 mm/YR)	
USA/Gulf	59*	fluvial
Europa/West	12*	fluvial
Huangho	1400*	fluvial
SE-Asia, Himalaya-Indus	796*	fluvial/glacial
Southern Alaska	1000*	glacial/fluvial
Kongsvegen, Svalbard	1250	glacial
Eastern Svalbard	420	glacial/(fluvial)
Nigardsbreen, Norway	730+(max)	glacial
1968-1971	255+(min)	

*:- Milliman & Mead (1983), +:- Kjeldsen (1983)

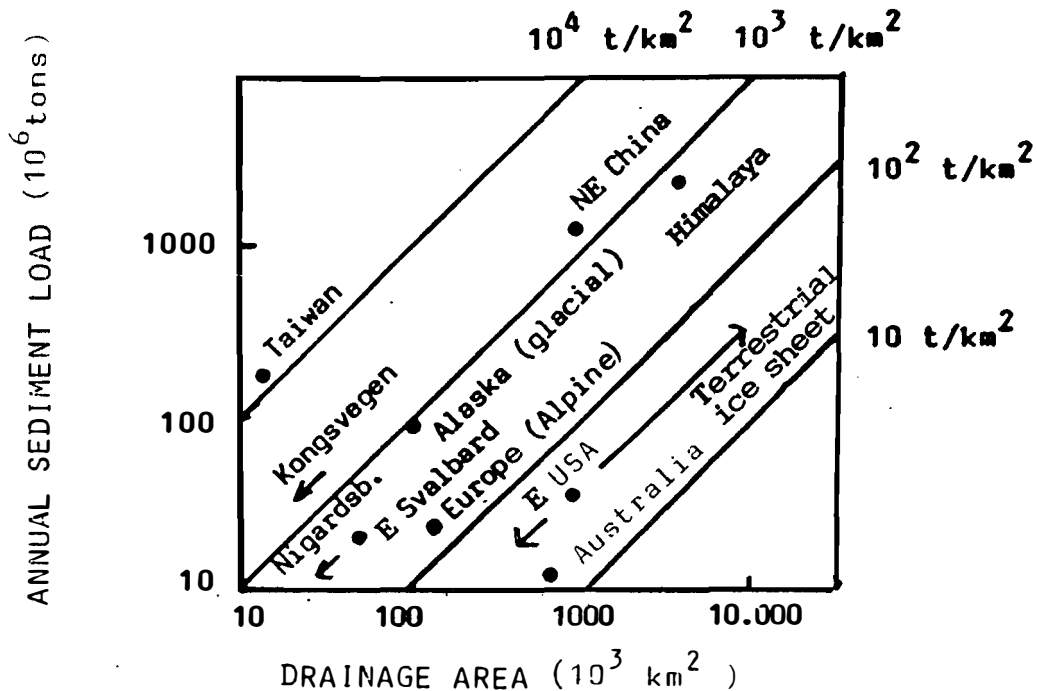


Fig. 2.24. Relationship between sediment yield and drainage area for various environments

The new datings of the glacial sediments off the southwestern Barents Sea are very important for understanding the Late Cenozoic development of the region. If the datings and the calculation of the volume of glacial sediments are correct, it may lead to the following two alternative conclusions:

- The Barents Sea has been ice covered during considerable parts of the Pliocene/Pleistocene - "Permanently Ice Covered" (based on the assumption of 0.5 -1.0 mm annual erosion)

- The idea of glacial erosional rates in the range of 0.5 - 1.0 mm per year has to be revised and increased significantly - in the order of tens of mm per year (based on the assumption of alternating ice-free and ice-covered periods through the Pliocene/Pleistocene)

Alternatively, the dating and estimates of sediment volume and erosional rate may be incorrect, and it is essential to confirm these values before further calculations of erosional rates are undertaken.

3. PERMAFROST IN SVALBARD AND EVALUATION OF THE POSSIBILITIES FOR SUBMARINE PERMAFROST AND GAS HYDRATES IN THE BARENTS SEA AND SVALBARD

3.1. Permafrost conditions in Svalbard

3.1.1 Spitsbergen (based on Liestøl 1980)

Permafrost covers the entire land area on Spitsbergen with depths varying between 200 and 450 m in the central parts. The mean air temperature is well below zero; in the period 1931-60 the annual standard normals of the air temperatures were -3.9°C for Isfjord Radio and -4.8°C for Longyearbyen. This period, however, was extremely warm, and the temperature has been lower both earlier and later. Besides, there is a considerable variation in temperature between the coast and the inland.

a) Permafrost depth

Few direct measurements of the permafrost thickness have been made. According to Orvin (1944), the temperature in the coal mines at Ny-Ålesund on NW Spitsbergen passed melting temperature at 130 - 140 m near the foot of the steep mountain side of Zeppelinfjellet, but further out on the plain 0°C was not reached at 150 m depth. In 1976 a permafrost depth of 140 m was measured in a borehole near Brøggerbreen in the same area (for locations see figure 3.1). Lutkevich (1937) reports that the USSR for coaldrilling in Colesbukta penetrated the permafrost at a depth of 75 m. In the coal mines in Adventdalen the thickness is between 250 and 450 m. These mines go through steep mountains where deep permafrost would be expected. The temperature has also been measured in a "stoll" underneath the glacier tongue of Larsbreen (Fig. 3.1). Where the overlying rock was about 50 m thick and the glacier thickness above about 100 m, the temperature was -2.4°C . With a temperature gradient of 1°C to 40 m, the 0° isotherm should be found at about 250 m. Under the glacier Foxfonna nearly the same temperature conditions were found. In a 64 m deep borehole at the bottom of this glacier the temperature was -3.3°C and in the mine 220 m below the surface -0.2°C . In 1956 H. Major measured temperatures in two boreholes on the southern side of Adventdalen and three near the Svea coal mines at the head of Van Mijenfjorden (Liestøl 1973).

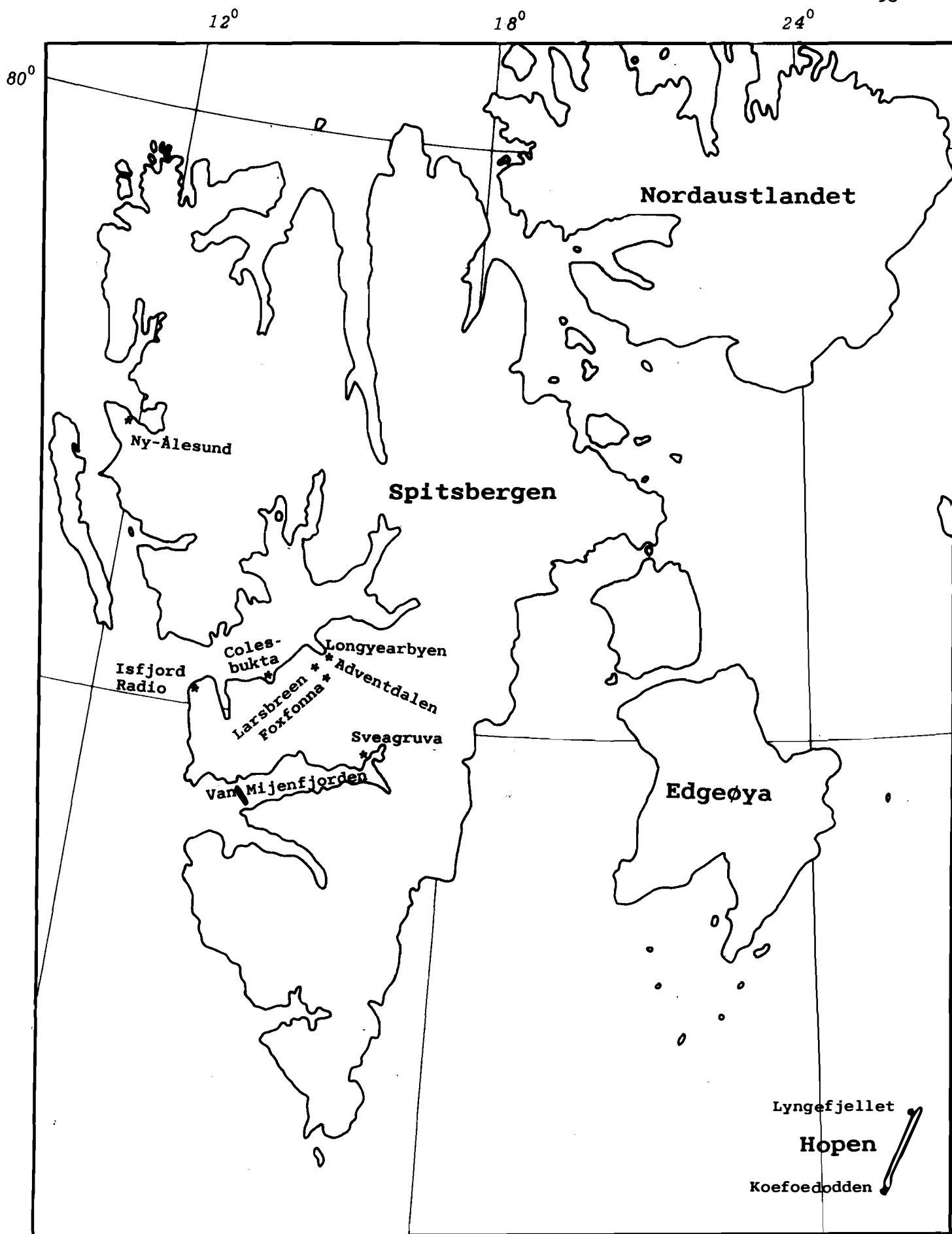


Fig. 3.1. Map showing localities where permafrost thicknesses have been measured in Svalbard.

The permafrost depth in Sarkofagen, a 500 m high mountain ridge SW of Longyearbyen, was 450 m, and the temperature gradient about 50 m/°C in the lower part. The other measurement, made 5 km further south at the bottom of Endalen, showed a depth of 200 m and a temperature gradient of about 40 m/°C. One of Major's measurements near Sveagrava was made in a hole 500 m a.s.l. halfway up the slope of Liljevalchfjellet. The depth to the 0° isotherm was 280 m. The other two holes were drilled in the flat area between the sea and the mountain foot. The reliability of measurements made in these two holes was not as good as in the others, but gave an indication of a permafrost thickness of more than 200 m. A much deeper permafrost would be likely at the first hole on Liljevalchfjellet. Reasons for this shallow depth might be the influence of adjacent glaciers and the black shale absorbing more radiation energy in the south-facing mountain slope. As figure 3.2 shows, the upper part of the temperature curve has an almost vertical gradient. The explanation might be the warm climatic period between 1920 and 1960. Such large and longlasting warm periods should manifest themselves in a warming-up of the upper layers of the permafrost. Theoretic calculations also show that the depth of this heat wave caused by the climatic change is reasonable. The same phenomenon is observed in boreholes in Alaska (Gold & Lachenbruch 1973).

b) Glaciers and lakes, influence on permafrost depth

Close attention should be given to the glaciers and their influence on the permafrost and the ground-water system. All glaciers of some magnitude on Spitsbergen are of the so called subpolar type with melting temperatures in the higher accumulation area. This phenomenon causes openings in the continuous permafrost layer, through which water will sink into the ground below the glacier bed and cause a groundwater stream to flow downwards under the permafrost layer and out to the coast and the sea (Fig. 3.3). The greater part of the meltwater will, however, particularly in the summer, follow the glacier bottom through tunnels in the ice and emerge in the front of the glacier.

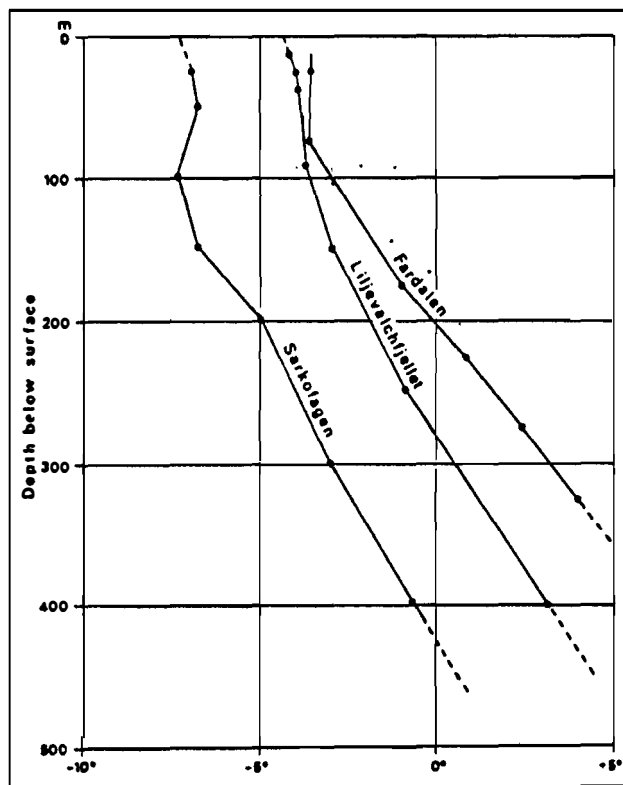


Fig. 3.2. Temperature curves from three boreholes on Spitsbergen (from Liestøl 1980).

Also during winter, water will come out from underneath the glacier snout, but in much smaller quantities, making conspicuous large icings, some more than 5 m thick, and covering areas of more than one square kilometre. These icings show whether a glacier is polar or subpolar. They are very noticeable in the field, and are clearly visible on air photos taken in mid-summer when the snow cover has melted while these thick layers of ice still remain. Measurements of the water in the winter show a conductivity more than ten times higher than the ordinary summer melt water. This difference indicates that a high percentage of groundwater is mixed with the "glacial" groundwater and the sub-glacial bottom meltwater. The bottom melting is in the order of $0.2 \text{ l sec}^{-1} \text{ km}^{-2}$. The quantity of water stored in the glacier after the summer melting is unknown, but it must be assumed that part of this volume gradually drains during the winter. It has been presumed that salts in the glacier ice gradually migrate out of the ice. In the winter, when discharge from the glacier is low, this salt could be responsible for a part of the high conductivity measured.

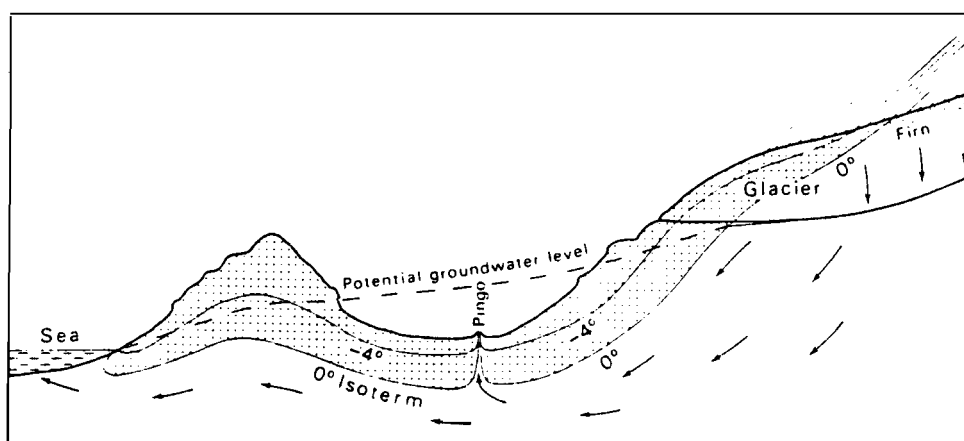


Fig. 3.3. Vertical profile of the permafrost layer and groundwater movement from the glacier accumulation out to the coast (from Liestøl 1980).

Lakes will also greatly influence the permafrost. Lake ice seldom exceeds a thickness of 2 m, and even small lakes have large heat reservoirs. Werenskiold (1922) made some theoretical calculations of the permafrost depth and the influence of sea and glaciers. He found that the permafrost would stretch some 200 m off shoreline in shallow water with a sea temperature of 0°C . The same would be the case with a lake or a glacier with a bottom temperature of 0°C . If lakes and glaciers measure less than 400 m across, the permafrost should form a continuous layer underneath.

3.1.2 Bjørnøya

The mean air temperature on Bjørnøya during the period 1951-80 is -2.1°C (Steffensen 1982). The permafrost depth is shallow, varying from about 20 m to 100 m below the highest mountains.

3.1.3 Hopen

The mean air temperature was as low as -6.1°C during the period 1951-80 (Steffensen 1982). The Fina Group drilled two wells on Hopen in 1973. One was drilled at Koefoedodden, in the shoreline area, near the southern end of Hopen. This well penetrated the permafrost at a depth of 138 m. The other well was drilled on Lyngfjellet, a 250 m high mountain, near the northern part of the island. The permafrost boundary was here at 238 m depth.

3.2 Thermal regimes and geological history

The existence of permafrost and gas hydrate is closely linked to the thermal history of an area. Based on the previous section: "Late Cenozoic Geological History", the thermal regime for the Late Cenozoic can be outlined. In broad terms the main geological events of the last 1 mill. years can be divided into glacial and interglacial cycles and their associated fluctuations of the sea level. Our knowledge of the pre-Weichselian Quaternary geological history is very limited and we therefore confine our discussions to the Weichselian and the Holocene. However, the principles outlined for this period will also account for older glacial - interglacial cycles.

3.2.1 Mid Weichselian/Early stage of the Late Weichselian (~50 - 20 ka)

In accordance with our model, the Barents Sea was not glaciated during the Mid Weichselian. However, due to the global sea level lowering of approximately 50 -75 m, Spitsbergenbanken was subaerially exposed. As regards the Late Weichselian ice sheet we have indicated two modes of formation (Fig. 2.14); one with a "delayed" growth at about 20 ka, while the other concept suggests glacial expansion at about 25 ka. According to the first idea, Spitsbergenbanken was subaerially exposed down to 120 m at the onset of the Late Weichselian glaciation (Fig. 3.4). Considering isostatic adjustment, it is probable that the relative sea level may have been lower, down to depths of 150 m. In figure 3.4 we have indicated the thermal regime for an early stage of glaciation (delayed glaciation). During this stage, the shallower parts of the Barents Sea were exposed to tundra conditions, while the deeper parts were covered by Arctic water. We have indicated a significantly greater ice cover for Svalbard than the present, but the ice sheet had not expanded into its adjacent marine areas.

3.2.2 Late Weichselian (18 - 14 ka)

For the last glaciation (i.e. Late Weichselian), the Barents Sea and the Svalbard archipelago were covered by grounded ice, leaving the shelf north and west of Svalbard non-glaciated and subaerially exposed

(Landvik et al. 1988). The temperature distribution is indicated in figures 3.5. and 3.6. The surface temperature of the tundra areas north and west of Svalbard is tentatively taken as -15°C (Fig.3.4).

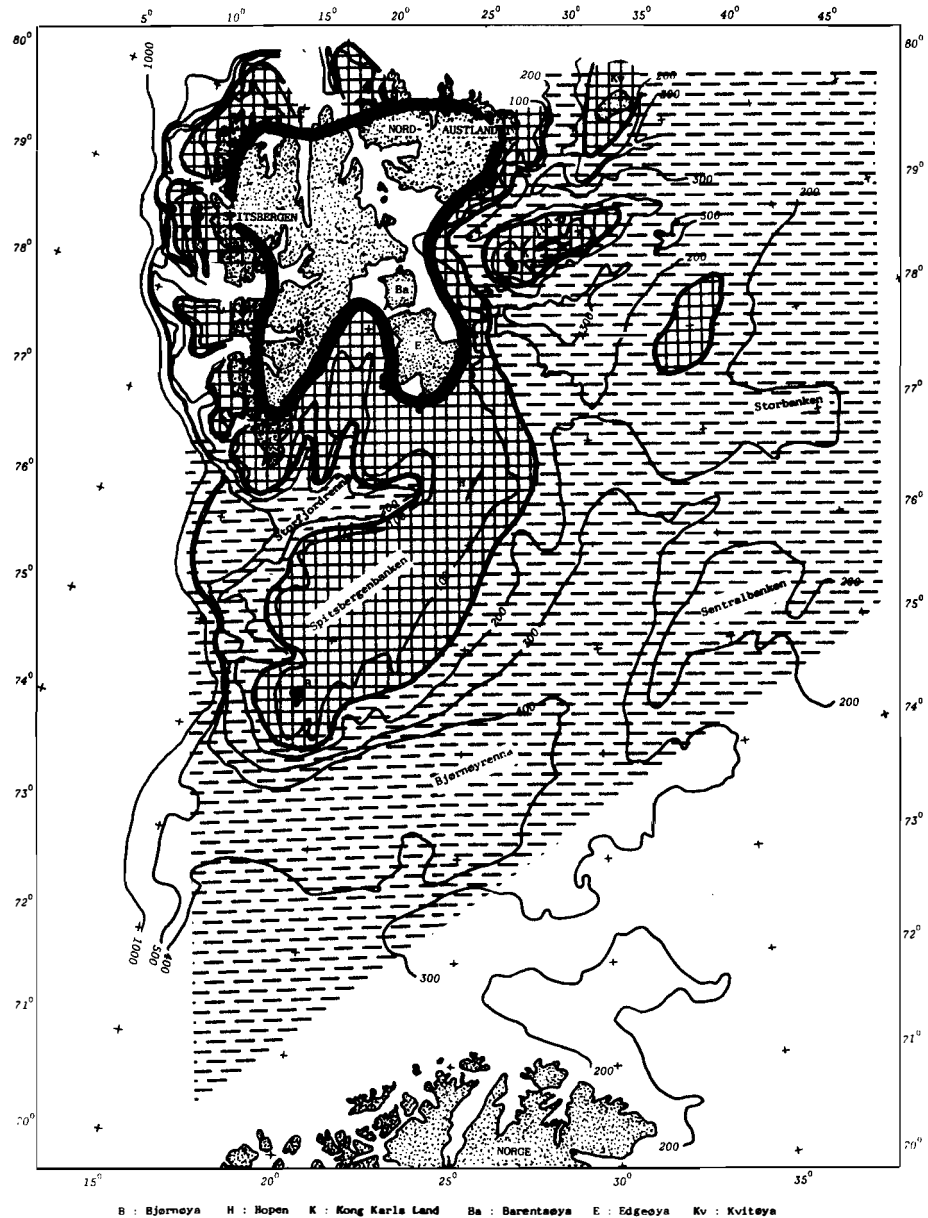


Fig. 3.4. Thermal regime: Early stage of the Late Weichselian glaciation: "delayed" model.

which is similar to the estimates of the temperature during glacials for other parts of the Arctic (Carter et al. 1986). For the internal parts of the Svalbard/Barents Sea Ice Sheet, the basal temperature is in the range of -1 to -2°C . In marginal parts the temperature is below the pressure melting point, except for areas occupied by ice

streams. The thermal regime for a limited ice model is shown in figure 3.6. The main difference between the two models is the possibilities of temperatures below pressure melting point along the margins of Spitsbergenbanken in the limited model. It is to be noted that the bottom temperature in the outer part of Bjørnøyrenna is independent of the model used. In both cases the bottom temperature is estimated to $-1,5^{\circ}\text{C}$, whether the area is covered by ice at pressure melting point or by Arctic Water.

3.2.3 End of the Late Weichselian (14 - 10 ka)

The main part of the marine based Barents Sea Ice Sheet probably disintegrated by calving relatively early, approximately at 13 - 12 ka, and at that time, Atlantic water was not yet flowing into the area (Hald & Vorren 1987) (Fig. 3.7). Emergence curves from the eastern islands in the Svalbard archipelago show 50 - 100 m Holocene glacioisostatic uplift (Hoppe 1970; Salvigsen 1981). Thus, at the transition from glacials to an early stage of interglacial, the water depth in the central, northern Barents Sea was up to 100 m deeper than at present. During this period, Arctic Water ($\sim -1,5^{\circ}\text{C}$) entered and covered the entire Barents Sea. The duration of these transitional periods seems to have been short, in the order of 1-3 ky.

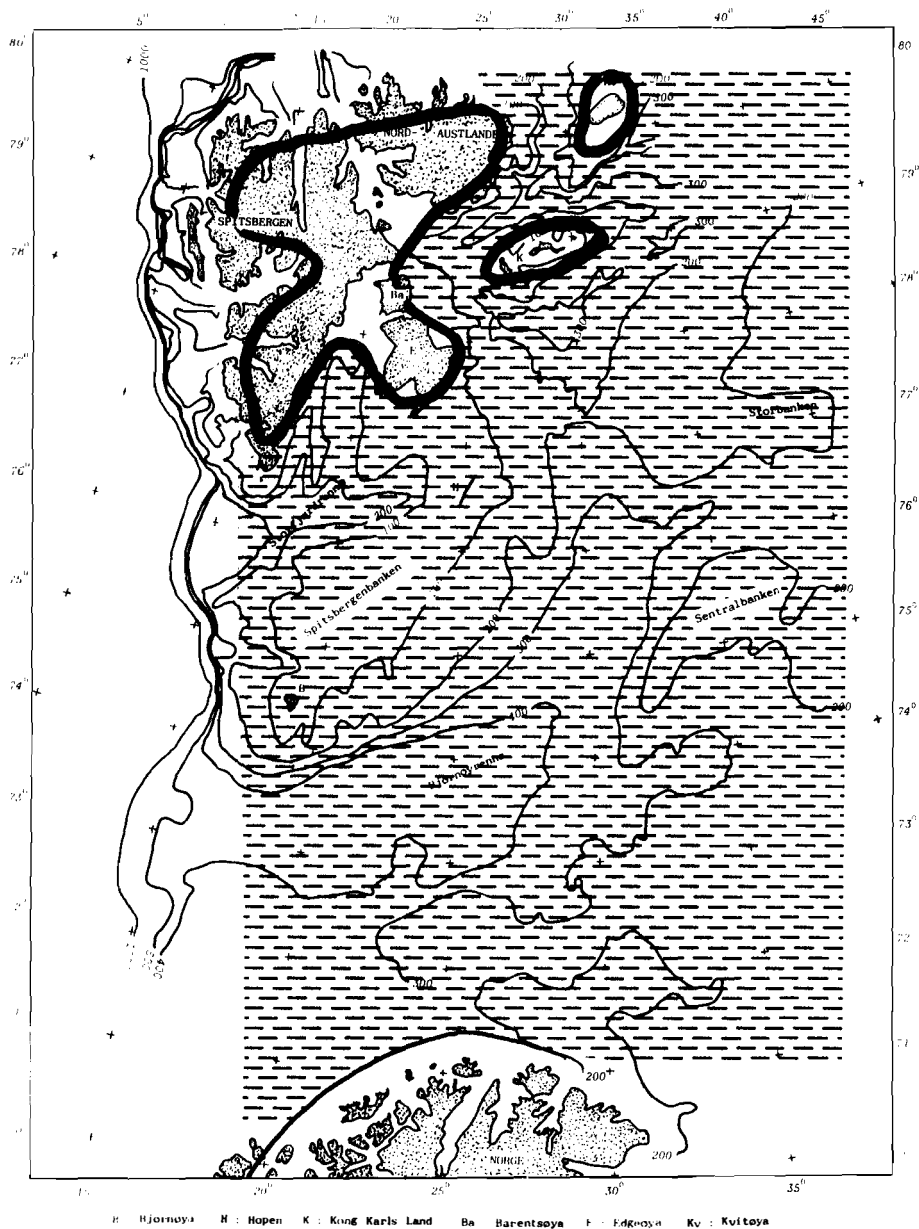
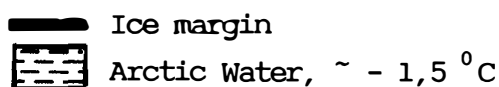


Fig 3.7. Thermal regime: End of Late Weichselian



3.2.4 Holocene

The present day situation can be compared to an interglacial period: Atlantic Water (+ 2-4⁰C) flows northwards into the southwestern parts of the Barents Sea and along the shelf west and north of Svalbard. Additionally, Atlantic Water also enters the Barents Sea from the north. The boundary between the warm Atlantic Water and the cold Arctic Water is approximately located at the 200 m depth contour (Fig. 3.8.), leaving the shallower parts of the Barents Sea with sub-zero temperatures (~ - 1.5 to -1⁰C) throughout the year. It is important to note that during the summer months (July/August), the temperature rises above zero at the shallowest parts of

Spitsbergenbanken (< 50 m water depth).

The distribution of Atlantic and Arctic Water is partly controlled by the seabed topography. During the early stages of an interglacial period, with greater water depths (due to glacioisostatic depression), the Atlantic Water may have penetrated further to the north. Analyses of mollusc faunas on Spitsbergenbanken show, however, that Arctic Water has been steadily flowing across the area during the Holocene. By analogy, we suggest that the present day water and temperature distribution can be applied as a first approximation for interglacial periods.

3.2.5 Conclusions

The discussion of the thermal regime has been concentrated to the last 50 ky. Our knowledge of the previous Cenozoic geological history is too limited for any longer time perspective. This period illustrates, however, the pattern of Late Cenozoic climatic variations: 1) glaciations, sea level lowering and sub aerial exposure, and 2) ice recession and transgression of Arctic Water in the northern part and Atlantic Water in the southern part of the Barents Sea. Several ideas on the Weichselian glaciations exist, and in the forthcoming discussion, we have proposed two models. Model I has the lowest probability for formation and preservation of permafrost and ice-bearing strata, while model II presents the most extreme concept in terms of permafrost.

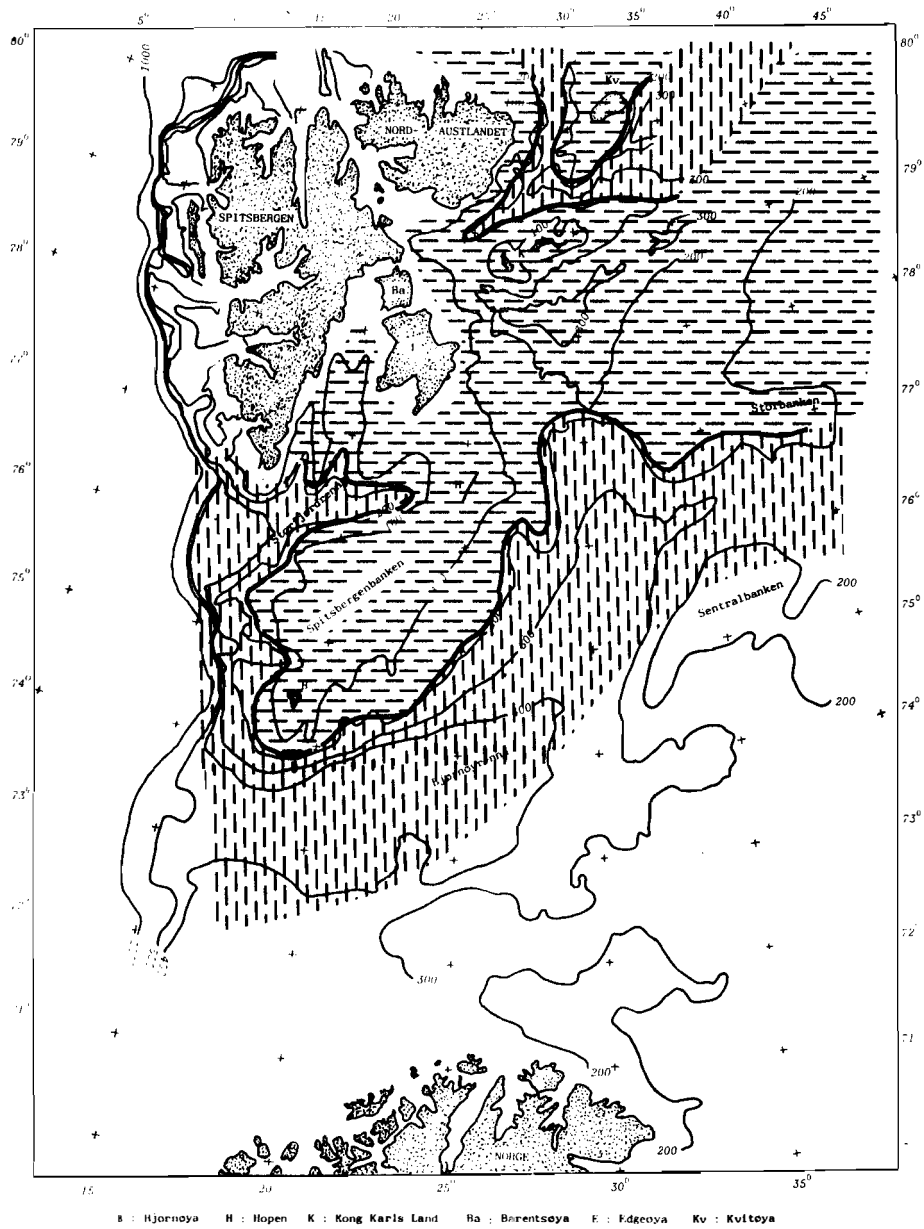


Fig. 3.8. Thermal regime: Holocene (interglacials)



Arctic Water, -1°C



Atlantic Water, $+2 - +4^{\circ}\text{C}$

Model I

- 1) A limited sea level lowering in Mid Weichselian of approximately 40 m. Only the most shallow part of Spitsbergenbanken and the shelf north and west of Svalbard are subaerially exposed.
- 2) Atlantic Water extends into the outer part of Bjørnøyrenna and flows along the west coast of Svalbard in Mid Weichselian time.
- 3) The Barents Sea Ice Sheet forms and expands from Svalbard into the adjacent marine areas. This expansion was at the end of O-isotope stage 3, ~30ka.
- 4) The Barents Sea is entirely covered by grounded ice, extending to the shelf edge, ~20 -18 ka.
- 5) At 16 ka, the ice sheet receded to the shallower areas, leaving Bjørnøyrenna as a calving bay.
- 6) The Barents Sea Ice Sheet calved off at 13-12 ka and Arctic water covered the entire area.
- 7) The onset of the present day conditions occurred at 10 ka.

Model II

- 1) A limited sea level lowering in Mid Weichselian, approximately 40 m, and only the very shallowest part of Spitsbergenbanken and the shelf north and west of Svalbard are subaerially exposed.
- 2) The formation of the Barents Sea Ice Sheet occurred at Late Weichselian max. sea level lowering, leaving areas down to 150 m present day water depth subaerially exposed. The rest of the shelf was covered by Arctic Water.
- 3) The shallower parts of the Barents Sea are covered by grounded ice, "limited model", leaving Bjørnøyrenna and areas deeper than 300 m as calving bays. The formation of the ice sheet starts at 18 ka.
- 4) The Barents Sea Ice Sheet is calved off at 13-12 ka, and the Arctic water covered the entire shelf.
- 5) The onset of the present day conditions occurred at 10 ka.

As seen from both models, the sea floor temperature in the central, shallower parts (< 200 m water depth) of the Barents Sea is independent of the two models, and would have remained stable at approximately -1 to -2 °C throughout the Weichselian. These regions have either been covered by cold Arctic Water, or they have been covered by grounded glacial ice being at the pressure melting point, e.g. -1 - -2 °C.

On Spitsbergenbanken the models indicate large variations in physical setting: In model I, the shallowest parts (< 50 m water depth) should have been subaerially exposed to low annual mean temperatures, approximately -15 °C for more than 20 ky. In model II, areas down to the present-day 150 m contour are exposed, and the period of exposure is expanded. The duration of subaerial exposure for the area between 50 and 150 m is 4 ky. In interglacial periods like the Holocene, the area is submarine and the temperature is in general -1 to -1.5 °C, while the temperature in the shallowest part of the Spitsbergenbanken may rise slightly above zero in July and August.

In Bjørnøyrenna, the sea floor temperature during interglacial periods is approximately +2 °C, while during glacials, the temperature drops to i) -1 to -2 °C, e.g. covered by Arctic Water (Model II) or ii) covered by ice at pressure melting point, -1 °C (Model I).

The greatest temperature variations are found for the shallow shelf areas west and north of Svalbard. During glacials, these areas (except for when the ice expanded to the shelf edge) have had tundra conditions, and annual temperature may be lowered to -15 °C. Transgression of warm Atlantic water during the end of the glacials/early stage of interglacials, causes a rise of the sea floor temperature to +2 - +4 °C.

Table I: Maximum ice model

Area	Time: 50-30ka		Time: 30- 22ka		Time: 22-16ka		Time: 16-12ka		Time: 12-10ka		Time: 10-	
	Temp	Environ.	Temp	Environ.	Temp	Environ.	Temp	Environ.	Temp	Environ.	Temp	Environ.
Spitsbergenbanken.<50m	-15	subaerial	-1.5	subgl	-2.0	subgl	-1.5	subgl	-1.5	Arctic W	-1.5	Arctic W
Spitsbergenbanken.>50m	-1.5	Arctic W.	-1.0	subgl	-1.5	subgl	-1.0	subgl	-1.5	Arctic W	-1.5	Arctic W
Spitsbergenbanken.W parts					-5.0	subgl						
Bjørnøyrenna, outer part	+2.0	Atlantic W	-1.5	Arctic W	-1.5	subgl	-1.5	subgl	-1.5	Arctic W	+2.0	Atlantic W
Bjørnøyrenna, inner part	-1.5	Arctic W.	-1.5	subgl	-2.0	subgl	-1.5	subgl	-1.5	Arctic W	+2.0	Atlantic W
Central Barents Sea/ Storbanken	-1.5	Arctic W.	-1.5	subgl	-2.0	subgl	-1.5	subgl	-1.5	Arctic W	-1.5	Arctic W
Kong Karls Land area.<50m	-15	subaerial	-1.5	subgl	-2.0	subgl	-1.5	subgl	-1.5	Arctic W	-1.5	Arctic W
Shelf areas NEW of Svalbard.<50m	-15	subaerial	-15	subaerial	-15	subaerial	-15	subaerial	+2.0	Atlantic W	+2	Atlantic W

(NB: 120m)

Table I: Limited ice model

Area	Time: 50-30ka	Time: 30- 22ka	Time: 22-18ka	Time: 18-12ka	Time: 12-10ka	Time: 10-
	Temp Environ.	Temp Environ.	Temp Environ.	Temp Environ.	Temp Environ.	Temp Environ.
Spitsbergenbanken, <50m	-15 subaerial	-15 subaerial	-15 subaerial	-1,5 subgl	-1,5 Arctic W	-1,5 Arctic W
Spitsbergenbanken, 50-150	-1,5 Arctic W.	-1,5 Arctic W	-15 subaerial	-1,5 subgl	-1,5 Arctic W	-1,5 Arctic W
Spitsbergenbanken, 150-300	-1,5 Arctic W	-1,5 Arctic W	-1,5 Arctic W	-5 subgl	-1,5 Arctic W	
Björnøyrenna, outer part	-1,5 Arctic W	-1,5 Arctic W	-1,5 Arctic W	-1,5 Arctic W	-1,5 Arctic W	+2,0 Atlantic W
Björnøyrenna, inner part	-1,5 Arctic W.	-1,5 Arctic W	-1,5 Arctic W	-5 subgl	-1,5 Arctic W	+2,0 Atlantic W
Central Barents Sea/ Storbanken	-1,5 Arctic W.	-1,5 subgl	-1,5 Arctic W	-1,5 subgl	-1,5 Arctic W	-1,5 Arctic W
Kong Karls Land area, <50m	-15 subaerial	-15 subaerial	-1,5 subaerial	-1,5 subgl	-1,5 Arctic W	-1,5 Arctic W
Shelf areas NEW of Svalbard, <50m	-15 subaerial	-15 subaerial	-15 subaerial	-15 subaerial	+2,0 Atlantic W	+2 Atlantic W

(NB: 120m)

3.3 Distribution of permafrost and ice-bearing sediments and rocks in the Barents Sea

According to the thermal definition of permafrost, considerable parts of the upper sediment sequence in the Barents Sea have permafrost. However, in marine environments with saline pore water, ice-bonded or bearing sediments will not be present at temperatures above $-1,8^{\circ}\text{C}$. The exact freezing point will depend on salinity and also the lithology. As stated in the introduction chapter, the water in clayey sediments is affected by the clay mineralogy, and ice-free clays have been reported even with temperatures below -10°C (S. Blasco pers. comm. 1988). When discussing permafrost in marine environments, it is common to discuss ice-bearing or ice bonded material.

In accordance with the two models, ice-bearing strata may have formed in the following regions:

- The shelf west and north of Svalbard
- Spitsbergenbanken and the coastal areas of eastern Svalbard exposed during low sea levels (e.g. Kong Karls Land)

Essential for the preservation of sub-marine permafrost and ice-bearing strata is the sealing of frozen fresh-water bearing sediments by transgression of cold Arctic Water. This has only been the case for Spitsbergenbanken and the coastal areas in eastern Svalbard. As shown from temperature modelling in the Beaufort Sea (Fig.1.9), the

temperature in the 600 m thick sub-marine permafrost zone will rise to barely sub-zero ($-2 - 3^{\circ}\text{C}$) conditions within 2000-3000 years after the transgression of cold Arctic Water. However, on the Svalbard shelf the thickness of the Weichselian permafrost zone is suggested to be significantly less. The present-day permafrost depth in Svalbard, 200-400 m is a possible analogue. The ice will melt due to migration of "warm" saline pore water into sediments from above and geothermal heat from below. Lachenbruch et al. (1982) have estimated the thaw rate from below caused by the geothermal heat flux to be 15 m/1000 years. The melting rate from above is not known, but most likely it will be higher due to the circulation of pore water. Melting of ice is a slow and energy consuming process (80 cal/g). However, as indicated from the numbers above, the time-span of almost 10 ky is sufficient to thaw the ice-bearing layers, at least in a 150 m thick zone. Due to interglacial transgression of warm Atlantic Water, we conclude that there is no sub-sea permafrost or ice-bearing strata left on the shelf west and north of Svalbard.

In the Barents Sea, ice-bearing strata may have formed in shallower parts of Spitsbergenbanken during the Mid Weichselian. According to the "delayed model" (Chapter 2), the area of subaerial exposure on Spitsbergenbanken increased during the early stage of the Late Weichselian, and ice-bearing strata may have formed down to present-day 120-150 m waterdepth.

Another important factor for the possible occurrence of ice-bearing strata in the Barents Sea is the thin, < 10 m cover of unlithified sediments. The ice-bearing layers have to form in the Mesozoic bedrock, and not in unlithified sediments, which is the case in the Beaufort Sea. The formation of ice-bearing layers in the Barents Sea will therefore be very different from the Beaufort Sea. Here, the ice-bearing strata is generally localized to fossil fresh-water bearing fluvial channels, formed under sub-aerial exposure during glacials.

The formation, and also the preservation, of ice-bearing layers is influenced by the existence of saline porewater in the submerged marine areas. At temperatures $-1 - -2^{\circ}\text{C}$, it is fundamental that if ice-bearing strata is going to be preserved under i) a grounded ice at pressure melting point and/or ii) Arctic Water, the saline porewater has to be replaced by fresh water. This replacement will depend on the porosity and permeability of the bedrock, as the thickness of unconsolidated sediments deposited under a fresh water regime (the till) is very thin (< 5 m) in these regions. In general, the Mesozoic rocks in Svalbard have low porosity,

approximately 10% (Elverhøi & Grønlie 1981), and low porosity values are also suggested for the Mesozoic rocks sub-cropping at Spitsbergenbanken. The development of permafrost in the surface will also represent an effective barrier for percolation of fresh water into the underlying bedrock during subaerial exposure. Migration of fresh water through subsurface aquifers is also unlikely due to the reduced topographic gradient. Accordingly, the probability for formation of ice-bearing strata seems low, with the lowest probability for the "maximum glaciation model", due to the limited time interval of subaerial exposure compared to the "delayed model" (Chapter 2).

3.3.1 In situ temperature measurements

In situ measurements of the sub-bottom temperature at 110 m water depth south of Hopen show sub-zero temperatures for the upper 15 metres (IKU News 1988) (Fig. 2.27). The measurements have been obtained in a region which may have been subaerially exposed during the Late Weichselian sea level lowering. The positive temperatures observed already at 15 m depth strongly suggest that if ice-bearing strata was formed in the early phase of the Late Weichselian, these features have now melted. The sub-zero temperature in the upper 15 m reflects the present-day conditions in the region, which is permanently covered by cold ($\sim -1,5$ °C) Arctic Water.

The observation of positive temperatures in the upper part of the sediments on the southern part of Spitsbergenbanken is very important for the conclusion of possible ice-bearing strata. Spitsbergenbanken is the only region in the western Barents Sea which may have been sub-aerially exposed and flooded by cold Arctic Water in post-glacial time. Up to now, only one in situ test has been carried out, but from our paleoclimatic model of the region, we conclude that ice bearing strata will not be present in water depths exceeding ~ 100 m. For the shallower parts of Spitsbergenbanken, we still lack reliable information, and further investigations are needed for finally proving the existence or non-existence of ice bearing strata on shallower parts of Spitsbergenbanken.

3.3.2 Temperature profiles: Hopen - the Barents Sea

One possible formational mode of submarine permafrost is continuation of onshore permafrost into offshore regions. To test this in Svalbard, model calculation has been carried out for Hopen, where onshore exploration drilling close to the shoreline indicated ice-bearing permafrost down to approximately 140 m. Static temperature calculations were carried out along a profile running from onshore Hopen and 1 km out from the shoreline. Constant temperatures were anticipated for onshore Hopen, at 540 m depth in the ground (Fig. 3.9).

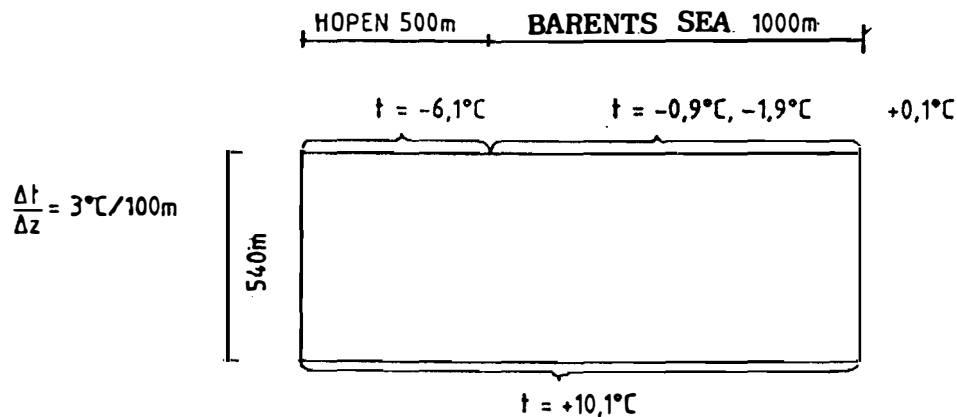


Fig. 3.9. The model for the temperature calculations

Three examples with different, but constant water temperatures, $t = -0.9^{\circ}\text{C}$, -1.9°C and 0.1°C are shown in figures 3.10.- 3.12. The calculations are carried out independently of the local geology. A top cover of unconsolidated sediments would have reduced the permafrost depth. The temperature gradient ($30^{\circ}\text{C}/\text{km}$) is based on measurements on Spitsbergen (Fig. 2.11). The calculations show that the onshore conditions only influence the temperature in the nearshore area, 50 - 100 m from the shoreline. Further out, the sub-bottom temperatures are influenced only by the bottom water temperature and the geothermal gradient. Hence, as a conclusion, onshore permafrost in Svalbard is in general unlikely to continue significantly more than 100 m offshore.

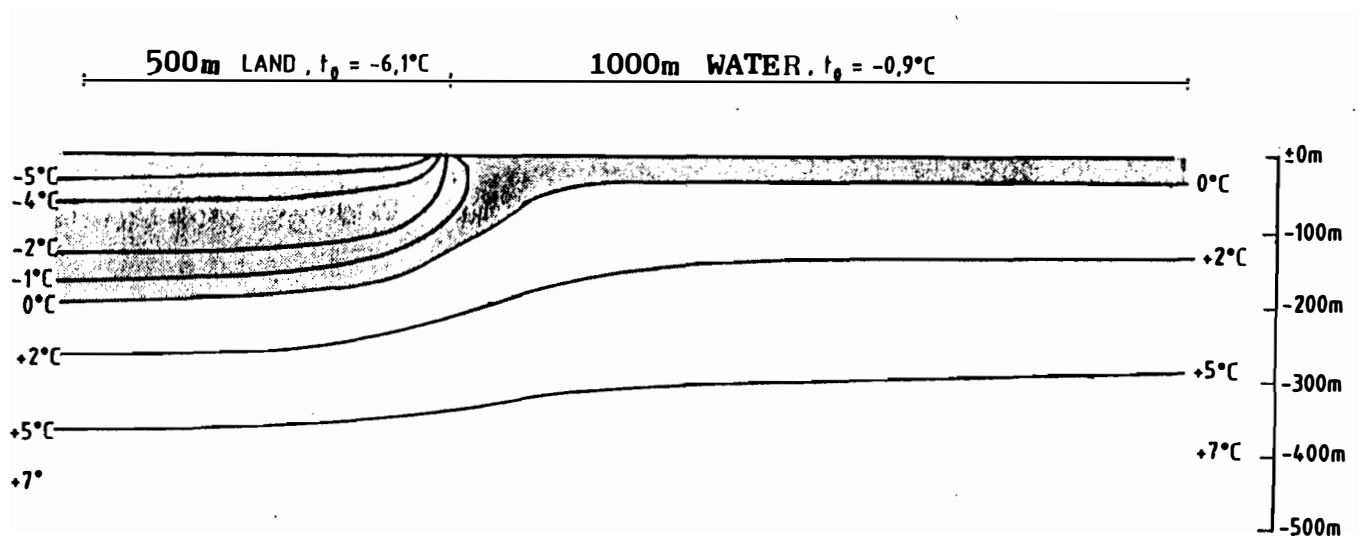


Fig. 3.10. Calculated temperature profile with a sea bottom temperature corresponding to -0.9°C .

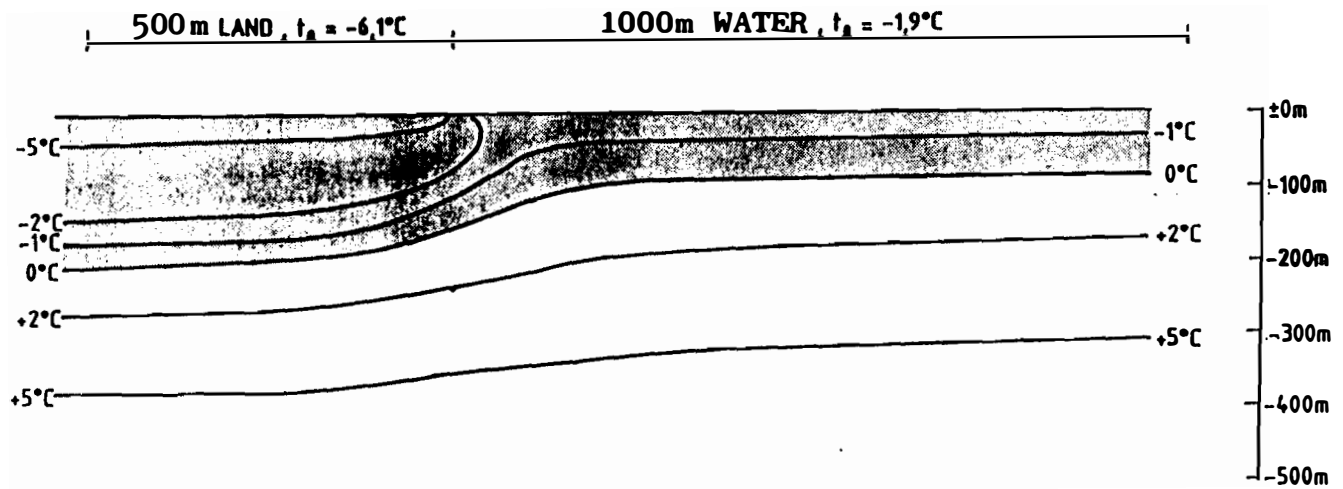


Fig. 3.11. Calculated temperature profile with a sea bottom temperature corresponding to -1.9°C .

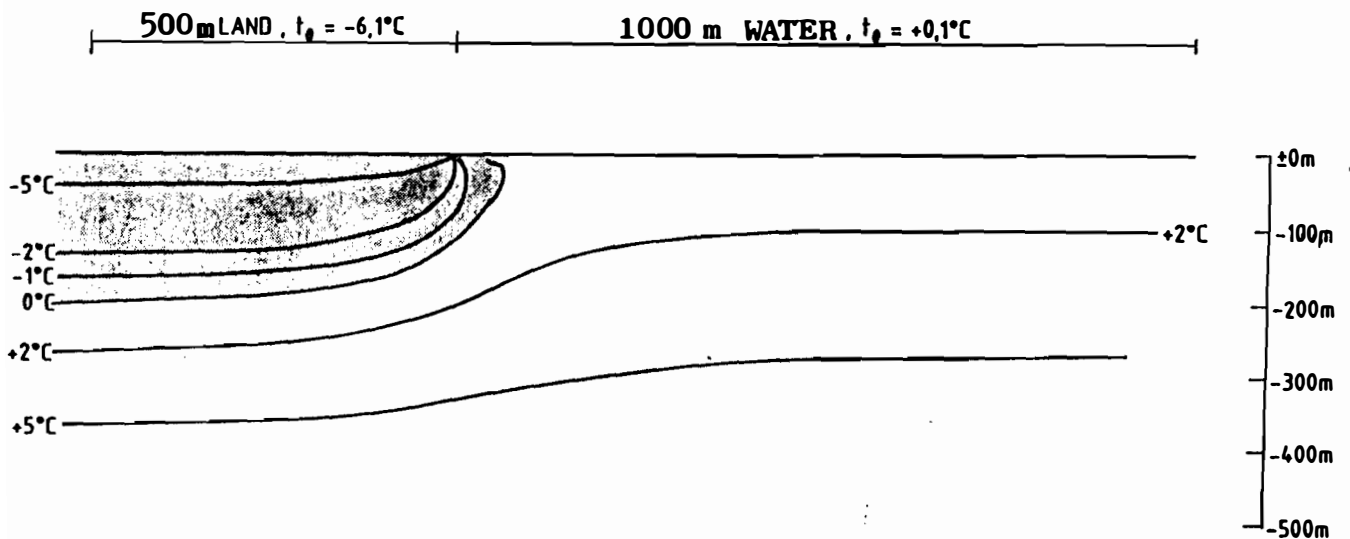


Fig. 3.12. Calculated temperature profile with a sea bottom temperature corresponding to 0.1°C .

3.3.3 Conclusions

In accordance with the paleothermal regime and the geological settings of the area, the discussion on the existence of permafrost and ice-bearing layers can be summarized as follows:

- 1) Permafrost is defined in terms of temperature, and thus areas covered with Arctic Water are by definition permafrost areas, because the temperature at the sea bed is less than 0°C throughout the year.
- 2) The main part of the unconsolidated sediments is marine deposits. Due to the saline porewater, causing a depression of the freezing point, ice bearing layers will not form in temperatures above -1.8°C .
- 3) In situ temperature measurements at 110 m water depth at the southern slope of Spitsbergenbanken show positive temperatures below 15 m. Combined with the paleoclimatic history, we therefore conclude that ice-bearing strata cannot exist in this region at water depths greater than 100 m.
- 4) For shallower (< 100 m) parts of Spitsbergenbanken ice-bearing layers may have formed in periods of low sea level (Mid Weichselian and early phase of Late Weichselian). However, to preserve this permafrost in the subsequent thermal regime of approximately -1.5°C , the saline porewater would have to be replaced by freshwater. The low porosity of Mesozoic rocks subcropping at Spitsbergen-banken is, however, an efficient barrier to such a process. We therefore consider the existence of ice bearing layers unlikely also in this area.
- 6) There is still lack of in situ data from the shallow part of Spitsbergen, and in order to finally prove the idea of no ice-bearing strata in this region either, we recommend further in situ testing.

3.4 Possible occurrence of gas hydrates in the Barents Sea and in Svalbard

An evaluation of the possibilities of the existence of gas hydrates in the Barents Sea must be based on the present-day physiographic conditions. During several glaciations, the sub-ice temperatures most likely remained in the same range as the present-day bottom water

temperatures, but the pressure was significantly higher, due to the ice overburden. This may have changed the hydrate stability zone. However, hydrates formed under conditions in which they are unstable during interglacials are expected to be decomposed at present.

3.4.1 Thermal prediction of gas hydrate occurrence in the Barents Sea.

As shown in Chapter 1, the actual distribution of gas hydrates depends on specific temperature and pressure conditions and on the availability of hydrocarbon gases. In this chapter temperature and pressure data from the Barents Sea are evaluated to provide a rough identification of potential areas of gas hydrate stability.

Subsurface temperature data and a typical bottom water temperature can be superimposed on the hydrate stability curve to determine whether gas hydrates are stable in an area and, if stable, the depth range over which their occurrence might be expected.

As there is a general lack of deep borehole temperature data from the Barents Sea, a geothermal gradient of $31\text{ }^{\circ}\text{C}/\text{km}$ measured in a shallow well on Spitsbergenbanken (IKU News 1988) is here used for the whole area. Judge (1982) used a gradient of $26\text{ }^{\circ}\text{C}/\text{km}$ as typical for the Scotia and Labrador shelves, but pointed out the importance of lithology; the gradient in individual formations was found to vary from $17\text{ }^{\circ}\text{C}/\text{km}$ in sand to $35\text{ }^{\circ}\text{C}/\text{km}$ in shale.

The bottom water temperatures in the Barents Sea are discussed in Chapter 2 and shown on figure 2.4. In the areas of interest, i.e. areas in the northern part with water depth exceeding 200 m, a typical bottom water temperature of $1\text{ }^{\circ}\text{C}$ is used. In figure 3.13 the assumed values for the geothermal gradient and bottom water temperature are plotted on the methane hydrate stability curve, showing the resulting depths of hydrate stability for different water depths. Methane hydrate will be stable in areas with water depths exceeding approximately 280 m, and the zone of stability extends to a depth of approximately 400 m. Increasing the water depth to 350 m results in a hydrate stability zone extending down to approximately 550 - 600 m. If the bottom water temperature increases to $2\text{ }^{\circ}\text{C}$ (a probable bottom water temperature in Bjørnøyna), a water depth of 300 m is a minimum for hydrate stability. In that case, the hydrates will be stable to a depth of approximately 350 to 400m.

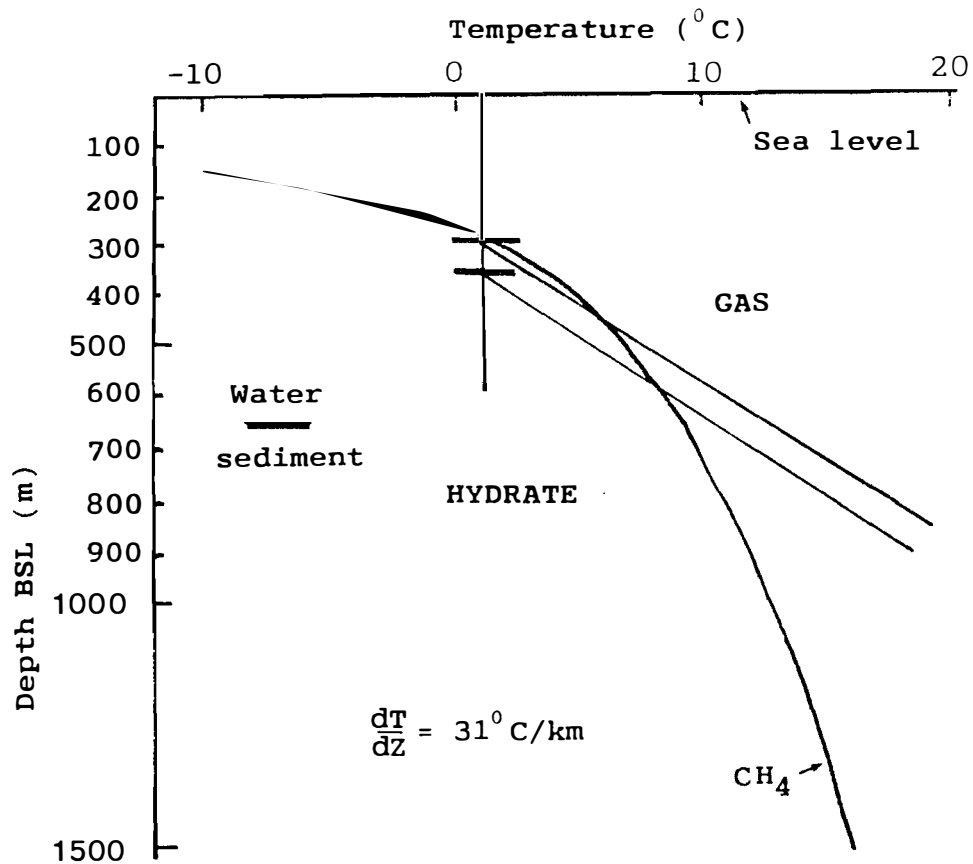


Fig. 3.13. Gas hydrate-prone zones in different water depths (280 m and 350 m) based on a typical bottom water temperature (1°C) and geothermal gradient (31°C/km) for the northern Barents Sea. The methane hydrate stability curve is taken from Judge (1982).

Figure 3.14 shows the resulting areas of methane hydrate stability in the northern Barents Sea. In Bjørnøya and Storfjordrenna a minimum water depth of approximately 300-350 m is indicated. Further north, 280-300 m of water is regarded as sufficient for methane hydrate stability.

These results do not imply that hydrates are present within the stable areas, rather they indicate that if methane gas and water exist in any horizon within that zone, hydrates will form given sufficient time.

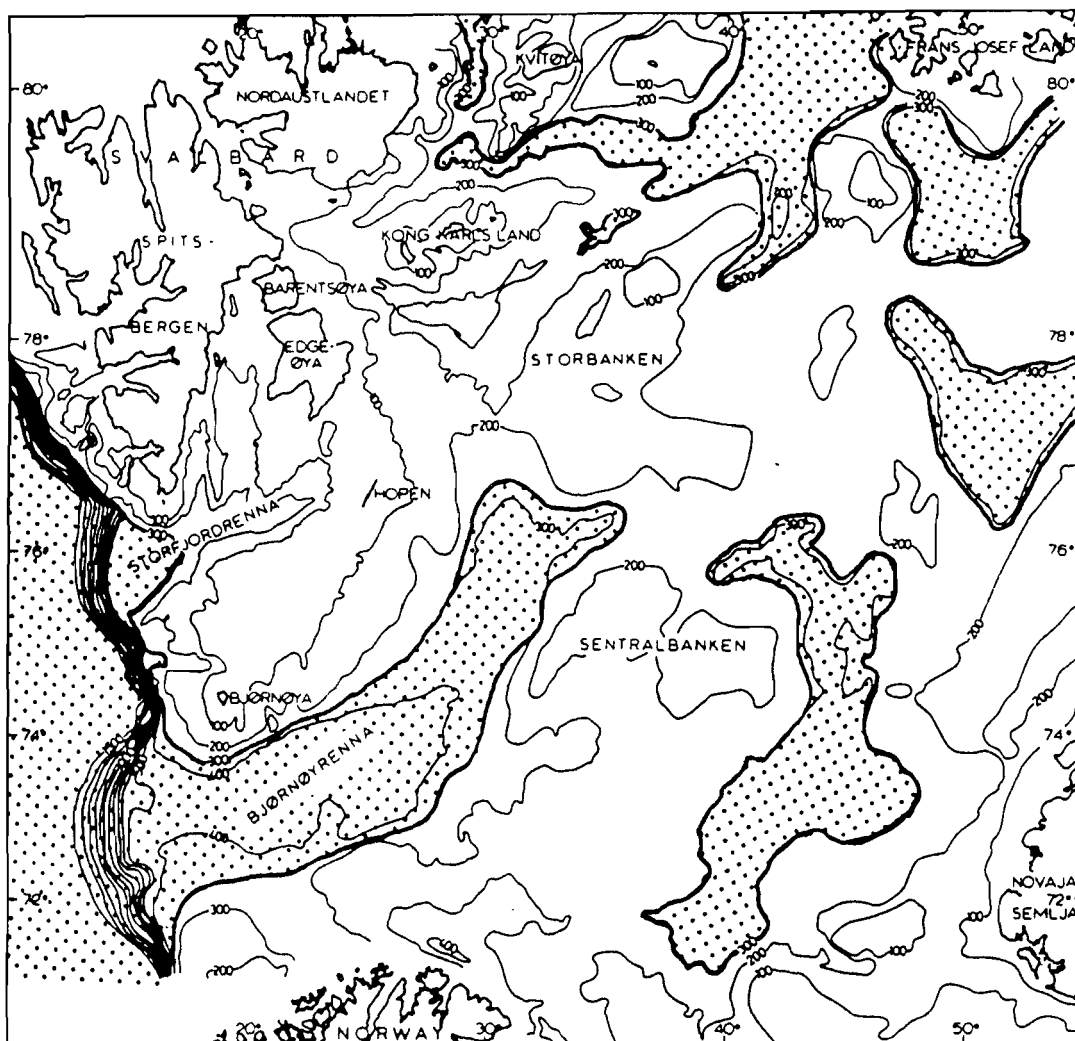


Fig. 3.14. Areas of methane hydrate stability (dotted) in the Barents Sea, based on thermal prediction.

3.4.2 Gas composition and hydrate stability

In Chapter 1, hydrate stability conditions for other systems than pure methane are discussed. Figure 1.1 shows that the effect of adding slight amounts of other gases, such as ethane or CO_2 , is hydrate stability at higher temperatures and lower pressures. Increasing salinity of the porewater has the opposite effect. Structure II hydrates, composed of heavier hydrocarbons such as propane and isobutane, are stable at both shallower and greater depths than Structure I hydrates, mainly formed by methane and ethane (Judge 1982). Hence, if natural gas in the Barents Sea contains other components than pure methane, stability conditions are changed and hydrates may be encountered in significantly shallower water depth than suggested in figure 3.14.

The gas composition of a possible hydrate in the Barents Sea is unknown and one can only speculate about it. If the gas originates

from migration from deeper sources (thermogenic gas), it may consist of higher-molecular weight hydrocarbons and inorganic gases, in addition to methane. However, in the progress of migration the gas composition is prone to be enriched in methane.

Analysed samples of gas hydrates from DSDP and ODP wells, discussed in chapters 1.1.4 and 1.1.5, generally contained more than 99 % methane. Carbon isotopic analysis of these gases showed a biogenic origin (Kvenvolden & Barnard 1983b; Kvenvolden & McDonald 1985; Kvenvolden & Kastner 1988). So far, gas hydrates with a proven thermogenic source have not been recognized, although several authors suggest migration of thermogenic gas from deeper reservoirs as the origin of the gas in the shallow gas hydrates (Shipley et al. 1979; Katz 1982; Collett et al. 1988).

When predicting the areas of gas hydrate stability in the Barents Sea, the possibility of gas composition other than pure methane cannot be ruled out. Thereby a greater zone of stability than shown in figure 3.11 is possible.

3.4.3 Thermal prediction of gas hydrate occurrence in Svalbard

Similar predictions of gas hydrate stability in Svalbard can be done. However, there is a lack of available deep, subsurface temperature data. As mentioned in chapter 3.1, the permafrost thickness has been measured in some places on Spitsbergen. In general, permafrost covers the entire land area with depths up to 450 m in the central part (Liestøl, 1980). There are no available temperature measurements from the zone beneath the permafrost.

To get a rough evaluation of the possibility for gas hydrate occurrence on Spitsbergen, the method of Collett (1983), described in chapter 1.1.2, is applied. The mean annual ground temperature and known permafrost depth provide a value for the thermal gradient within the permafrost layer. At the base of the ice-bearing permafrost zone the geothermal gradient increases abruptly (Lachenbruch, 1982). Given a regional value for the gradient increase at the permafrost base, the geothermal gradient below the base of the permafrost can be calculated. In a study in Prudhoe Bay, Alaska, Collett (1983) used a value of 1.75 for the gradient increase at the permafrost base.

The thermal gradients above and below the base of the permafrost zone can then be plotted on a methane hydrate stability curve, and the intersections between the gradients and the phase curve mark the zone of hydrate stability. As a first approximation, the same value of the

thermal gradient increase at the base of the permafrost (1.75) is used. Given a representative annual ground temperature of -5°C , an equilibrium temperature at the base of the ice-bearing permafrost of -0.5°C , and assuming a lithostatic pressure gradient, the resulting zone of hydrate stability is shown on figure 3.15. In order to get an intersection between the methane hydrate stability curve and the geothermal gradients in Spitsbergen, the permafrost depth has to be a minimum of approximately 260 m.

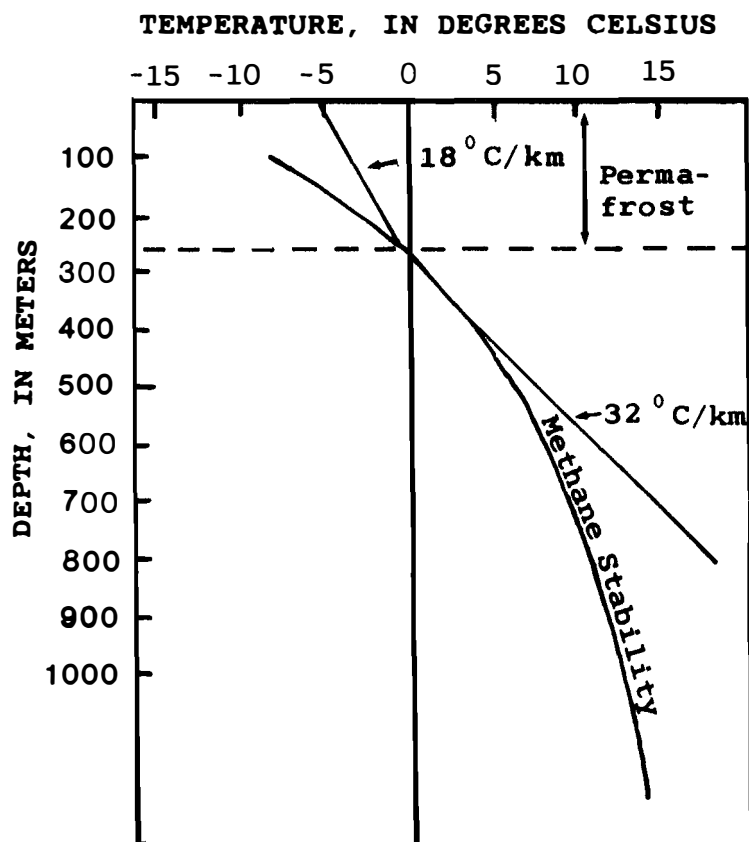


Fig. 3.15. Tentative calculation of permafrost thickness and gas hydrate stability. Methane hydrate stability curve is taken from Collett (1983).

4. SEISMIC DATA ANALYSIS

4.1 Seismic interpretation

The present project includes seismic interpretation from different areas in the Barents Sea, where anomalous reflectors have been observed. The first area is situated in the Bjørnøya South region, on the southern slope of Bjørnøyrenna in approximately 350 m water depth (Fig.4.1). The other area covers part of Sentralbanken and the northern extension of Bjørnøyrenna in water depths up to more than 300 m. Furthermore, some seismic lines from the Olga Basin (Fig.4.1) have been interpreted.

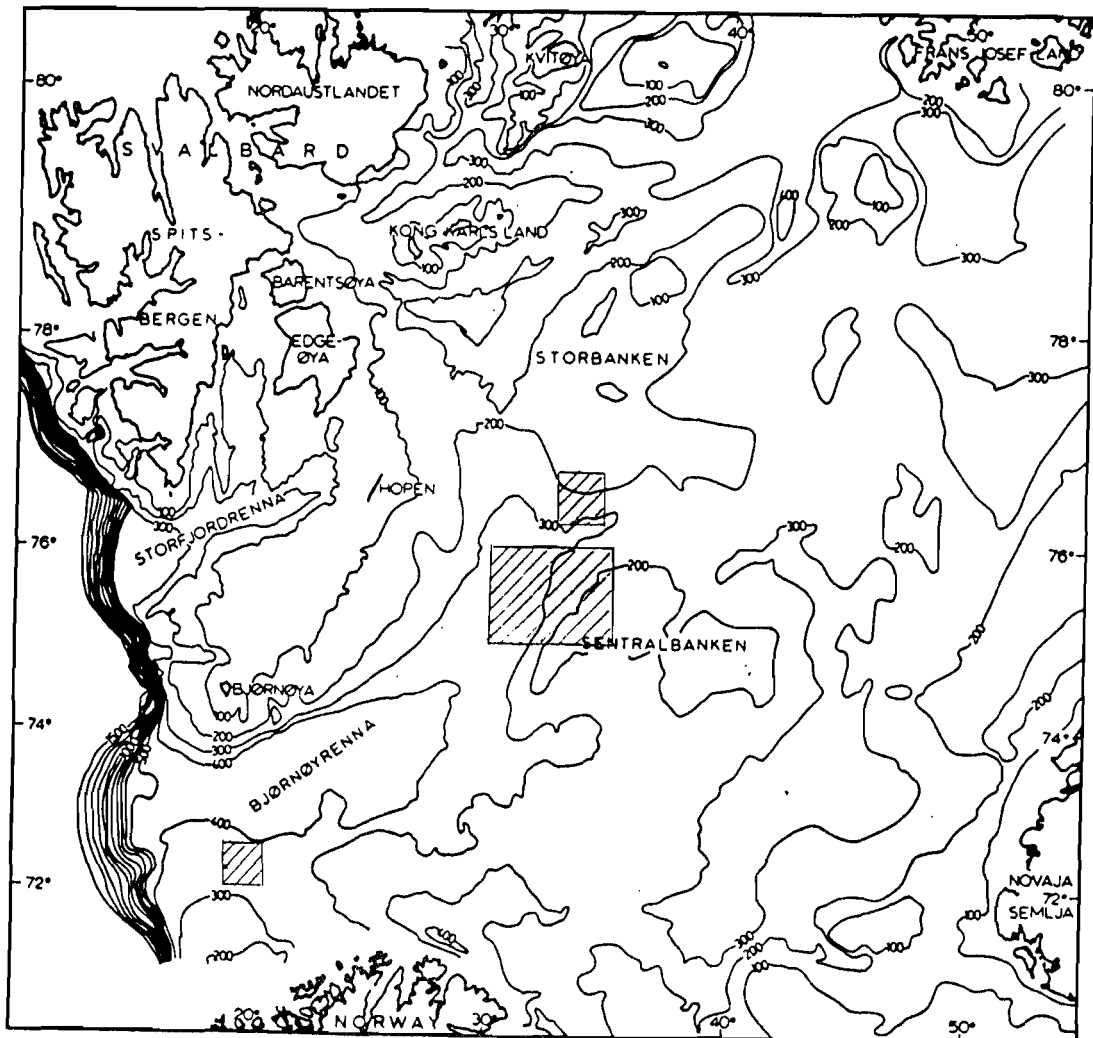


Fig. 4.1. Location of the study area of seismic interpretation.

In the Bjørmøya South area, the anomalies appear as shallow, high amplitude reflectors with restricted lateral extension. In the Olga Basin and the Sentralbanken area, one significant reflector parallels the seabed at a relatively shallow depth.

4.1.1 Bjørmøya South

The investigated area is situated between 72° and $72^{\circ}30'N$, 19° and $21^{\circ}E$ in water depth ranging from 320 to 380 m. Structurally, the area covers the western part of Loppa High, a part of the NNE-SSW trending Bjørmøyrenna Fault Complex, parts of Helgøy High to the west and Bjørmøya Basin to the northwest.

One well, 7219/9-1, has been drilled in the area (Fig.4.2). Base Quaternary, at approximately 130 m below sea bottom, is marked by the transition from sandy, silty clay with few pebbles and rock fragments to a more homogeneous, non-calcareous, silty claystone below. The Tertiary sediments are consolidated, and characterized by monotonous sequences of claystone with a gradual increase in consolidation grade with depth. Well logging indicates few intervals with increased sand/silt content in the claystone. No distinct sand layers and no shallow gas were encountered. Reflectors within the Tertiary sediments are probably related to changes in the consolidation (density) of the clayey layers. The Tertiary sequence is relatively thick, up to 1000 m.

In addition to the well-information, both high-resolution and conventional deep seismic data were interpreted. The high-resolution sections provided the best information in the shallow layers where the anomalous reflections were found.

The seismic anomalies consist of high amplitude reflectors, some of which cut across the bedding, while others are parallel. On several lines, the seismic character below the anomalies is masked. Push-down of underlying reflectors is also observed. All anomalies occur within the Tertiary sequence, but the subsea depth varies between 0.6 and 1.3 seconds two way time (s twt). Correlation between seismic lines allowed mapping of the individual anomalous areas (Fig.4.2).

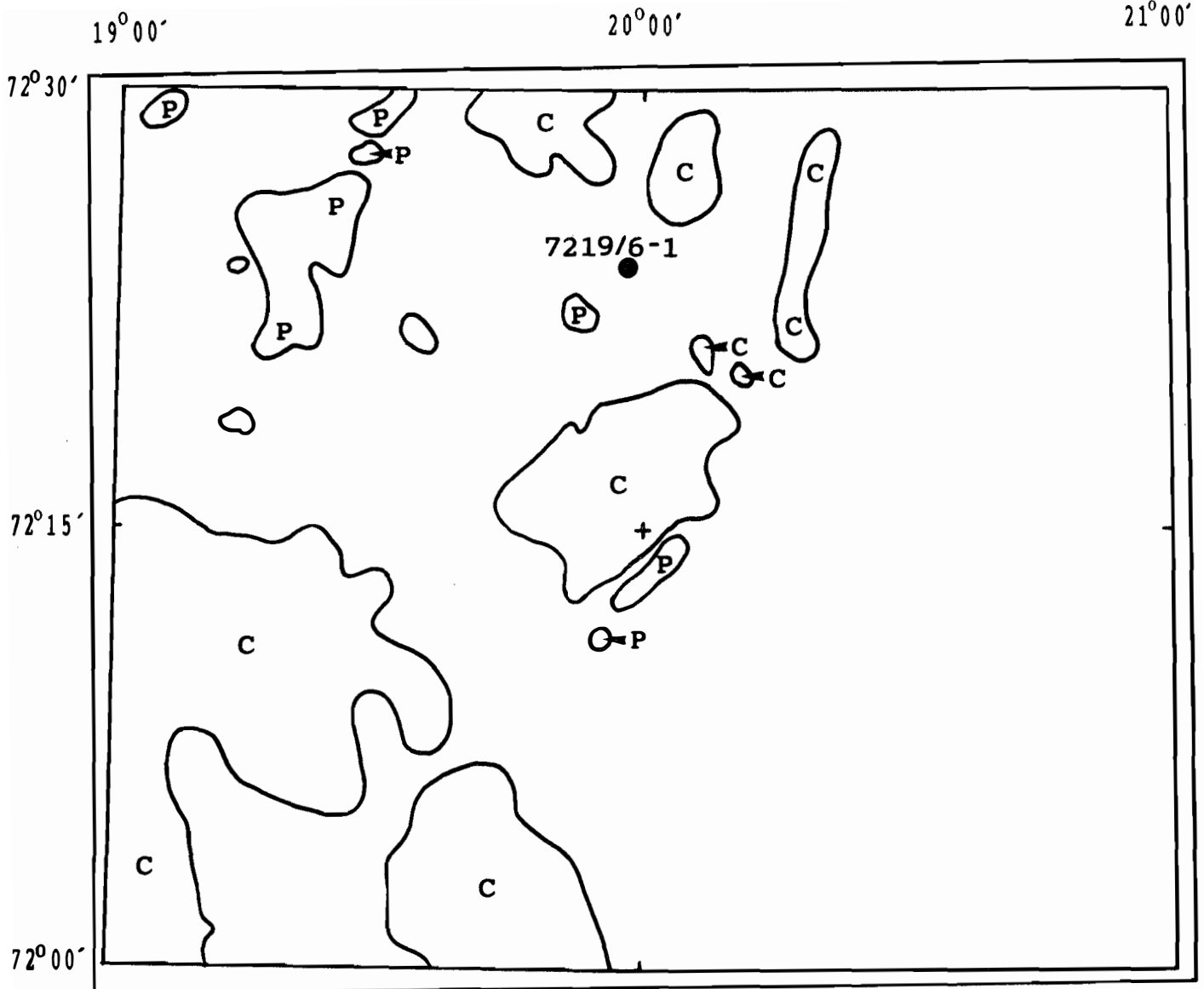


Fig. 4.2. Distribution of the anomalous, shallow seismic reflectors.
 P - the anomalous reflector is parallel with the bedding.
 C - the anomalous reflector cuts across the bedding.

Possible explanations for the anomalies are:

- shallow gas
- gas hydrates
- diagenesis
- intrusions
- multiples/ghosts

To evaluate the different possibilities, the following steps of interpretation were performed:

- 1) Three internal reflectors in the Tertiary sequence were chosen from the well and mapped in the area in order to determine the stratigraphic depth of the anomalies.
- 2) The different anomalies were grouped in two: the first cutting across the reflecting horizons, the second paralleling the horizons.
- 3) The depth to the anomalies was determined.

In the well, the Tertiary lithology is dominated by claystone, indicating that the anomalies are not restricted to specific coarser-grained horizons. The interpretation of the three reflectors in the Tertiary sequence supported this hypothesis. The anomalies are all localized in different depths with regard to the three reflectors. The northeastern anomaly is stratigraphically deepest, while the southern and southwestern anomalies are the most shallow. This is consistent with the thickness variation of the Tertiary sequence; increasing from the northeast to the southwest.

Most of the anomalies were found to cut across the bedding (Fig.4.2). Of the larger anomalies, only the northwesterly one paralleled the bedding. However, most of the smaller anomalies follow the stratification (Fig.4.2).

Three of the greater anomalies in the east-northeastern part were found to parallel the seabed at approximately the same subsea depth, 0.65 - 0.70 s twt (about 0.2 s subbottom depth) (Fig.4.3). The others were found at greater depths, from 0.80 to more than 1.25 s twt, and the anomalous reflectors were dipping with regard to the seafloor.

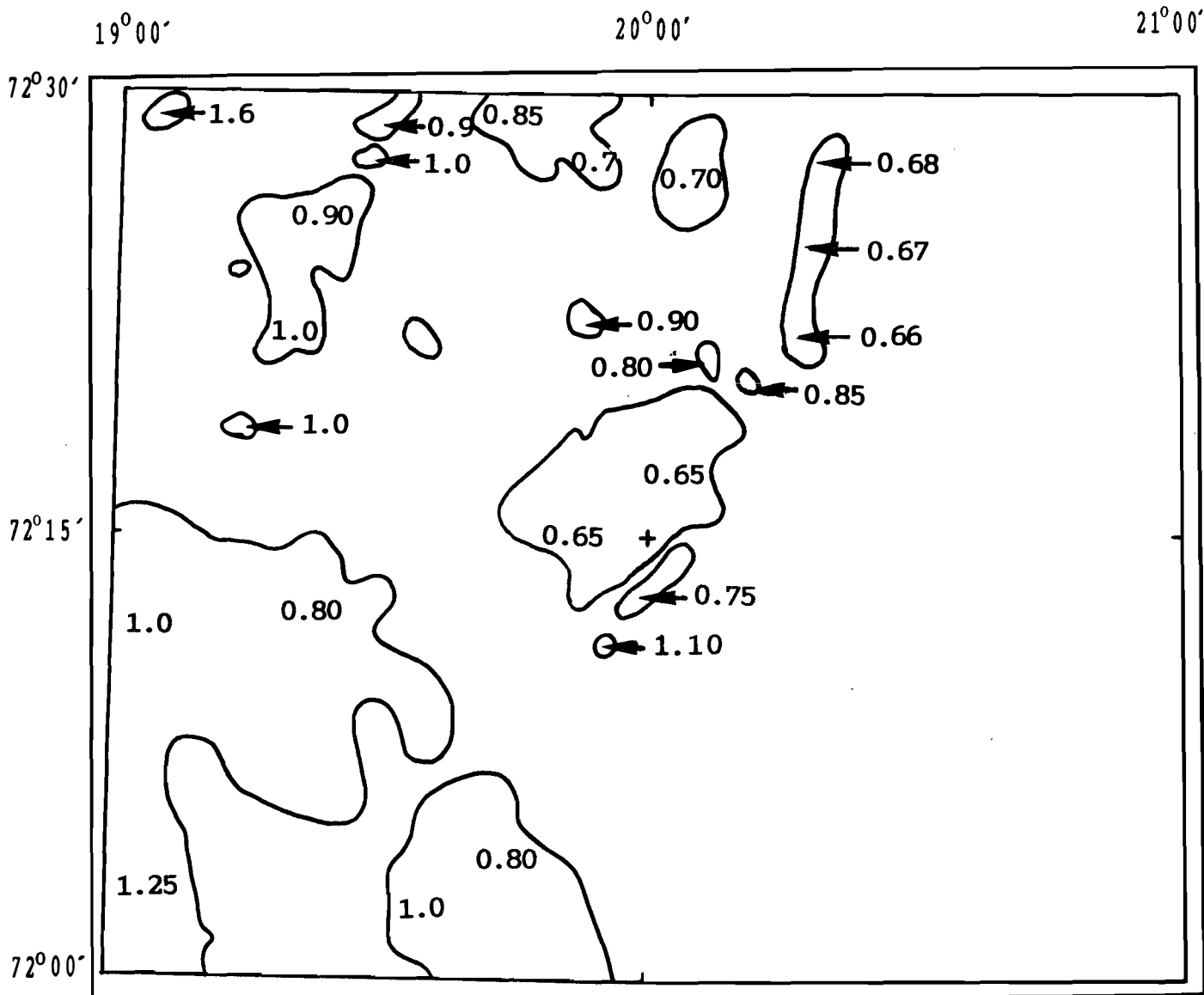


Fig. 4.3. Subsea depth in seconds two way time to the anomalous reflectors (water depth varies between 0.45 and 0.50 s twt).

This leads to the following interpretation of the origin of the anomalies (Fig.4.4):

- gas hydrates/free gas: the three easternmost anomalies may consist of gas hydrates with the possible existence of free gas trapped beneath.
- shallow gas: the northwestern great anomaly and most of the smaller, probably consist of gas trapped in the shallow layers.
- diagenesis: the two great anomalies in the south and the one to the north are probably caused by a diagenetic front, leading to a density and velocity change.

a) Gas hydrates/free gas

The three east-northeastern anomalies are probably caused by gas hydrates. The anomalous reflectors cut across other reflecting horizons and parallel the seabed. Accordingly, the reflectors fulfil the requirements of a bottom simulating reflector (Chapter 1.3). The subbottom depth to the reflectors is approximately 0.2 s twt. This corresponds to 220 m, using a seismic velocity of 2200 m/s obtained from the sonic log in the shallow part of the Tertiary sediments. The thickness of the possible gas hydrate zone compares well with the stability considerations presented in chapter 3.

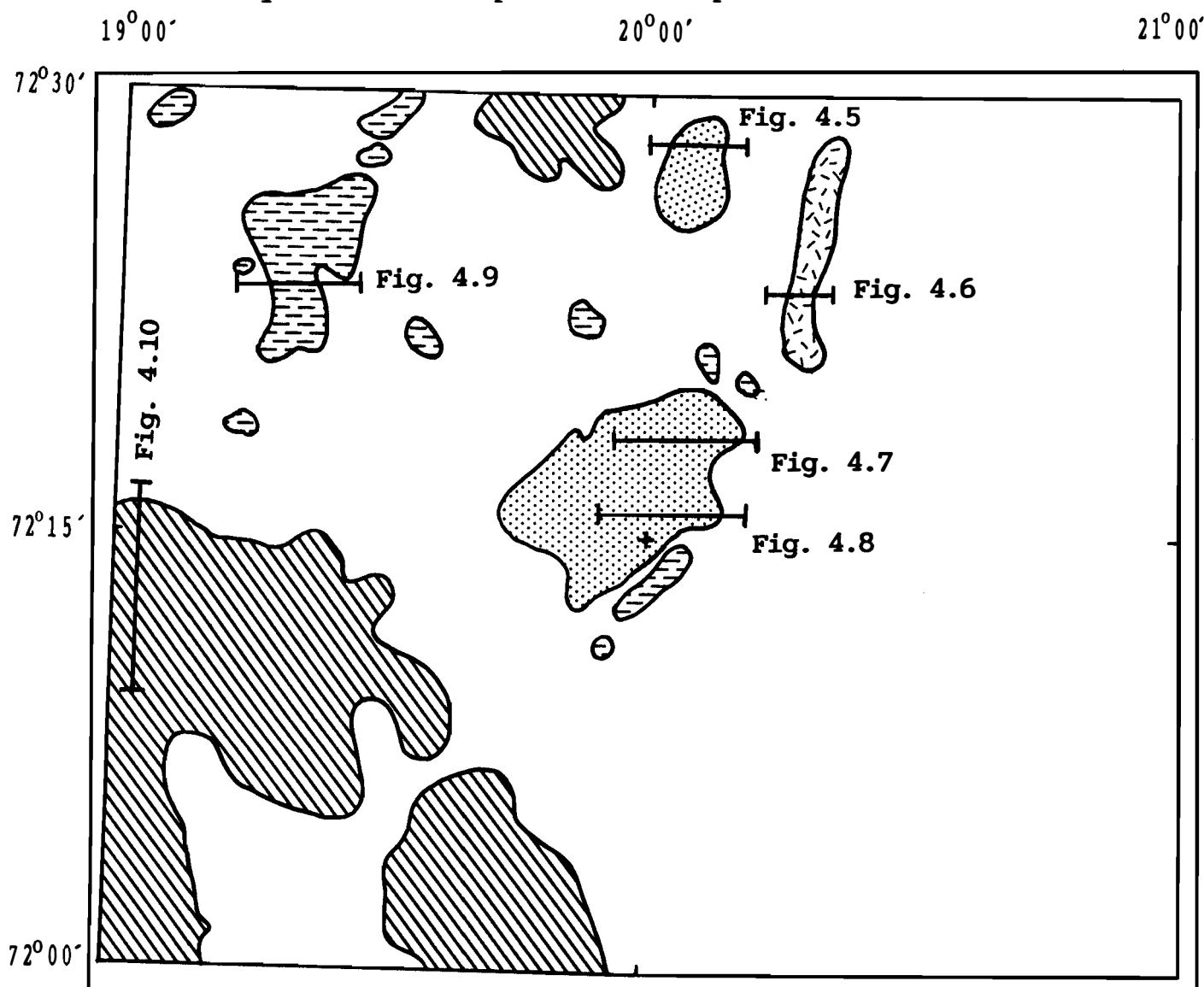
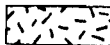
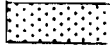
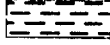



Fig. 4.4. Possible origin of the seismic anomalies

-  - gas hydrates
-  - gas hydrates with possible shallow gas trapped below
-  - shallow gas
-  - diagenesis

The locations of the seismic examples (Figs. 4.5.-4.10.) are shown.

There are indications of the presence of free gas beneath at least two of the anomalies. The indications include push-down and masking of underlying reflector, and diffractions at the edges of the anomalies, which may be caused by an abrupt transition to water-saturated layers. Furthermore, the anomalies are situated above tectonically disturbed areas, where large faults may enable the upward migration of gas.

Figure 4.5 shows a high resolution section crossing the northernmost gas hydrate area. The gas hydrate reflector is seen at a depth of approximately 0.7 s twt, running parallel to the seafloor and cutting across the bedding. Below is evidence of free gas: gas blanking, diffractions at the edges and a significant push-down. In the deeper part of the section, there is a fault zone with the downthrown side to the west.

Figure 4.6 shows a section from the northeastern anomaly (Fig.4.4). The anomalous reflector clearly cuts across the reflecting horizons. There is no significant evidence of the presence of trapped gas below. The anomaly is situated above several large faults.

Figures 4.7 and 4.8 are sections crossing the central anomaly interpreted as gas hydrate/free gas (Fig.4.4). The reflector is partly discontinuous. On the northern section, the reflector has a hummocky character (Fig.4.7). In the southern part, there are "holes" (up to 1.25 km in extension) between the segments of the reflector (Fig.4.8). On both lines the reflectors are conformable with the seafloor and cut across the bedding. The seismic records are completely masked below the anomalous reflector. The reflector is suggested to be caused by gas hydrates with gas possibly trapped below. The origin of the "holes" is unclear. They may be caused by changes in the lithology, influencing the distribution of gas hydrates. In Chapter 1.1.b), the effect of grain size variations on gas hydrate equilibrium is discussed. Collett et al.(1988) indicate that fine-grained material may reduce the temperature of gas hydrate equilibrium. Another explanation for the "holes" could be that there is a lack of gas to create a hydrate at these sites, or that the hydrates are lost.

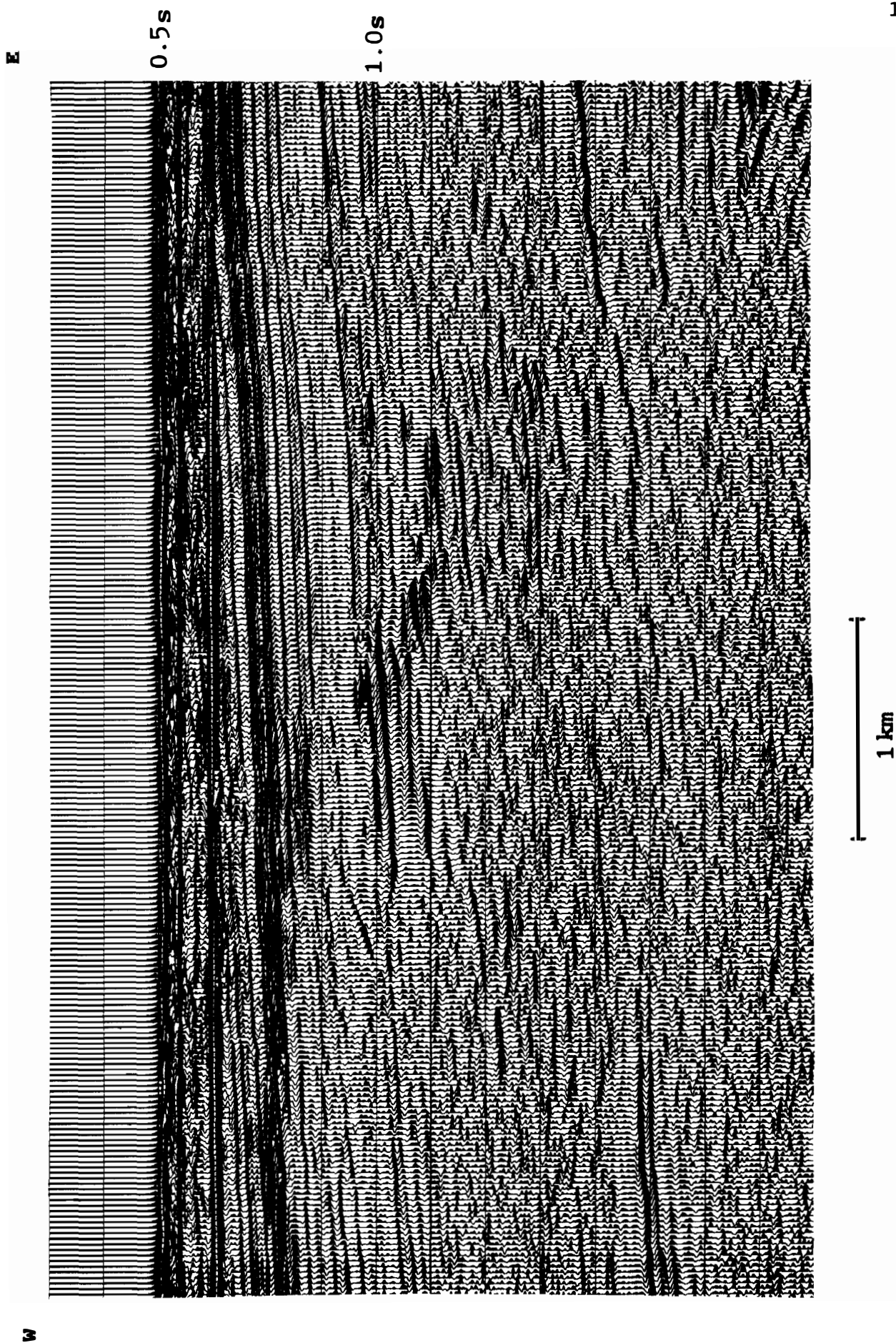


Fig. 4.5. Seismic example crossing the northern anomaly interpreted as gas hydrates with free gas trapped below. A bottom simulating reflector is seen at a depth of 0.7 s twt. Courtesy A/S Geotem

W

E

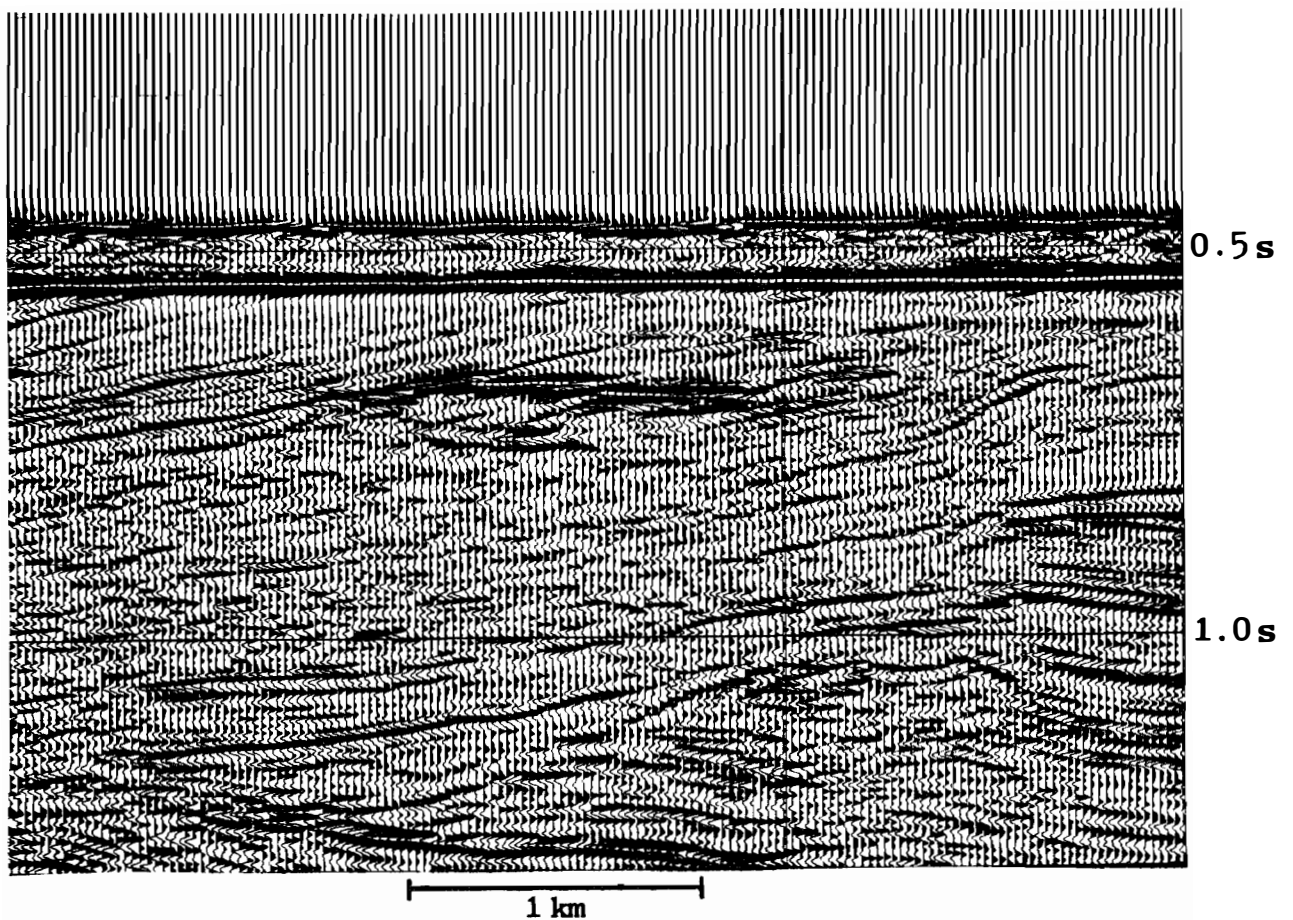


Fig. 4.6. Seismic example crossing the northeastern anomaly interpreted as gas hydrates. A bottom simulating reflector is seen at a depth of approximately 0.67 s twt. Courtesy A/S Geoteam

b) Shallow gas

The large northwestern anomaly and several of the small anomalies are suggested to be caused by shallow gas. The anomalous reflectors seem to follow the stratification, and do not parallel the seabed. There is gas masking in the area beneath the reflectors and push-down of underlying reflectors. Besides, the anomalies are situated at varying subbottom depth, from 0.3 to 0.6 s twt. Assuming a seismic velocity of 2200 m/s, the depth will be between 330 to 660 m below the sea floor, i.e. approximately 680 to 1100 m below sea level. Because the temperature increases with depth, this is probably below the lower limit for gas hydrates. According to the stability considerations in Chapter 3, the anomalous reflectors are situated below the stability zone for gas hydrates at the present water depth.

Figure 4.9 is a section crossing the northwestern anomaly. The reflector follows the bedding in the Tertiary sediments that are dome-shaped above an underlying structural high. Gas masking and push-down are seen beneath the anomalous reflector.

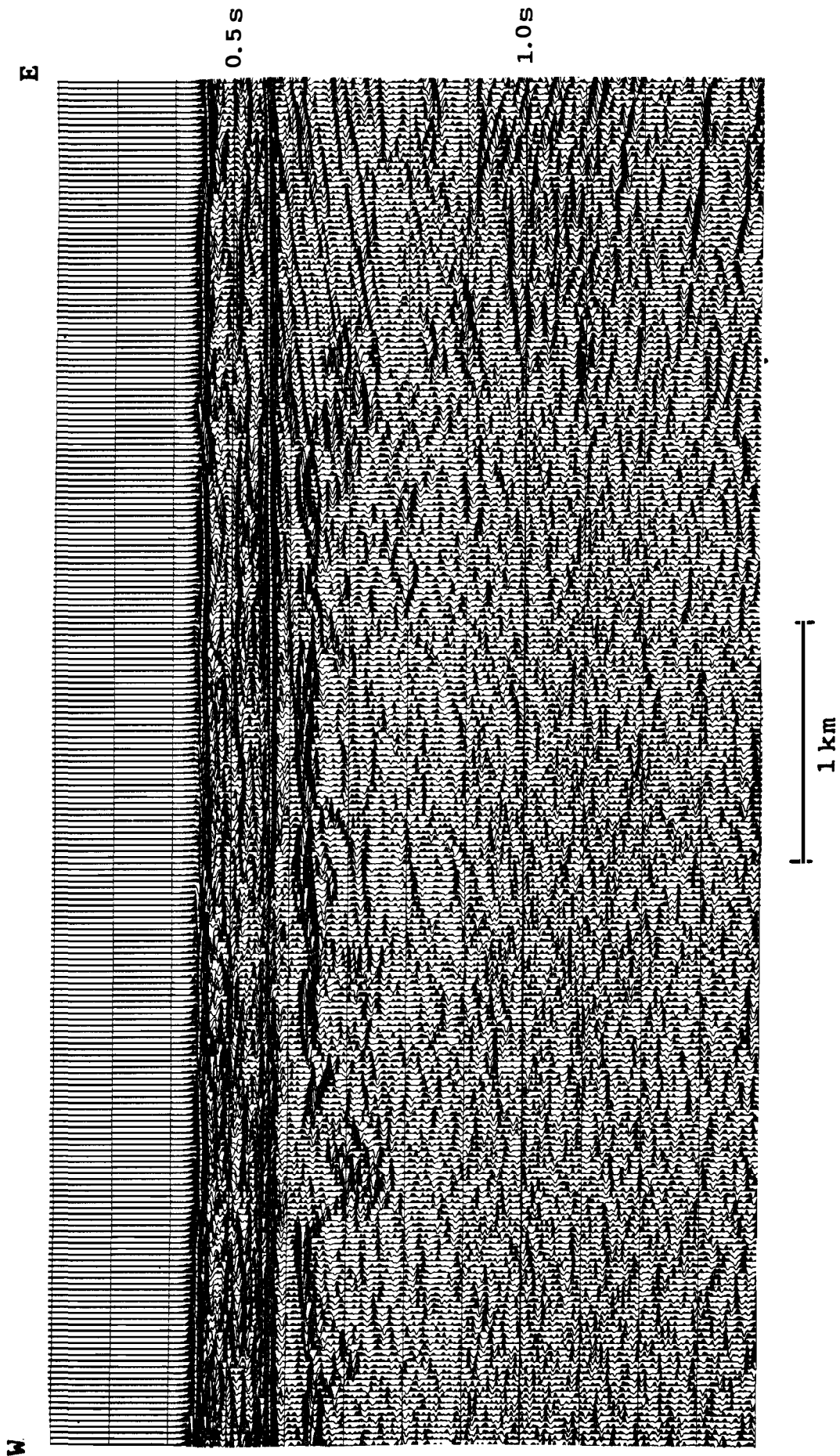


Fig. 4.7. Seismic example from the central anomaly interpreted as gas hydrates with free gas below. The bottom simulating reflector is seen at a depth of approximately 0.64 s twt. Courtesy A/S Geoteam

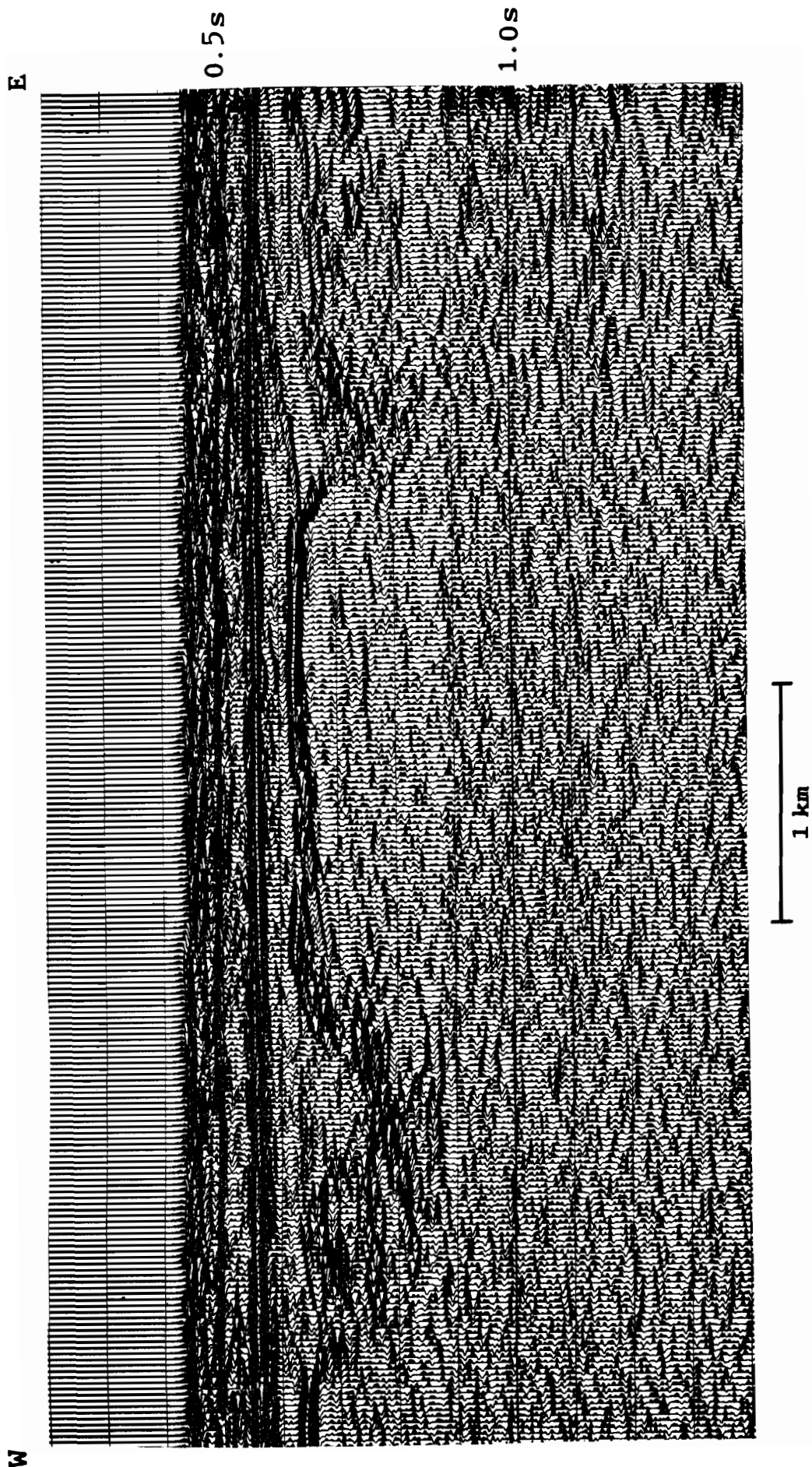


Fig. 4.8. Seismic example from the central anomaly interpreted as gas hydrates/free gas. Courtesy A/S Geoteam

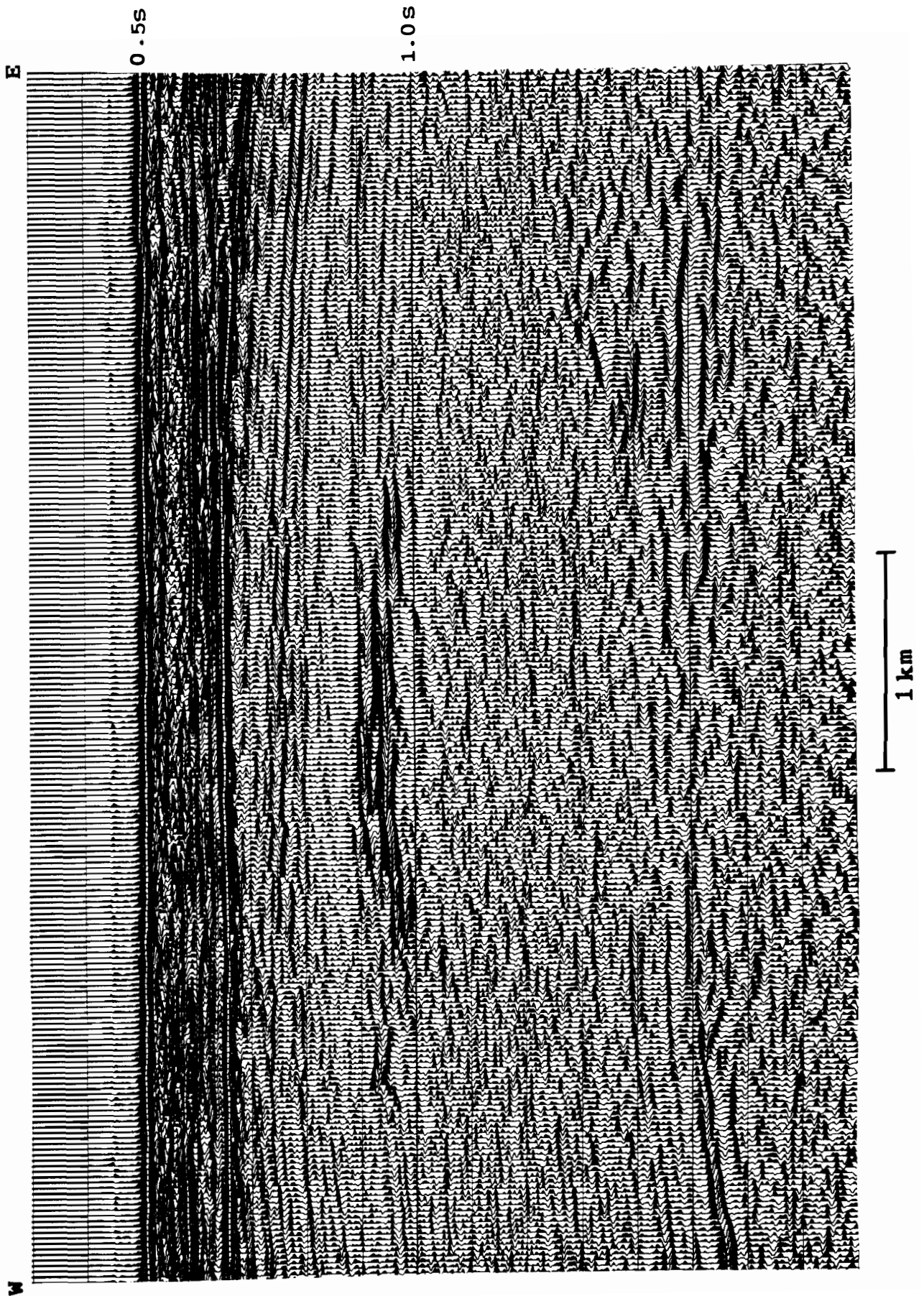


Fig. 4.9. Seismic examples from the northwestern anomaly interpreted as shallow gas. Courtesy A/S Geoteam

c) Diagenesis

The anomalous reflector in the southwestern and northern anomalies appears as a significant reflector cutting across other reflecting horizons and dipping towards the southwest (Fig.4.10). The reflector occurs at depths ranging from 0.75 s to 1.25 s twt, i.e. approximately 680 to 1230 m below sea level. This is too deep for gas hydrates at the present water depth, because of the increasing temperature (see stability considerations in chapter 3). Thus, the presence of gas hydrates can be excluded. In parts of the anomaly-areas, the seismic records beneath the reflector are totally masked. As no other indications of gas are apparent, this masking is probably not caused by gas. Furthermore, free gas migrating from below would not have been trapped beneath the strongly dipping, anomalous reflector. The masking is probably caused by the strong reflection from the anomaly, inhibiting penetration of seismic energy into the deeper layers.

The reflectors are interpreted to represent a diagenetic boundary, most likely the transition from opal-CT to quartz. This transition occurs at a temperature of approximately 80°C, and the velocity and density change may result in a bottom simulating reflector as described in Chapter 1.3.a. The present depth of the diagenetic boundary is therefore a function of the history of uplift and erosion (F.Riis pers.comm. 1988).

4.1.2 The Sentralbanken and the Olga Basin areas

The investigated area is located between 75° and 76°N, 30° and 35°E, covering the northwestern part of Sentralbanken and the eastern slope of the northern extension of Bjørnøyrenna (Fig.4.1). The water depth ranges from 170 to 350 m.

The seismic anomaly consists of a shallow, bottom simulating reflector cutting across other reflecting horizons.

Possible explanations for the reflector are:

- A geological feature: gas hydrates or diagenesis.
- A non-geological feature: bubble pulse or ghost.

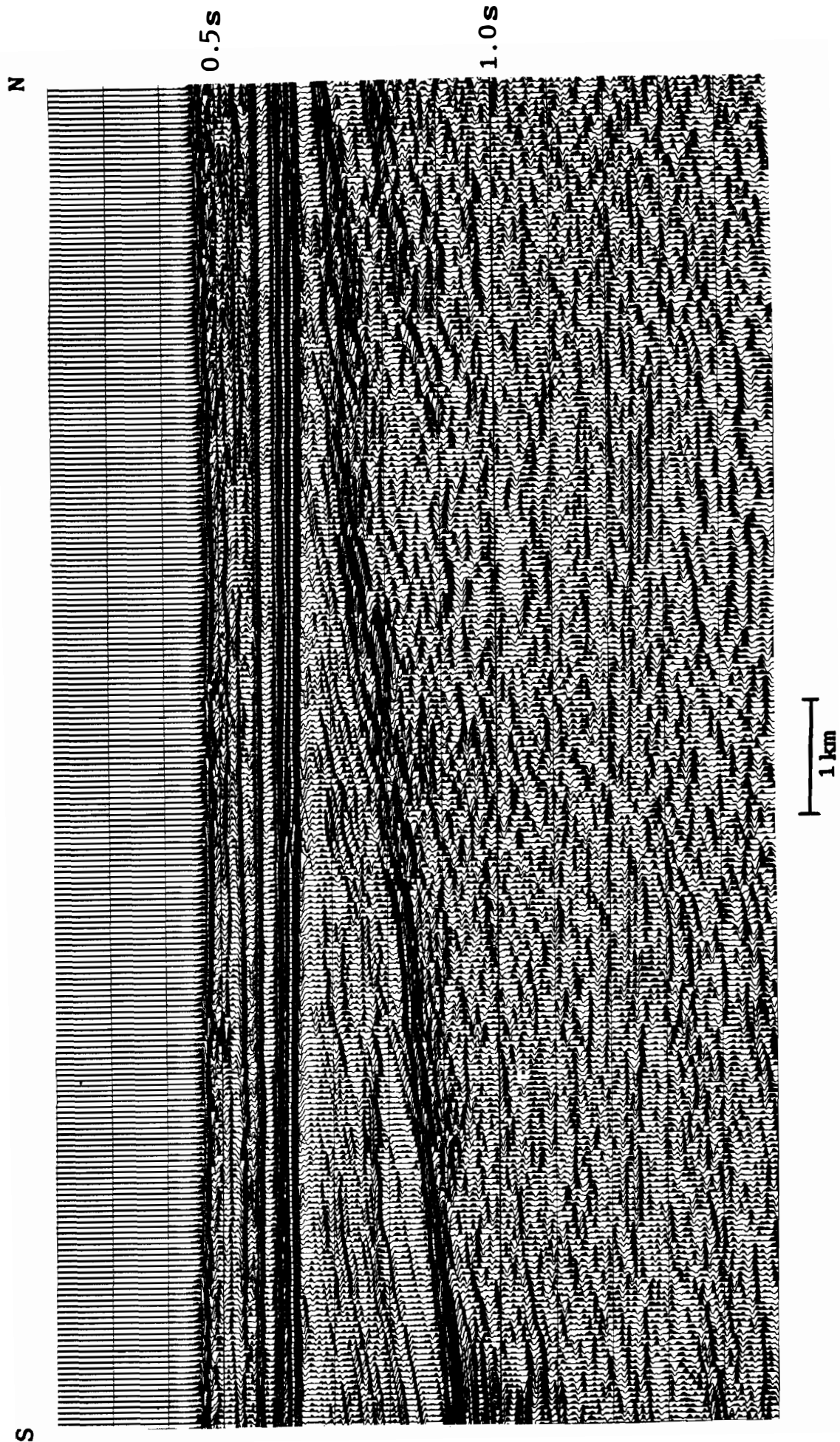


Fig. 4.10. Seismic example from the southwestern anomaly interpreted as a diagenetic front. Courtesy A/S Geoteam

Data from three different seismic surveys were interpreted, and the bottom simulating reflector was found to be present in all three. However, the reflector is most clearly seen in areas with dipping layers, cutting across the reflecting horizons. In one east-west running section, the reflector can be followed continuously from 35°E on Sentralbanken to 30°E in Bjørmøyrenna, i.e. the whole of the studied area. The great lateral extension disfavors a geological explanation of the anomaly.

The character of the reflector does not change significantly in the area (Fig.4.11). Amplitude anomalies, bright spots, gas blanking, or any other evidence of shallow gas are not observed. The water depth in the study area increases from 170 m on Sentralbanken to 350 m in Bjørmøyrenna. However, the subbottom depth to the anomalous reflector was found to be constant, approximately 0.14 s twt. Thus, the possibility of a geological cause for the anomaly can be excluded. Furthermore, the great subbottom depth precludes ghost as a possible explanation.

The remaining explanation for the origin of the bottom simulating reflector is that it probably represents a bubble pulse reflection. This interpretation is supported by interpretation of seismic lines from the Olga Basin. A bottom simulating reflector was found at a depth of 0.07 s twt. On one seismic line the reflector is relatively continuous for approximately 40 km, while on some of the other lines the reflector occurs in restricted areas. The reflector does not change character or subbottom depth along the lines, although the water depth varies, indicating a non-geological origin for the reflection. The company that designed the airgun source confirmed the interpretation, expecting a bubble pulse reflection at the measured depth (L.Eikum pers.com. 1988).

The reason for the fact that the bubble pulse reflection only exists on some of the lines from the same seismic survey, which are recorded and processed with more or less constant parameters, may be attributed to varying geology in the survey area. The lithology of the shallow layers may influence the character of the bubble pulse reflection. In the Olga Basin, the bottom simulating reflector is most clearly seen in areas with flat-lying layers and relatively few reflecting horizons. Changing acoustic impedance of the sea floor may also affect the bubble reflection. The higher the acoustic impedance contrast, the more energy is reflected, and the reflectors (both sea floor and bubble pulse) get higher amplitudes.

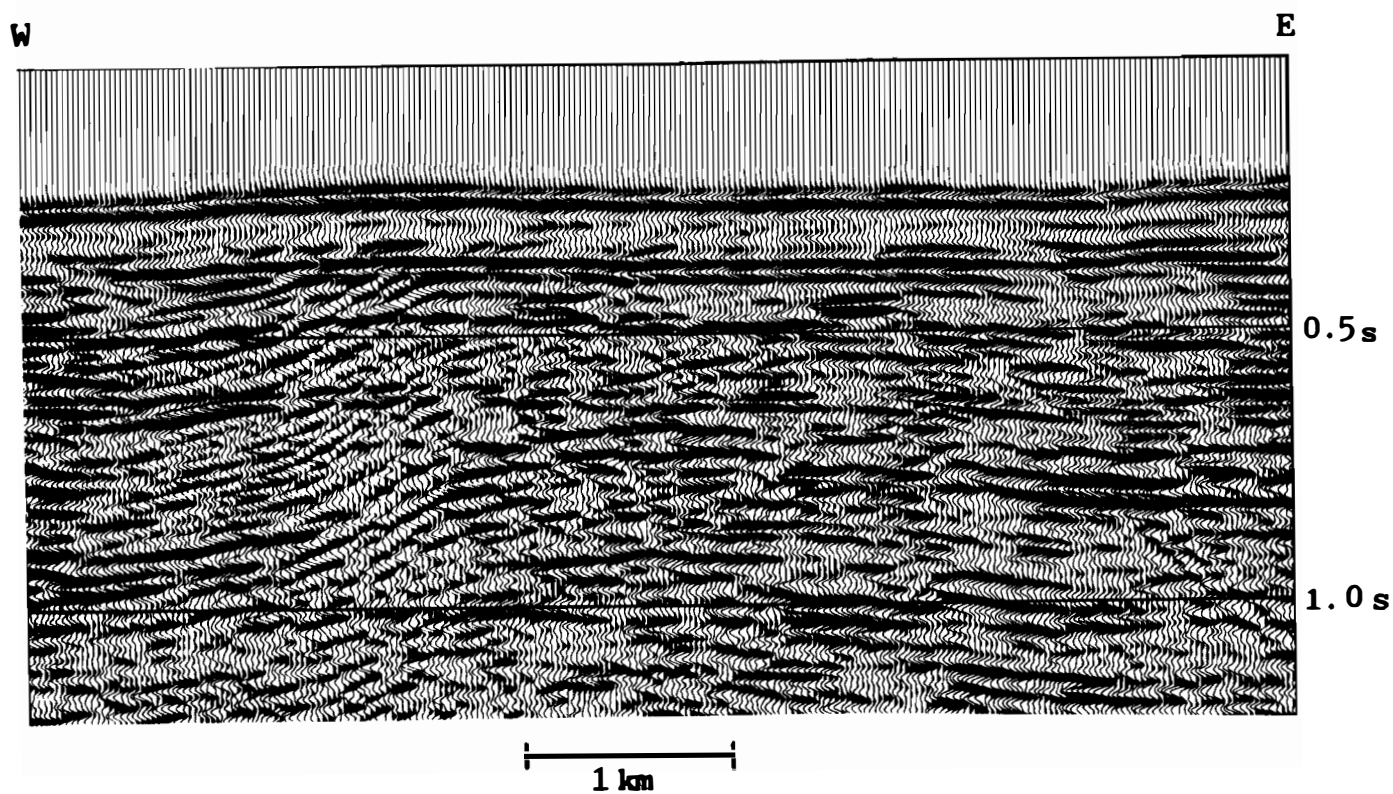


Fig. 4.11. Seismic example from the Sentralbanken area showing a bottom simulating reflector at a subbottom depth of approximately 0.14 s twt interpreted as a bubble pulse reflection. Courtesy A/S Geoteam

5. WELLS AND BOREHOLES IN OFFSHORE ARCTIC REGIONS WHERE PERMAFROST AND GAS HYDRATES MIGHT BE ENCOUNTERED.

5.1 Introduction

In Arctic offshore regions relict permafrost and gas hydrates below the seabed present a technical problem for drilling and production operations. These operations will thaw permafrost and decompose gas hydrates unless a system is used to prevent heat flow from the wellbore into the formation. In unlithified sediments thaw of permafrost imposes horizontal and vertical stresses on the casing and causes hole instability, sloughing and washouts. Hydrate decomposition can generate high gas pressure in the wellbore, thaw loads and borehole instability.

5.2 Permafrost and gas hydrate thaw/freeze loads in wells and boreholes.

Thaw/freeze and hydrate decomposition or sublimation will impose a change of stresses within the unlithified sediments. This change of stresses can be transmitted to the borehole or well. This new state of stresses can cause borehole instability and/or collapse of the casing. The mechanisms of thaw/freeze loads are stated below.

5.2.1 Thaw subsidence

As permafrost thaws, the soil mass will consolidate and induce loads on the well or borehole. Thaw subsidence can be caused by various processes (Goodman 1978):

a) Excess ice

In addition to ice forming the permafrost, there might be excess ice distributed in discrete ice lenses, wedges and veins. In Prudhoe Bay and the Mackenzie Delta excess ice exist at depths shallower than 50 feet (Howitt 1971, Rampton & Mackay 1971). It seems that excess ice is typical of shallow depth permafrost. During thawing, the excess ice melts, there is a volume contraction and the soil mass subsides to occupy the space created by the volume contraction from ice to water.

b) Thaw-consolidation with fluid expulsion

If potentially underconsolidated conditions exist in a permafrost zone (i.e. permafrost has been buried by new sediments and or presently loaded by surface ice), excess pore pressure will develop during permafrost thawing. Thawed permafrost will consolidate due to the overlying weights of sediments until the excess pore pressure in the meltwater is dissipated. Consolidation of the thawed permafrost zone can cause subsidence of the overlaying layers.

c) Pore pressure reduction

"Pore pressure reduction" is considered the main mechanism for thaw-subsidence in deep permafrost (Goodman 1978). In normally consolidated permafrost, thaw causes contraction of the pore ice bounding the sedimentary grains. This volume contraction causes a "pore pressure reduction" in the meltwater between the grains. Because of the "pore pressure reduction", the effective stress between the grains increases and the grains can come closer together with the consequent reduction of volume within the thawed zone and subsidence of the overlaying layers.

d) Stiffness reduction

Thawed permafrost soil can deform more easily than the surrounding unaffected permafrost. The difference in stiffness between frozen and thawed material can induce inward pressure towards the borehole, soil deformation and thaw subsidence.

5.2.2 External freezeback

In a thawed permafrost area after the drilling or during the oil or gas production shut-down periods, refreeze can occur. Refreeze of thawed permafrost or waterbased fluids outside the casing can generate inward radial loads around the wellbore. Mechanically, thawing and refreezing are not completely reversible. Consolidated soil due to thawing will not return to its initial volume during refreezing. The volume expansion of the water saturated zone during refreezing is

primarily towards the borehole. The expansion of the refrozen zone that requires more than its original volume when it refreezes determines the magnitude of the compressive stresses on the wellbore.

5.2.3 Hydrate decomposition

Wellbore loads caused by hydrate decomposition are not well understood. More research is needed to determine the mechanical behaviour of decomposed hydrate formations. Since the pressure required to form gas hydrates increases logarithmically while the temperature increases linearly, in most sedimentary basins hydrates will decompose naturally at depths around 1500 m (21-27°C). Obviously, areas of high geothermal gradient will form thinner hydrate zones than areas of low geothermal gradients. Figure 5.1 shows gas hydrates from Prudhoe Bay (Holder et al. 1976) and Messoyakah field, USSR (Makogon et al. 1971). The permafrost in Prudhoe Bay extends to about 600 m. The potential-hydrate depth extends to about 1100 m (1200 m for a 0.6 gravity-gas). At Messoyakah field the hydrate interval has been measured down to 900 m (Hunt 1979). Hydrates form initially near the surface (i.e. on the continental slope or outer shelf) and if later buried by sediments to decomposition depth will release a large amount of water creating underconsolidated conditions and high gas pressure. Hedberg (1974) has indicated that such decomposition at the base of hydrates could cause mud diapirs and other features related to overpressuring in formations. Pressures up to 100,000 psi have been measured from trapped decomposed hydrates in the USSR. Deposits of gas hydrates in Siberia have been estimated to be in the order of $15 \cdot 10^{12}$ m³ (Hunt 1979).

The naturally decomposed gas hydrates represent a serious technical problem and a potential geological hazard for drilling. Drilling technical problems are faced to stabilize a formation that behaves as a gelatinous mass. The drilling geological hazard is represented by the potential high pressure gas accumulated below the frozen hydrate surface. If hydrates are decomposed or thawed during drilling operations and no permeable path exists within the formation to dissipate excess pore pressure, high lateral loads and gas flow into the wellbore may result. Before drilling, it is important to know if the hydrates exist as thin discontinuous layers of local extent or as thick continuous zones.

5.3 Examples of measured parameters in thaw/freeze processes

5.3.1 Radius of thawing around a well

Thaw estimates for non-insulated wells at Prudhoe Bay and Mackenzie Delta indicate that during a normal drilling operation, a 1 m radius zone will be thawed around the wellbore. For a 20 year oil production period, the total thawed zone around the well will have a radius of 15 m (Pui et al. 1975, Perkins et al. 1975). But this is only a guess, as thermal gradient and thermal conductivity of the sediments are poorly known.

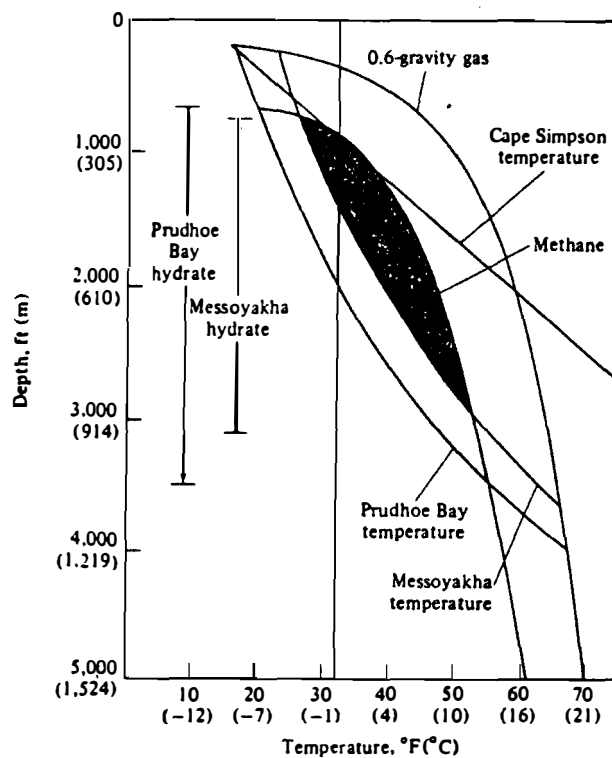


Fig. 5.1. Depth-temperature curve for predicting the depth and thickness of gas hydrates. Geothermal gradients are lower in permafrost than in deeper sections at Messoyakha and Prudhoe Bay (data from Holder et al. 1976, Makogon et al. 1971).

5.3.2 Thaw-subsidence induced loads

Few field tests due to thaw-subsidence induced loads have been reported in the literature. The best documented test was performed by Arco/Exxon in Prudhoe Bay (Goodman 1978). In 1973-74 a five spot thaw subsidence test was conducted. Figure 5.2 shows the results obtained after thawing an approximately 12 m radius zone (equivalent to 20 year production). These results show that significant deformations can be induced at the surface. Alternating compression and tension loads resulted in the permafrost zone. These alternating loads can be attributed to lithological variations. Above the base of the permafrost peak compressive stresses were measured, immediately below the base of permafrost tensile stresses were measured. This was interpreted as an uplifting force at the base of the permafrost. In 1972 Arco/Exxon recorded freezeback pressures in wells where hot fluid circulation had thawed a 1 m radius around the wells. The results of these measurements (Goodman & Wood 1975, Perkins et al. 1974) are shown in figure 5.3. It is interesting to note that freezeback stress can be 1.6 time higher than the state of stresses resulting from lithological overburden.

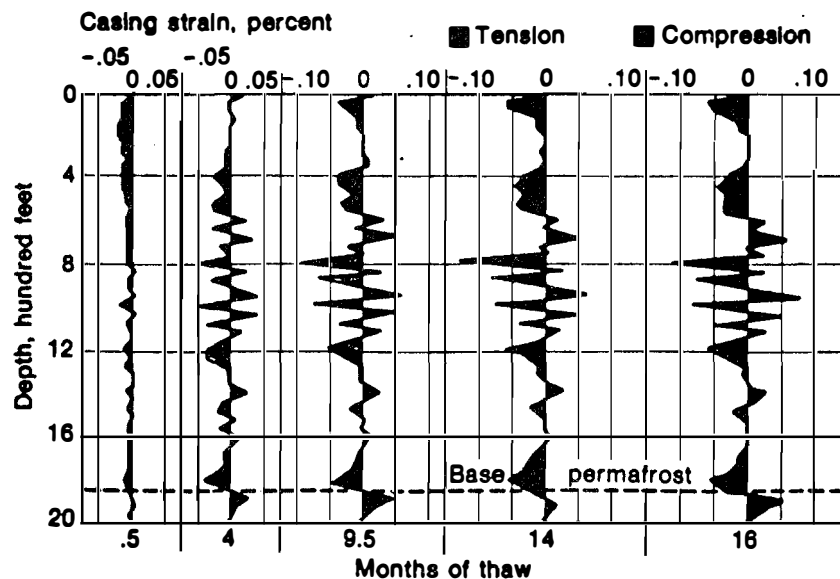


Fig. 5.2. Casing strain versus depth during progress of Arco/Exxon thaw test at Prudhoe Bay illustrates alternating strain in central region due to lithology and uplifting at the base of the permafrost (after Perkins et al. 1974).

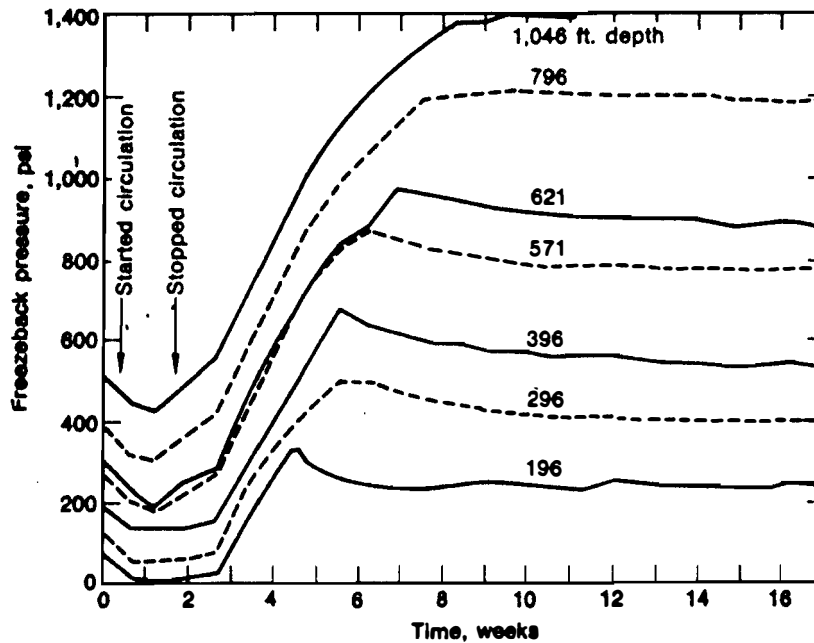


Fig. 5.3. Pressure buildup in a freezback test at Prudhoe Bay.

Maximum pressure increases with depth and shows only slight decline after complete freezback. Initial thaw radius was about 2.5 feet (after Goodman & Wood 1975).

5.4 Drilling problems in permafrost areas

5.4.1 Hole sloughing and washouts

In zones of thawed permafrost in unconsolidated sediments borehole sloughing and washout problems can be severe due to:

1. Frozen soil impermeability, which hinders filter cake build-up and limits differential pressure (overbalance) needed for well bore support.
2. Lateral loads across the thaw front which tend to squeeze the thawed material inward, and
3. Intergranular stress relief which tends to fluidize the thawed material.

5.4.2 Drilling through hydrates

While drilling through gas hydrates, two problems can be expected. The first and most important is to be able to control the well if gas under pressure is encountered below the hydrate layer. The second problem is the stability of the hole in the hydrate zone if this

begins to decompose. Increasing mud weight is not effective in controlling mud gasification from hydrates. Furthermore, it increases risk of losing circulation in normally pressured free-gas or water-bearing sands. However, careful wellsite supervision and mud-weight control are important, should abnormally pressured gas sands be encountered below the hydrate section.

To ensure maximum safety, hydrate zones should be anticipated and diagnosed quickly, and drilled at controlled rates with mud cooled to the hydrate equilibrium temperature. To prevent problems after hydrate zones are penetrated, cooled muds should continue to be used. And, where possible, hydrate zones should be cased off with high-collapse-strength casing (Goodmann 1978).

5.5 Drilling mud in permafrost areas

5.5.1 Mud types and properties

To minimize permafrost thaw it is important to drill the permafrost zone as rapidly as possible and with the least heat transfer from the wellbore to the formation. The drilling mud for permafrost should fulfill at least the following requirements : - Be effective in the removal of cuttings and coarse clastic sediments

to permit an adequate hole cleaning and assure fast penetration rates through permafrost.

- Inhibit mudstone and shale swelling.
- Increase the yield point.
- Depress the freezing point of the fluids.

Experience has shown that Bentonite-XC Polymer fluid with added potassium chloride (KCl) is effective to drill through shales and mudstones within a permafrost zone. In permafrost zones without shales, operators have found that the standard Bentonite-XC Polymer fluid together with controlled hydraulics are sufficient to clean the hole and maintain rheology.

5.5.2 Air and foam

Air and foam have been used successfully to minimize permafrost melting. In drilling 10 wells in the Yukon (Canada), Mobil Oil Canada, Ltd., used air to drill a 17¹/₂-inch hole to 750 feet. Standard Oil

Co. of California used stable foam to drill two 17¹/₂-inch surface holes through 350 feet permafrost. Penetration rates with foam were 2-3 times faster than drilling with lightweight gel muds. Advantages of foam, compared to air, are lower compressor requirements and better hole cleaning capacity.

Stable foam, generated by mixing compressed air and a special foam solution, can be treated with 10-15% by weight NaCl solution to depress the foam freezing point. Foam disposal is not a problem. Meeting subzero surface temperatures, foam freezes immediately into a brittle mass that readily collapses into a powder. Foam can be destroyed by a fine spray of diesel oil containing foam suppressant.

Formation sampling and gas detection with stable foam can be a potential problem, unless special means are used to separate cuttings and gas from the foam (Goodman 1978). The use of foam reduces the risk of casing collapse due to freezeback, because the foam mixture contains less than 2 % of water by volume. The principal disadvantage of stable foam is that special equipment is required.

5.6 Casing and completion equipment in permafrost areas

5.6.1 Casing design

There is no general procedure for casing design in permafrost areas, and each arctic region should be evaluated separately for local geological engineering conditions. In general the following aspects should be specially evaluated:

- Casing strain limits for permafrost casing
- Maximum thaw-subsidence and freezeback loads for casing/coupling selection.
- Wellhead material and seal requirements for low temperature application.

5.6.2 Completion equipment (Goodman 1978)

Because of conditions caused or related to permafrost in unlithified sediments, Arctic downhole completions must meet with unusual requirements. With the exception of insulated casing, equipment is standard, but its use is unique. For example, safety

valves are set deeper, provisions allow changes in tubing length and special methods are used to hang and cement production casing. Downhole production equipment in Arctic wells must be designed for maximum tubing movement caused by pressure effects, thermal strains and surface subsidence, as well as for potential disruptions because of unforeseen permafrost problems. The following special equipment can isolate permafrost and accommodate tubing movement.

- Surface controlled, subsurface safety valve (with dual control lines) placed below permafrost base.
- Tubing expansion joint placed above producing zone to withstand tubing length changes of nearly 20 feet.
- Hanger-tieback system for eliminating internal freezeback annuli during shut-in periods and for optional use of insulated casing.
- Full opening, multiple cycle cementing collars for circulating cement and/or insulating packer fluid into the annulus between surface casing and production casing.

5.6.3 Thermal production systems (Goodman 1978)

To reduce permafrost thaw around boreholes various thermal protection systems can be used. These systems normally have a dual effect: to reduce thaw and loads during drilling and to maintain permafrost undisturbed during production. Some of these thermal protection systems are:

- Non freezing, low water content packer fluids that are pumpable at permafrost temperatures but gel at producing temperatures to prevent thermal convection and decrease heat loss.
- Displacement mechanics developed for removal of water-based muds from wellbores in permafrost to prevent internal freezeback, and for placement of special packer fluids.
- Double-walled insulated tubing/casing that significantly reduces permafrost thaw and can be run with normal handling procedures.
- Refrigerated conductor casing and heat pipes (devices used on the Trans-Alaska pipeline) for keeping permafrost frozen and providing surface stability.

6. RELEVANT GEOPHYSICAL METHODS FOR DETECTION OF SUBSEA PERMAFROST AND GAS HYDRATES IN THE BARENTS SEA.

6.1 Detection of subsea permafrost

Most of the reported studies of offshore permafrost have been conducted on the Canadian and U.S. Beaufort Sea shelf. The physiography of this shelf is considerably different from that in the Barents Sea. As mentioned in Chapter 2, the cover of Quaternary sediments in the northern Barents Sea is generally thin, and locally missing. Subsea permafrost, if present, is therefore likely to occur in sedimentary rocks. In contrast, permafrost beneath the Beaufort Sea is mostly found in unlithified sediments with high porosity and low seismic velocity. Furthermore, the water depth in the Barents Sea averages 230 m, which is about 10 times deeper than the Beaufort Sea shelf. These differences are important concerning the geophysical methods for detection of subsea permafrost, discussed in Chapter 1.3.

In the Beaufort Sea, the seismic method (particularly the refraction method) has provided the best results concerning subsea permafrost identification. Different electrical methods have also been applied with limited success. Both the seismic and electrical methods depend upon changes in acoustic velocity and electrical resistivity in unfrozen and frozen ground.

Studies on unlithified sediments show a considerable increase in both acoustic velocity and electrical resistivity when temperature decreases to below 0°C (Rogers & Morack 1983) (Fig.1.10). In general, there is also a marked difference between the frozen and unfrozen state in lithified sediments (King 1977). However, the changes are affected by factors like porosity, pore fluid salinity, pore size and the mineral composition of the rocks. A sample of sandstone showed a smaller increase in seismic velocity compared to a sample of sand when frozen (Hnatiuk & Randall 1977). Furthermore, increasing shale content and decreasing porosity will cause the velocity change to decrease, and for tested shale samples, hardly any increase in compressional velocity was recorded when freezing the sample (King 1977). The electrical resistivity of shales of low porosity were also found to be relatively insensitive to freezing temperatures.

On southern Spitsbergen, the porosities in the near-surface sedimentary bedrock layers are known to be very low, 5-10% (Elverhøi &

Gronlie 1981). Similar values can reasonably be anticipated in the transect areas. However, the porosities are higher in the southern Barents Sea (F. Riis pers. comm. 1988), which is also indicated by the lowered seismic velocities in this area (Eldholm & Talwani 1977). Furthermore, the seismic velocities of the Mesozoic strata in the Barents Sea and in Svalbard overlap with the velocities of ice-bonded material (Eldholm & Talwani 1977, Elverhøi & Gronli 1981). Thus, seismic detection of possible ice-bonding in these low porosity, high velocity sediments seems very difficult.

Electrical methods may provide better results. However, there are restrictions in the use of several of the methods. Although the contrast necessary for successful differentiation of frozen and nonfrozen ground exists offshore, the critical problem is the high electrical conductivity of the sea water leading to an attenuation of the signals. Most of the electrical methods developed are only applicable in shallow water, and have been conducted either on sea ice over very shallow water, or on artificial islands.

A method that probably may be recommended for a local study in the Barents Sea, is the MOSES (Magnetometric Off-Shore Electrical Sounding) method, described in detail by Edwards & Wolfgram (1988). According to the authors, this method is particularly suitable for offshore electrical mapping as it can be made relatively insensitive to the shielding effects of the highly conductive sea water. The transmitter is a vertical, long-wire bipole, extending from the sea surface to the sea floor. A commuted current is fed to two large electrodes, one near the sea surface and the other on the sea floor (Fig. 6.1). The return current is through the sea water and the subjacent sediments. The receiver consists of two horizontal orthogonal coils located on the sea floor, and the data are measurements of two components of the magnetic field as a function of frequency and transmitter-receiver horizontal separation.

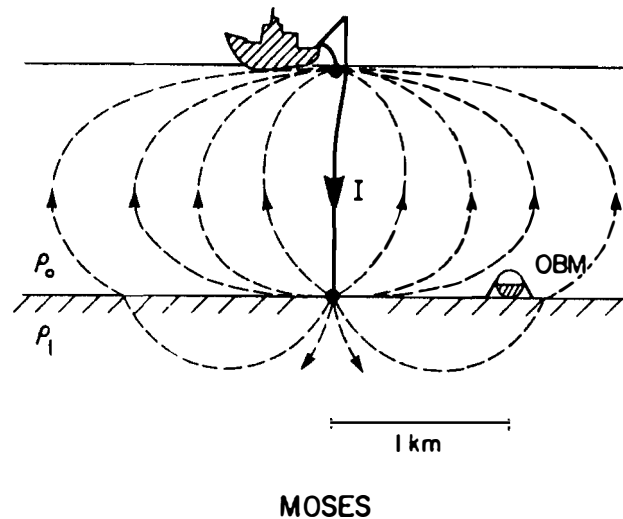


Fig. 6.1 The principle of physics behind the MOSES method. The current flow is axisymmetrical about the bipole source. The relatively small amount of current entering the resistive crust is inversely proportional to the ratio of the crustal resistivity to the sea resistivity. The magnetic field is a direct measure of the sea floor resistivity.

Due to the mentioned geological conditions in the northern Barents Sea, the seismic technique seems to be unappropriate as a detection method for subsea permafrost in the area. However, the MOSES method may be applicable for a local investigation of subsea permafrost in a restricted area, for instance on Spitsbergenbanken. It must be emphasized, however, that the electrical methods only provide spot soundings.

As geophysical methods only can provide indications of ice-banded permafrost, only drilling with subsequent temperature measurements and sampling can give the final verification.

6.2 Detection of gas hydrates

The most relevant method for detection of gas hydrates in the Barents Sea is seismic reflection. The occurrence of bottom simulating reflectors in an area which is regarded as being within the stability area for gas hydrates provides an indication for the presence of gas hydrates. However, to confirm the possible occurrence of gas hydrates, drilling data are required.

The seismic reflection method for detection of gas hydrates is described in Chapter 1.3.1, and will be briefly reviewed here. The base of the gas hydrate layer may give rise to a characteristic

seismic reflection which approximately parallels the sea floor and intersects the bedding reflectors. The reflection is caused by an acoustic impedance contrast between the gas hydrate zone and the underlying sediments. Free gas is often trapped beneath the gas hydrate layer, and will further enhance the acoustic impedance contrast. In general, these bottom simulating reflectors are characterized by a large reflection coefficient, an increasing subbottom depth with increasing water depth, and a reflection polarity reversal (Shipley et al. 1979).

Most of the reported occurrences of bottom simulating reflectors are from areas with relatively young, unlithified sediments. In Chapter 1.2 it is mentioned that laboratory tests show an increase in compressional velocity from 1850 m/s to 2700 m/s when unlithified sediments (sand) are filled with gas hydrates (Stoll 1974). So far, no studies concerning the effects of gas hydrates on rocks have been published.

In the northern Barents Sea the cover of unlithified sediments is generally thin and locally missing. Thus, gas hydrates, if present, will most likely be found in sedimentary bedrock. High seismic velocity and low porosity may cause difficulties with respect to the seismic method. Gas hydrates will not lead to any velocity increase if present in a rock with a seismic velocity of 2500-3000 m/s. Furthermore, the density is not likely to change enough to give rise to any significant change in acoustic impedance resulting in a seismic reflection. Thus, the presence of gas hydrates may be difficult to recognize in the case where there is no free gas.

Another problem with the seismic method is that most of the hydrocarbon exploration seismic reflection surveys are designed for deeper horizons. Events in the shallow layers may be suppressed, or even mistaken as multiples, ghosts, or bubble pulse reflections and thus, removed during processing of the data.

However, at present the seismic reflection method constitutes the most promising geophysical method for investigation of possible gas hydrate occurrence in the Barents Sea. Combined with a total evaluation of the geology, the latest geological history and a thermal prediction (discussed in Chapter 3.4), areas of interest may be pointed out. The final step in the detection of a gas hydrate occurrence is a correlation with well data, i.e. well logging and sediment sampling (described in Chapter 1.3.2 and 1.3.3).

7. CONCLUSIONS

In situ information on sub-sea permafrost, ice bearing sediments/rocks and gas hydrates in the Barents Sea is very limited. The evaluation of the possibilities for existence of these phenomena and their distribution is therefore largely based on the knowledge of the present day physical settings and the Late Cenozoic geological history of the Barents Sea, combined with information from other Arctic regions. The main conclusions are summarized in the following paragraphs:

7.1 Geological history and physical setting

1. In the northern Barents Sea, the flow of cold (-1°C) Arctic Water maintains the seabed below 0°C in areas where the water depth is shallower than 200 m. Below 200 m water depth, positive ($+1$ to $+4^{\circ}\text{C}$) sea floor temperatures are widely distributed due to influx of Atlantic Water.
2. Only minor changes in the Barents Sea floor temperatures are suggested during periods of glaciation, due to the pressure melting point conditions of -1 to -2°C at the base of the ice over large parts of the region. However, the loading of an up to 2500 m thick ice sheet implies a significant increase in the pressure.
3. The Barents Sea may have remained ice-free during glaciation of neighbouring land. Due to the global sea level lowering, shallow bank areas, down to approximately 150 water depth, may have been sub aerially exposed and may have experienced tundra conditions under which permafrost would develop.
4. The estimate of 1000 m glacial erosion in the central Barents Sea appears to be in conflict with the concept of waxing/waning ice sheets during the Late Cenozoic glacials and inter-glacials.

7.2 Permafrost

- 1) Permafrost is defined in terms of temperature, and thus areas covered with Arctic Water are by definition permafrost areas, because the temperature at the sea bed is below 0°C throughout the year.
- 2) The main part of the unlithified sediments is marine deposits. Due to the saline porewater, causing a depression of the freezing point, ice bearing layers will not form in temperatures above -1 to -1.5°C .
- 3) Sub-sea permafrost with formation of ice-bearing layers represents a major hazard for drilling and production in Arctic regions. The heating caused by drilling and, more seriously, the heating from warm oil or gas during a production phase can cause thawing and instability of the unlithified sediments.
- 4) If sub-sea ice-bearing layers are present in the Barents Sea, they will be located in sedimentary rocks, and therefore not represent the same hazards as in the other Arctic shelves where the ice-bearing layers mainly are found in originally unlithified sediments.
- 5) Seismic methods are widely used for identification of ice-bearing layers where these are situated within unlithified sediments and porous rocks, causing a distinct velocity increase.
- 6) In the Barents Sea, however, where low porosity rocks have seismic velocities close to those of ice, the use of seismic methods is inadequate. Under such conditions, electric measurements represent a more promising method.
- 7) Based on the Late Cenozoic geological history, present-day physical settings, in situ sub-bottom temperature measurement (only one) and composition and distribution of the unlithified sediments and underlying bedrock, there are most likely no ice bearing layers in the northwestern Barents Sea or on the shelf north and west of Svalbard.

- 8) Spitsbergenbanken is the only area of the Barents Sea where ice-bearing layers may have formed, and there is a total lack of in situ data from this region. Our recommendations for future work is therefore to carry out electrical measurements and/or shallow drilling in the shallowest parts of Spitsbergenbanken. These investigations should provide evidence to conclude if there are ice-bearing layers in the Barents Sea.

7.3 Gas hydrates

1. Although gas hydrates may have an economic potential, both as an energy source and as an impermeable seal for trapped free gas, the decomposition of gas hydrates represent a hazard for drilling and operation of production wells, posed by decomposition of gas hydrates. Decomposing gas hydrates may also be a potential source of greenhouse gases to the atmosphere. This effect was probably important during the last deglaciation.
2. The existence and distribution of gas hydrates depends on the temperature and pressure conditions, as well as on the availability of hydrocarbon gases, of which methane is the most important.
3. Using a Barents Sea thermal gradient of $31\text{ }^{\circ}\text{C}/\text{km}$, methane hydrate is stable (provided sufficient gas and time) in areas of water depth exceeding 280–300 m in the northern Barents Sea (bottom water temperature , 1°C) and 300–350 m in the southern parts of Bjørnøyrenna and Storfjordrenna (bottom water temperature , 2°C). Thickness of the hydrate layer, given the above numbers, may vary from 50 to 200 m, increasing with increasing water depth and decreasing temperature.
4. Adding gas components other than methane will lead to stability at shallower water depths and higher temperatures, i.e. a thicker hydrate layer.
5. The effect of glaciations will mainly result in an increased pressure, due to ice overburden. Hence, hydrates may, during glacials, form at depths in which they are unstable during interglacials.

6. Seismic reflection is the most relevant method for detection of gas hydrates. A bottom simulating reflection (BSR) marks the base of a hydrate layer and is characterized by a large reflection coefficient, reflection polarity reversal and increasing subbottom depth with increasing water depth.

7. As interpretation of seismic data from the Barents Sea has revealed seismic indications of gas hydrates, recommendations for future work in the region include:
 - Reprocessing of older seismic data, emphasizing on high resolution in the upper 1 second.
 - Acquisition of new high resolution seismic data, focusing in the areas in which this report suggests gas hydrates to be stable.
 - If possible, the acquisition parameters of exploration seismic data should be set to provide primarily seismic data for the exploration target, but also make it possible to reprocess the data to enhance resolution in the upper 1 second of the record.
 - Conduct exploratory drilling, coring and well logging in areas where seismic profiles indicate the possibility of hydrates.

REFERENCES

- Anderson, D.M., Tice, A.R., McKim, H.L., 1973; The unfrozen water and the specific heat capacity of frozen soils. In: Proc. 2nd Intern. Conf. Permafrost, Yakutsk, U.S.S.R., Nat. Acad. Sciences, Washington D.C., 257-288.
- Antonsen, P. & Flood, S.B., 1987: En studie av øvre berggrunn i det nordlige Barentshav. Unpubl. Cand. Scient thesis, University of Oslo, 212 pp.
- Antonsen, P., Elverhøi, A., Dypvik, H. & Solheim, A., in prep.: The shallow bedrock geology in the Olga Basin area, northwestern Barents Sea.
- Badley, M.E., 1985; Practical Seismic Interpretation. Reidel, 266 pp.
- Banin, & Anderson, 1974; Effects of salt concentration changes during freezing on the unfrozen water content of porous materials., Water resources research 10, (1).
- Bell, M. & Laine, E.P., 1985; Erosion of the Laurentide Region of North America by Glacial and Glaciofluvial Processes. Quaternary Research 23, 154-174.
- Berge, A.M. & Beskow, B., 1983; A method to determine the velocities in the seafloor and near-surface sediments. NPD contribution (12), 53 pp.
- Beskow, B., Berge, A.M. & Kanestrøm, R., 1984; Interpretation and modelling of seismic data from the Barents Sea. NPD contribution (16), 118 pp.
- Blasco, S, 1984; A perspective on the distribution of subsea permafrost on the Canadian Beaufort continental shelf. In: Final proceedings, Fourth Int. Conf. Permafrost, National Academy Press, Wash. D.C., 83-86.

- Boulton, G.S., 1974; Processes and pattern of glacial erosion. In: Coates, D.R. (ed.), *Glacial Geomorphology*. Binghamton, N.Y. State University of New York, 41-87.
- Boulton, G.S., 1976; The origin of glacially fluted surfaces - observations and theory. *Journal of Glaciology* 17, (76), 287-309.
- Boulton, G.S., & Jones, A.S., 1979; Stability of temperate ice caps and ice sheets resting on beds of deformable sediment. *Journal of Glaciology* 24, (90), 29-43.
- Boulton, G.S., 1981; Deformation of subglacial sediments and its implications. *Annals of Glaciology* 2, 114.
- Brigham-Grette, J., Matthews, J.V. & Schweger, C., 1988; Nearshore and Terrestrial Evidence for Pre-Glacial Arctic Environments across North America and Greenland. In: Bleil & Thiede (eds.), *Geologic history of the Polar Oceans: Arctic versus Antarctic*.
- Bryan, G.M., 1974; In situ indications of gas hydrates. In *Natural gases in marine sediments: Marine Science* 3, 299-308.
- Bugge, T., Befring, S., Belderson, R.H., Eidvin, T., Jansen, E., Kenyon, N.H., Holtedahl, H. & Sejrup, H.P., 1987; A giant three-stage submarine slide off Norway. *Geo-Marine Letters* 7, 191-198.
- Carpenter, G., 1981; Coincident sediment slump/clathrate complexes on the U.S. Atlantic continental slope. *Geo-marine Letters* 1, 29-32.
- Carter, D.L., Brigham-Grette, J., Marinovich, L., Pease, V.L. & Hillhausen, J.W., 1986; Late Cenozoic Arctic Ocean sea ice and terrestrial paleoclimate. *Geology* 14, 675-678.
- Clark, D.L., 1982; Origin, nature and world climate effect of Arctic Ocean ice cover. *Nature* 300, 321-325.

- Claypool, G.E. & Kaplan, I.R., 1974; The origin and distribution of methane in marine sediments. In Natural gases in marine sediments: Marine Sciences 3, 99-139.
- Collett, T.S., 1983; Detection and evolution of natural gas hydrates from well logs, Prudhoe Bay, Alaska. Proceedings Fourth Int. Conf. Permafrost., Natl. Res. Counc., Canada, 169-174.
- Collett, T.S., Bird, K.J., Kvernfolden, K.A. & Magoon, L.B., 1988; Geologic interrelations relative to gas hydrates within the North Slope of Alaska. Open File Rep. 88-389., 150 pp.
- Corwin, R.F., 1983; Marine permafrost detection using galvanic electrical resistivity methods. Offshore Technology Conference., Houston, Texas, 1983.
- Davidson, D.W., El-Defrawy, M.K., Fuglem, M.O. & Judge, A.S., 1978; Natural gas hydrates in northern Canada. Proceedings Third Int. Conf. Permafrost 1, 937-943.
- Davy, H., 1811; On some of the combinations of oxy-muriatic gas and oxygen, and on the chemical relations of the principles to inflammable bodies. Royal Soc. London Philos. Trans. 101, p.1.
- Drewry, D., 1986; Glacial Geologic Processes. Edward Arnold Ltd., London, 276 pp.
- Denton, G.H. & Hughes, T.J., 1981; The Arctic Ice Sheet: An outrageous hypothesis. In: G.H. Denton and T.J. Hughes (Eds.), The Last Great Ice Sheets, John Wiley & Sons, 437-467.
- Dowdeswell, E.K., 1988; The Cenozoic Stratigraphy and Tectonic Development of the Barents Shelf. In: Harland, W.B. & Dowdeswell, E.K. (Eds.), Geological Evolution of the Barents Shelf Region. Graham & Trotman, 131-155.
- Ehrenbard, R.L., Hoekstra, P. & Rozenberg, G., 1983; Transient electromagnetic soundings for permafrost mapping. Proceedings Fourth Int. Conf. Permafrost. National Academy Press, Washington, D.C., 272-277.

- Eide, L.I., 1983; Environmental conditions in the Barents Sea and near Jan Mayen. A report. Norsk Meteorologisk Inst.
- Eidvin, T., Fjeldskaar, W. & Riis, F., 1989; Ny datering av tertiær erosjon i Barentshavet. Abstract til Norsk Geologisk Forenings XI. Landsmøte Bergen 1989.
- Eilertsen, B., Loeng, H., Rey, F. & Tjelmeland, S, 1981; The feeding conditions of capelin during summer: Field observations in 1979 and 1980. Fisken Hav 3, 1-68.
- Eldholm, O. & Talwani, M., 1977; The sediment distribution and structural framework of the Barents Sea. Bull. Geol. Soc. Am. 88, 1015-1029.
- Eldholm, O., Sundvor, E. & Crane, K., 1984; Sonobuoy measurements during the "Ymer" Expedition. Norsk Polarinstitutt Skrift. 180, 17-23.
- Elverhøi, A., Grønli, G., 1981; Diagenetic and sedimentologic explanation for high seismic velocity and low porosity in Mesozoic - Tertiary sediments, Svalbard Regions. American Association of Petroleum Geologists, Bulletin 65 (1), 145-153.
- Elverhøi, A., Lønne, Ø. & Seland, R., 1983; Glaciomarine sedimentation in a modern fjord environment, Spitsbergen. Polar Research 1, 127-149.
- Elverhøi, A. & Solheim, A., 1983; The Barents Sea ice sheet - a sedimentological discussion. Polar Research 1, 23-42.
- Elverhøi, A. & Solheim, A., 1987; Shallow geology and geophysics of the Barents Sea. Norsk Polarinstitutt Rapportserie 37, 71pp.
- Elverhøi, A., Antonsen, P., Flood, S., Solheim, A. & Vullstad, A.A., 1988; The physical environment. Western Barents Sea, 1:1500000, Shallow bedrock geology - Structure, litho - and biostratigraphy. Norsk Polarinstitutt Skrift. 179D, 44 pp.

- Elverhøi, A., Pfirman, S.L., Solheim, A. & Larsen, B.B., 1989:
Glaciomarine sedimentation in epicontinental seas exemplified by
the northern Barents Sea. *Marine Geology* 85, 225-250.
- Elverhøi, A., Solheim, A., Berg, M.N. & Russwurm, L., in
press.: Deglaciation of the marine based Barents Sea Ice Sheet;
Sediments and sedimentary processes. NATO Advanced studies.
- Faleide, J.I., Gudlaugson, S.T. & Jacquart, G., 1984;
Evolution of the western Barents Sea. *Marine and
Petroleum Geology* 1, 123-150.
- Flint, R.F., 1957; *Glacial and Pleistocene Geology*. John Wiley and
Sons, New York, 553 pp.
- Flint, R.F., 1971; *Glacial and Quaternary Geology*. John Wiley and
Sons, New York, 892 pp.
- Forsberg, C.F., 1983; Sedimentation and early diagenesis of Late
Quaternary deposits in central parts of the Barents Sea. Unpubl.
Cand. Real thesis, University of Oslo, 120 pp.
- Gabrielsen, R.G., Færseth, R., Hamar, G. & Rønnevik, H.C., 1984:
Nomenclature of the main structural features on the Norwegian
continental shelf north of 62nd parallel. In: Spencer, A.M
et al. (Eds.). *Petroleum Geology of the North European
Margin*. Norwegian Petroleum Society/Graham & Trotman, London
1984, 41-60.
- Gabrielsen, R.G., Færseth, R., Jensen, L.J., Kalheim, J.E. & Riis,
in prep.: Nomenclature of structural elements in the Barents Sea,
Norwegian shelf, Norwegian Petroleum Directorate (NPD) Bulletin.
- Gammelsrød, T. & Rudels, B., 1983; Hydrographic and current
measurements in the Fram Strait, August 1981.
Polar Research 1, 115-126.
- Glen, J.W., 1955; The creep of polycrystalline ice. *Proc. R. Soc.
London, Ser. A* 228, 519-538.

- Gold, L.W. & Lachenbruch, A.H., 1973; Thermal Condition in Permafrost, Second International Conference, Washington D.C.
- Goodman, M.A., 1975; Mechanical properties of simulated deep permafrost. *Journal of Engineering for Industry*. Trans ASME 97, series BV 82.
- Goodman, M.A. & Wood, D.B., 1975; A mechanical model for permafrost freeze back pressure behavior. *SPE Journal* 1975, Trans. AIME V. 259.
- Goodman, M.A., 1978; Series of technical notes of non-proprietary technology on petroleum exploration in Arctic frontiers. World Oil Publication.
- Goodman, M.A., Giussani, A.P. & Alger, R.P., 1982; Detection and evaluation methods for in-situ gas hydrates. *Soc. Petr. Engin. Unconventional gas recovery symposium, Proc.*
- Hagen, J.O., Wold, B., Listøl, O., Østrem, G. & Sollid, J.L., 1983; Subglacial processes at Bondhusbreen, Norway: preliminary results. *Annals of Glaciology* 4, 91-98.
- Hald, M., & Vorren, T.O., 1987; Stable isotope Stratigraphy and paleoceanography during the last deglaciation on the continental shelf off Troms, Northern Norway., *Paleoceanography* 2 (6), 583-599.
- Hallet, B., 1979; Subglacial regelation water film. *Journal of Glaciology* 23, 321-333.
- Hallet, B., 1981; Glacial abrasion and sliding: their dependence on the debris concentration in basal ice. *Annals of Glaciology* 2, 23-28.
- Hammerschmidt, E.G., 1934; Formation of gas hydrates in natural gas transmission lines. *Ind. Eng. Chem* 26, 851 pp.

- Hand, J.H., Katz, D.L. & Verma, V.K., 1974; Review of gas hydrates with implication for ocean sediments. In: I.R. Kaplan (ed.), *Natural gases in marine sediments.*, Plenum Press, New York.
- Harrison, W.D. & Osterkamp, T.E., 1982; Measurements of the electrical conductivity of interstitial water in subsea permafrost. *Proceedings Fourth Can. Permafrost Conf.*, Calgary. Natl. Res. Counc. Canada, 229-237.
- Hedberg, H.D., 1974: Relation of methane generation to undercompacted shale, shale diapirs, and mudvolcanoes. *American Association of Petroleum Geologists, Bulletin* 58 (4), 661-673.
- Herman, Y. & Hopkins, D.M., 1980; Arctic Ocean climate in Late Cenozoic time. *Science* 209, 557-562.
- Hitchon, B., 1974; Occurrence of natural gas hydrates in sedimentary basins. In: I.R. Kaplan (ed), *Natural gases in marine sediments.*, Plenum, New York, 195-225.
- Hoekstra, P., 1969; The physics and chemistry of frozen soils. *Highway Research Board Special Report* 103, 78-90.
- Holder, G.D., Malone, R.D. & Lawson, W.F., 1985; The effects of gas composition and geothermal properties on the thickness and depth of natural gas hydrate zones. *Soc. Petr. Engineers, Annual Calif. Regional Meeting, Proc.*, 55.
- Holder, G.D., Katz, D.L. & Hand J.H., 1976; Hydrate formation in subsurface environments. *AAPG Bull.* 60, 981-988.
- Hooke, R. LeB., 1977; Basal Temperatures in Polar Ice Sheets: A Qualitative Review. *Quaternary Research* 7, 1-13.
- Hoppe, G., 1970; The Wurm ice sheets of northern and Arctic Europe. *Acta Geographica Lodziensia* 24, 105-115.
- Houtz, R.E., 1980; Seafloor and near-surface sound velocities from Barents Sea sonobuoy data. *Journ. Geoph. Res.* 85, 4838-4844.

- Howitt, F., 1971; Permafrost geology at Prudhoe Bay. World Petroleum, sept. 71.
- Hunt, J.M., 1979; Petroleum geology and geochemistry.
W.H. Freeman and Company, San Fransisco, California, 617 pp.
- Hunter, J.A.M., Neave, K.G., MacAulay, H.A. & Hobson, G.D., 1978;
Interpretation of sub-seabottom permafrost in the
Beaufort Sea by seismic methods, 1, Seismic refraction
methods. Proceedings, Third Int. Conf. Permafrost,
Natl. Res. Counc. Canada, 515-520.
- Hunter, J.A.M., 1984; Geophysical techniques for subsea
permafrost investigations. Final proceedings,
Fourth Int. Conf. Permafrost, National Academy Press,
Wash. D.C., 88-89.
- IKU news, 1988; Offshore permafrost in the Barents Sea. IKU news no. 3
1988.
- Jansen, E., Bleil, U., Heinrich, R., Kringstad, L. & Slettemark, B.,
1987; Climatic changes in the Norwegian Sea during the last
2.8 Ma., Polar Research 5, 329-332.
- Jansen, E., Bleil, U., Henrich, R., Kringstad, L. & Slettemark, B.,
1988; Paleoenvironmental changes in the Norwegian Sea and the
Northeast Atlantic during the last 2.8 m.y.: Deep Sea Drilling
Project/Ocean Drilling Program sites 610, 642, 643 and 644.
Paleoceanography 3 (5), 563-581.
- Jansen, E., Sjøholm, J., Bleil, U. & Erichsen, J.A., in press; Neogene
and Pleistocene Glaciations in the Northern Hemisphere and
Miocene-Pliocene Global Ice Volume fluctuations: Evidence from
the Norwegian Sea. In: Bleil & Thiede (eds.), Geologic history of
the Polar Oceans: Arctic versus Antarctic. NATO ASI Series,
Kluwer Acad. Publ. (Submitted Jan. 1989.)

- Johannessen, O.M. & Foster, L.A., 1978; A note on the topographically controlled oceanic Polar Front in the Barents Sea. Journ. Geoph. Research 63 (C9), 4567-4571.
- Jones, G.A., 1987; The central Arctic Ocean sediment record: Current progress in moving from a litho- to a chronostratigraphy. Polar Research 5, 309-311.
- Jones G.A. & Keigwin, 1988; Evidence from Fram Strait (78 N) for early deglaciation. Nature 336, 56-59.
- Judge, A.S., 1982; Natural gas hydrates in Canada. In: H.M. French (ed.), Proceedings, Fourth Can. Conf. Permafrost., Natl. Res. Council. Canada, 320-328.
- Katz, D.L. et al., 1959; Water-hydrocarbons systems. Handbook of natural gas engineering. New York: McGraw-Hill, 189-211.
- Katz, D.L., 1971; Depths to which frozen gas fields (gas hydrates) may be expected. Journ. Petr. Tech. 23, 419-423.
- Katz, H.R., 1982; Evidence of gas hydrates beneath the continental slope, East Coast, North Island, New Zealand. New Zealand Journal of Geology and Geophysics 25, 193-199.
- Kersten, M.S., 1948; Thermal conductivity of soils. Proc. Highway Res. Board 28, 391-409.
- King, M.S., 1977; Acoustic velocities and electrical properties of frozen sandstones and shales. Canadian Journal of Earth Sciences 14, 1004-1013.
- King, M.S., Pandit, B.I., Hunter, J.A. & Gajtani, M., 1982; Some seismic, electrical, and thermal properties of sub-seabottom permafrost from the Beaufort Sea. Proceedings, Fourth Canadian Permafrost Conf., Nat. Res. Council. Canada, 268-274.

- King, M.S., 1984; The influence of clay-sized particles on seismic velocity for Canadian Arctic permafrost. *Canadian Jour. of Earth Sciences* 14, 1004-1013.
- Kjeldsen, O., 1983; Materialtransportundersøkelser i norske breelver. Rapport 1 - 83. Vassdragsdirektoratet Hydrologisk Avdeling, Oslo, 39 pp.
- Kvenvolden, K.A. & McMenamin, M.A., 1980; Hydrates of natural gas - a review of their geologic occurrence. *U.S. Geol. Surv. Circ.* 825, 11 pp.
- Kvenvolden, K.A., 1982; Occurrence and origin of marine gas hydrates. *Proceedings, Fourth Can. Conf. Permafrost., Natl. Res. Council. Canada*, 305-311.
- Kvenvolden, K.A. & Barnard, L.A., 1983; Hydrates of Natural Gas in Continental Margins. In: Watkins & Drake (eds.), *Studies in continental margin geology. AAPG Memoir* 34, 631-640.
- Kvenvolden, K.A. & Barnard, L.A., 1983b; Gas Hydrates of the Blake Outer Ridge, Site 533, DSDP Leg 76. *Init. Reports DSDP 76, Washington*, 353-366.
- Kvenvolden K.A., Barnard, L.A. & Cameron, D.H., 1983; Pressure Core Barrel: Application to the study of gas hydrates, DSDP Site 533, Leg 76. *Init. Reports DSDP Leg 76, Washington*, 367-375.
- Kvenvolden, K.A. & McDonald, T.J., 1985; Gas Hydrates of the Middle America Trench DSDP Leg 84. *Init. Reports DSDP 84, Washington*, 667-682.
- Kvenvolden, K.A. & Kastner, M., 1988; Gas Hydrates of the Peruvian continental margin. *Proc. ODP Leg 112*.
- Lachenbruch, A.H., Sass, J.H, Marshall, B.V. & Moses, T.H. Jr., 1982; Permafrost, Heat Flow, and the Geothermal Regime at Prudhoe Bay, Alaska. *Jour. Geophys. Res.* 87, 9301-9315.

- Ladd, C.C., Jeffery, S.W. & Germaine, T.J., 1984; Strength-deformation properties of Arctic silts. ASCE Arctic Conference San Francisco.
- Landvik, J.Y., Mangerud, J. & Salvigsen, O., 1988; Glacial history and permafrost in the Svalbard area. *Proceedings 5. International Conference on Permafrost*, Tapir, 194-198.
- Lehman, S.J. & Forman, S.L., 1987; Glacier extent and sea level variation during the Late Weichselian on northwest Spitsbergen. *Polar Research* 5, 271-272.
- Lindner, L., Marks, L. & Pekala, K., 1987; Quaternary chronostratigraphy of south Spitsbergen. *Polar Research* 5, 273-274.
- Liestøl, O., 1974; Glaciological work in 1972. Norsk Polarinstitutt Årbok 1972
- Liestøl, O., 1980; Permafrost conditions in Spitsbergen. *Frost i jord* nr. 21.
- Loeng, H., 1979; Isforholdene i Barentshavet og vest av Spitsbergen. En oversikt. *Fisken og havet* (2), 29-75.
- Loeng, H., 1980; Fysiske oceanografiske undersøkelser i sentrale deler av Barentshavet i juli 1979. *Fisken og Havet* (3), 29-60.
- Loeng, H., 1983; Klimavariasjoner i tre hydrografiske snitt i Barentshavet i perioden 1977-1982. *Fisken Hav* (3), 5-21.
- Loeng, H. & Skjoldal, H.R., 1987; Physical and biological oceanographic features across the Polar Front in the Western Barents Sea. 22nd Europ. Marine Biol. Symp., Barcelona August 1987.
- Lutkevich, E.M., 1937; Geology of the Tertiary Coalbearing Deposits of Spitsbergen in the Ice-Fjord Region. *Trans. Arctic Inst.* 76, 7-24.

- MacAulay & Hunter, 1982; Detailed seismic refraction analysis of ice-banded permafrost layering in the Canadian Beaufort Sea. Proceedings, Fourth Can. Permafrost Conf. Calgary, Natl. Res. Council. Canada, 256-267.
- Macleod, M.K., 1982; Gas hydrates in ocean bottom sediments. Am. Ass. Petr. Geol. Bull. 66 (12), 2649-2662.
- Makogon, Y.F., T...in, F.A., Tsarev, V.P. & Cherkizy, N.V., 1971; Detection of a pool of natural gas in a solid (hydrated gas) state. Dokl. Akad. Nauk. SSSR 196.
- Mangerud, J., Bolstad, M., Elgersma, A., Helliksen, D., Landvik, J.Y., Lycke, A.C., Lønne, I., Salvigsen, O., Sandahl T. & Seirup H.P., 1987; The late Weichselian glacial maximum in western Svalbard. Polar Research 5, 275-278.
- Manley, P.L. & Flood, R.D., 1988; Cyclic sediment deposition within Amazon Deep-Sea Fan. Am. Ass. Petr. Geol. Bull. 72 (8), 912-925.
- Markl, R.G., Bryan, G.M. & Ewing, J.I., 1970; Structure of the Blake-Bahama Outer Ridge. Jour. Geophys. Research, 75, 4539-4555.
- Markussen, B., Zahn, R., & Thiede, J., 1985; Late Quaternary sedimentation in the Eastern Arctic Basin. Stratigraphy and depositional environment. Palaeogeography, Palaeoclimatology, Palaeoecology 50, 271-284.
- McIver, R.D., 1982; Role of naturally occurring gas hydrates in sediment transport. Am. Ass. Petr. Geol. Bull. 66 (6), 789-792.
- Midttun, L., 1985; Formation of dense bottom water in the Barents Sea. Deep Sea Res. 32 (10), 1233-1241.
- Midttun, L. & Loeng, H., 1987; Climatic variations in the Barents Sea. Proc. 3. Soviet-Norwegian Symp., Murmansk May 1986.

- Miller, G.H., 1982; Quaternary depositional episodes, western Spitsbergen, Norway: aminostratigraphy and glacial history. *Arctic and Alpine Research* 14, 321-340.
- Miller, G.H., Sejrup, H.P., Lehman, S.J. & Forman, S.L., 1987; The last glacial-interglacial cycle, western Spitsbergen, Svalbard archipelago. *Polar Research* 5, 279-280.
- Milliman, J.D. & Meade, R.H., 1983; World wide delivery of river sediment to the oceans. *Journal of Geology* 91, 1-21.
- Morack, J.L. & Rogers, J.C., 1982; Marine seismic refraction measurement of near-shore subsea permafrost. *Proceedings Fourth Can. Permafrost Conf.*, Calgary Natl. Res. Counc. Canada, 249-255.
- Morack, J.L., MacAulay, H.A. & Hunter, J.A., 1983; Geophysical measurements of subbottom permafrost in the Canadian Beaufort Sea. *Proceedings Fourth Int. Conf.*, National Academy Press, 866-871.
- Murzin, R.R., Bogolepov, A.K. & Junov, J.A., 1984; New data on the geological make-up of the northeastern part of the Barents Sea. In *Neftegazoznosit' Mirovogo okeano: sbornik nauchnykh trudov.*- Leningrad, PGO Semorgeologija, 40-47.
- Neave, K.G. & Sellmann, P.V., 1984; Determining distribution patterns of ice-banded permafrost in the U.S. Beaufort Sea from seismic data. In: P.W. Barnes, D.M. Schell & E. Reimnitz (eds.), *The Alaskan Beaufort Sea, Ecosystems and Environments.* Academic Press Inc., 237-258.
- O'Connor, M.J., 1981; Distribution of shallow acoustic permafrost in the Southern Beaufort Sea. *Geological Survey of Canada, Open File Report* 953.
- Orvin, A.K., 1944; Litt om kilder på Svalbard. *Norsk Geografisk Tidsskrift* X (1).

- Osterkamp, T.E., 1975; Structure and properties of ice lenses in frozen ground, Report No. UAG-R233, Geoph. Inst., University of Alaska, Fairbanks, Alaska. 36 pp.
- Osterkamp, T.E. Payne, M.W., 1981; Estimates of permafrost thickness from well logs in northern Alaska. Cold Regions Science and Technology 5, 13-27.
- Osterkamp, T.E. & Harrison, W.D., 1982; Temperature measurements in subsea permafrost off the coast of Alaska. In: H.M. French (ed.), Proceedings Fourth Can. Permafrost Conf., Calgary, Natl. Res. Council, Canada, 238-248.
- Panayev, V.A., 1987; Gas hydrates in the oceans. International Geology Review.
- Parent, J.D., 1984; A survey of United States and total world production, proved reserves, and remaining recoverable resources of fossil fuels and uranium as of December 31, 1982: Inst. Gas Tech., Chicago, Illinois.
- Paterson, W.S.B., 1981; The Physics of Glaciers. Pergamon, 380 pp.
- Pewe, T.L., 1974; Permafrost, New York, Encyclopedia Britannica.
- Perkins, T.K., Rechow, J.A. & Knowlas, C.K., 1974; Studies of pressures generated upon refreezing of thawed permafrost around a wellbore. JPT 1974.
- Perkins, T.K., Rechow, J.A., Ruedrich, R.A., Schuh, F.S. & Wooley, G.R., 1975; Prudhoe Bay field permafrost casing and well design for thaw-subsidence protection. Atlantic Richfield Co., North American producing dillitaton. Report to State of Alaska.
- Pfirman, S.L., 1985; Modern sedimentation in the northern Barents Sea: Input, dispersal and deposition of suspended sediments from glacial meltwater. Woods Hole Oceanographic Inst., Unpubl. Ph.D. thesis, 284 pp.

- Plafker, G., 1981; Late Cenozoic glaciomarine deposits of the Yakataga Formation, Alaska. In: Hambrey, M.J. and Harland, W.B., (Eds.), *Earth's pre-Pleistocene glacial record*, (Cambridge University Press), 694-699.
- Potential Gas Agency, 1981; Gas Hydrates. In: Potential supply of natural gas in the United States (as of December 31, 1980): Colorado School of Mines, Golden, Colorado, 76-89.
- Pui, N.K. & Kljuec, N.H., 1975; Temperature simulation while drilling permafrost. Paper presented at the 26th. annual technical meeting of CIM. Banff. can.
- Rampton, V.N. & Mackay, J.R., 1971; Marine ice and icy sediments throughout the Tuktoyaktuk Peninsula, Richards Island and nearby areas. District of Mackenzie. Geological Survey of Canada. Dept. of Energy and Resources, Ottawa.
- Roldalset, E. & Rosenquist, I.Th., 1971; Absorbed rare earth elements as a clue to the origin of some glacial clays. Bull. Group franc. Argiles XXIII, 191-194.
- Rogers, J.C. & Morack, J.L., 1980; Geophysical evidence of shallow near-shore permafrost, Prudhoe Bay, Alaska. Jour. Geoph. Res. 85, (B9), 4845-4853.
- Rothlisberger, H., 1972; Water pressure in intra- and subglacial channels. Journal of Glaciology 11 (62), 177-203.
- Rothlisberger, H. & Iken, A., 1981; Plucking as an effect of water-pressure variations at the glacier bed. Annals of Glaciology, vol 2, 57-62.
- Rønnevik, H.C., Beskow, B. & Jacobsen, H.P., 1982; Structural and stratigraphic evolution of the Barents Sea. Norw. Petrol. Soc., Geol. Mem. 8, 431-440.

- Rønnevik, H.C. & Jacobsen, H-P., 1984; Structural highs and basins in the western Barents Sea. In Graham & Trotman (eds): Petr. Geol. of the North European Margin., Norw. Petr. Soc., 19-32.
- Salvigsen, O., 1981; Radiocarbon dated raised beaches in Kong Karls Land, Svalbard, and their consequences for the glacial history of the Barents Sea Area. Geographical Annual 63A, 283-291.
- Salvigsen, O. & Østerholm, H., 1982; Radiocarbon dated beaches and glacial history of northern coast of Spitsbergen, Svalbard. Polar Research 1, 97-115.
- Sartorelli, A.M. & French, R.B., 1982; Electromagnetic methods for mapping permafrost along northern pipeline corridors. Proceedings Fourth Can. Permafrost Conf., Calgary, Natl. Res. Counc. Canada, 283-295.
- Sayles, F.H., 1966; Low temperature soil mechanics. Tech. Note U.S. Army CRREL, Hanover, N.H.
- Schei, B., Eilertsen, H.G., Falk-Larsen, S., Gulliksen, B. & Taasen, J.P., 1979; Marinbiologiske undersøkelser i Van Mijenfjorden etter oljesøllekkasje ved Sveagrava 1978. Trosø Mus. Rapportser., Naturvitenskap 2, 50 pp.
- Sellmann, P.V. & Hopkins, D.M., 1984; Subsea permafrost distribution on the Alaskan shelf. Final proceedings, Fourth Int. Conf. Permafrost, Natl. Academy Press, Wash. D.C., 75-82.
- Shackleton, N.J., 1987; Oxygen Isotopes, Ice Volume and Sea Level. Quaternary Science Reviews 6, 183-190.
- Shcheglova, O.P. & Chizhov, O.P., 1981; Sediment transport from the glacier zone, Central Asia. Annals of Glaciology 2, 103-108.

- Shiple, T.H., Houston, M.H., Buffler, R.T., Shaub, F.J.,
McMillen, K.J., Ladd, J.W. & Worzel, J.L., 1979;
Seismic evidence for widespread possible Gas Hydrate
horizons on Continental Slopes and Rises.
AAPG Bull. 63 (12), 2204-2213.
- Shreve, R.L., 1984; Glacier sliding at subfreezing temperature.
Journal of Glaciology 30 (106), 341-347.
- Solheim, A. & Kristoffersen, Y., 1984; The physical environment,
Western Barents Sea, 1:1500000, sheet B; Sediments above the
upper regional unconformity: Thickness, seismic stratigraphy and
outline of the glacial history. Norsk Polarinstitutt Skrift.
179B, 26 pp.
- Solheim, A., & Elverhøi, A., 1985; A pockmark field in the central
Barents Sea; gas from a petrogenic source?
Polar Research 3, 11-19.
- Solheim, A., 1988; Glacial geology of the northern Barents Sea, with
emphasis on the surge related, ice proximal depositional
environment. Norsk Polarinstitutt Rapportserie 47, 343pp.
- Solheim, A., Milliman, J.D. & Elverhøi, A., 1988; Sediment
distribution and sea floor morphology of Storbanken, implications
for the glacial history of the northern Barents Sea. Canadian
Journal of Earth Sciences 25, 547-556.
- Solheim, A., Elverhøi, A., Russwurm, L. & Berg, M. N., in press; The
Marine Barents Sea Ice Sheet, Sub- and Pro Glacial features and
Processes.
- Steel, R.F. & Worsley, D., 1984; Svalbard's post Caledonian strata-
an atlas of sedimentational patterns and paleogeographic
evolution. In Graham & Trotman (eds): Petr. Geol. of the
North Europ. Marg., Norw. Petr. Soc., 109-135.
- Steffensen, E.L., 1982; The climate at Norwegian Arctic stations.
Klima 5, 44 pp.

- Stoll, R.D., 1974; Effects of gas hydrates in sediments.
In: I.R.Kaplan (ed.), Natural gases in marine sediments., Plenum Press, New York, 235-248.
- Stoll, R.D. & Bryan, G.M., 1979; Physical properties of sediments containing gas hydrates. Journal of Geophysical Research 84 (B4), 1629-1634.
- Tantsiura, A.I., 1959; On the currents of the Barents Sea. In: Kripovic (Ed.). Polar Sci. Res. Inst. Fish. Econ. Oceanogr. (PINRO), Murmansk, 11, 35-53.
- Trondsen, T. & Bjærke, T., 1983; Palynodebris analysis of a shallow core from the Barents Sea. Polar Research 1 (1), 43-47
- Tsyтович, N.A., 1975; The mechanics of frozen ground.
Translated by Scripta Book Company, Washington, D.C.
- Ulmishek, G., 1985; Geology and petroleum resources of the Barents-Northern Kara Shelf in light of new geologic data.
Argonne National Laboratory, report ANL/ES-148, 89 pp.
- Verba, M.L., 1984; Barents Sea.
In I.S. Gramberg & Y.Y. Pogrebitskiy (eds): Geological structure and economic minerals of the USSR (9): Seas of the Soviet Arctic, Nedra, Leningrad, USSR, 11-38.
- Vinje, T.E., 1985; Drift, composition, morphology and distribution of the sea ice field in the Barents Sea. Norsk Polarinstitutt Skrift. 179C, 26 pp.
- Vorren, T.O., Hald, M., Lebesbye, E. & Vorren, K.-D., 1987; Late Cenozoic stratigraphy and environment in the Barents Sea. Polar Research 5, 303-304.
- Vyalov, S.S., 1965; Rheological properties and bearing capacity of frozen soils. Translation 74, U.S. Army CRREL, Hanover, N.H.

- Watt, B.J., 1982; Hydrocarbon extraction in Arctic frontiers. SOA Paper . Proc. 3rd. Conf. - On behavior of offshore structures. Cambridge Ma. MIT.
- Weaver, J.S. & Stewart, J.M., 1982; In situ hydrates under the Beaufort Sea shelf. Canadian Permafrost Conference, 4th. Proceedings, 312-319.
- Wellman, P. & Tingey, R.J., 1981; Glaciation, erosion, and uplift over part of Antarctica. Nature 291, 142-144.
- Werenskiold, W., 1922; Frozen earth in Spitsbergen. Geophysical Publication 2 (10).
- White, W.A., 1972; Deep erosion by continental ice sheets. Geol. Soc. Am. Bull. 83, 1037-1056.

